THE SYNTHESIS OF GRAPHENE FILMS VIA GRAPHENE OXIDE REDUCTION USING GREEN TEA POLYPHENOL AND ELECTROPHORETIC DEPOSITION FOR BIOMEDICAL APPLICATION

MUHAMMAD FAIQ BIN ABDULLAH

UNIVERSITI SAINS MALAYSIA

2013

THE SYNTHESIS OF GRAPHENE FILMS VIA GRAPHENE OXIDE

REDUCTION USING GREEN TEA POLYPHENOL AND

ELECTROPHORETIC DEPOSITION FOR BIOMEDICAL APPLICATION

By

MUHAMMAD FAIQ BIN ABDULLAH

Thesis submitted in fulfillment of the requirements

for the degree of

Master of Science

December 2013

ACKNOWLEDGEMENT

characterization. Lastly, my deepest appreciation also goes to all my fellow friends who had always stick with me through hardship and happiness.

Muhammad Faiq bin Abdullah, 2013

TABLE OF CONTENTS

Page

CHAPTER 1: INTRODUCTION

CHAPTER 2: LITERATURE REVIEW

CHAPTER 5: CONCLUSION AND RECOMMENDATIONS

LIST OF TABLES

LIST OF FIGURES

LIST OF PLATES

LIST OF ABBREVIATIONS

AFM	Atomic force microscope
BE	Binding energy
BSA	Bovine serum albumin
B3LYP	Becke-3-parameter-Lee-Yang-Parr
c-GO	Control-graphene oxide
CMA	Cylindrical mirror analyzer
CMG	Chemically modified graphene
CNDs	Nanodiamonds
CNHs	Carbon nanohorns
CNTs	Carbon Nanotubes
CRFK	Crandell-Rees feline kidney
CRG	Chemically reduced graphene
CRGO	Chemically reduced graphene oxide
CVD	Chemical vapor deposition
DC	Direct current
DFT	Density functional theory
DGU	Density gradient ultracentrifugation
DI	Deionized
DMEM	Dulbecco's Modified Eagle's Medium
DMF	Dimethylformamide
DMSO	Dimethylsulfoxide
DNA	Deoxyribonucleic acid
EC	Epicatechin
ECG	Epicatechin gallate
EDA	Ethylenediamine
EDS	Energy dispersion spectroscopy
EGC	Epigallocatechin
EGCG	Epigallocatechin gallate
EPD	Electrophoretic deposition
FBS	Fetal bovine serum
FET	Field-effect transistor
FTIR	Fourier transform infrared
GFs	Graphene films
GO	Graphene oxide
GTP	Green tea polyphenol
HA	Hydroxyapatite
HF	Hartree-Fock
HI	Hydroiodic
HMIH	1-hexyl-3-methylimidazolium hexafluorophosphate
HOPG	Highly oriented pyrolytic graphite
HRP	Horseradish peroxidase

HRTEM	High resolution transmission electron microscope
ILs	Ionic liquids
ITO	Indium tin oxide
KE	Kinetic energy
MAS	Magic angle spinning
MP	Moller-Plesset
NMP	N-methylpyrrolidone
NMR	Nuclear magnetic resonance
O.D.	Optical density
ORR	Oxygen reduction reaction
PE	Polyethylene
PEG	Polyethylene glycol
PEI	Polyethylenimine
PES	Potential energy surface
PET	Polyethylene terephthalate
PP	Polypropylene
PPD	P-phenylene diamine
PSS	Poly(sodium-4-styrenesulfonate
PTCA	Perylene tetracarboxylic acid
QDs	Quantum dots
RG	Reduced graphene
RGO	Reduced graphene oxide
ROS	Reactive oxygen species
SC	Sodium cholate
SDBS	Sodium dodecylbenzene sulfonate
SEM	Scanning electron microscopy
SOP	Standard order procedure
SS	Stainless steel
STQN	Synchronous Transit-Guided Quasi Newton
SWCNTs	Single-wall carbon nanotubes
TGA	Thermogravimetric analysis
TS	Transition state
UHV	Ultrahigh vacuum
UV-Vis	Ultraviolet-visible
XPS	X-ray photoelectron spectroscopy
XRD	X-ray diffraction
0D	Zero-dimensional
1D	One-dimensional
2D	Two-dimensional
3D	Three-dimensional

LIST OF SYMBOLS

μ	Electrophoretic mobility
ε_0	Permittivity of free space
ε_r	Permittivity of suspension medium
η	Viscosity of suspension medium
ζ	Zeta potential
$f(\kappa r)$	Henry coefficient
Ψ	Wavefunction
m	Mass of particle
h	Planck's constant
V	Potential field
∇	Operator del
r	Spatial functions
t	Time functions
m/S	Deposition weight per unit area
C_s	Solid loading
E	Electric field
Δ	Change of
H	Enthalpy
G	Gibbs free energy
S	Entropy

SINTESIS FILEM GRAFIN MELALUI PENURUNAN GRAFIN OKSIDA MENGGUNAKAN POLIFENOL TEH HIJAU DAN PEMENDAPAN ELEKTROFORETIK UNTUK APLIKASI BIOPERUBATAN

ABSTRAK

Dalam beberapa tahun kebelakangan ini, grafin telah muncul sebagai bahan nano yang paling berpotensi untuk pelbagai aplikasi terutamanya di dalam bidang bioperubatan disebabkan oleh struktur-nano dua dimensinya (2D) yang unik dan sifat fizik-kimianya yang menarik. Satu kaedah ringkas untuk menghasilkan grafin telah dibangunkan melalui penurunan grafin oksida (GO) menggunakan polifenol teh hijau (GTP) di dalam satu reaktor berkelompok. Kaedah yang disebutkan ini tidak memudaratkan persekitaran, kos yang efektif dan boleh diskalakan untuk penghasilan dalam kuantiti yang besar. Produk yang terhasil daripada proses penurunan dikenali sebagai grafin oksida yang diturunkan (RGO). Kesan nisbah berat GTP/GO dan suhu tindakbalas terhadap proses penurunan GO dikaji dengan teliti. Spektroskopi ultraungu-dilihat (UV-Vis), transformasi inframerah Fourier (FTIR), analisis gravimetrik terma (TGA) dan pengukuran keupayaan zeta serta pergerakan elektroforetik telah menunjukkan bahawa penurunan GO yang berjaya dan penyediaan larutan RGO yang stabil di dalam media berair boleh dicapai melalui tindakbalas penurunan GO dengan GTP pada suhu 90 ℃ menggunakan nisbah berat GTP/GO=1. Tambahan lagi, spektroskopi UV-Vis dan analisis spektroskopi fotoelektron X-ray (XPS) menunjukkan bahawa RGO yang disediakan menggunakan GTP mempunyai kedudukan akhir puncak penyerapan (271 nm) dan intensiti karbon sp^2 yang hampir sama dengan RGO yang dihasilkan menggunakan

larutan hidrazin (N_2H_4). Pemerhatian ini menunjukkan sifat penurunan GTP yang berkesan apabila dibandingkan dengan larutan N_2H_4 sebagai ejen penurunan piawai. Ujian ketoksidan menunjukkan bahawa RGO mempunyai kesan toksik yang rendah terhadap sel fibroblas kolon manusia (CCD-18Co) seperti yang dibuktikan oleh <30 % perencatan percambahan sel pada kepekatan yang rendah iaitu 6.25 µg/mL. Sementara itu, mekanisma untuk menyingkirkan kumpulan epoksi daripada GO melalui tindakbalas penurunan dengan GTP telah dikaji dengan melaksanakan kaedah fungsi hibrid Becke-3-parameter-Lee-Yang-Parr (B3LYP) digabungkan dengan set asas 3-21G, di mana semua pengiraan dilakukan menggunakan perisian Gaussian 09. Pengiraan tenaga dan frekuensi telah menunjukkan bahawa penurunan GO menggunakan GTP mempunyai perubahan entropi (ΔS) (0.039 kcal/mol·K) yang lebih tinggi dan halangan tenaga bebas Gibbs (G) (52.880 kcal/mol) yang lebih rendah daripada penurunan GO menggunakan larutan N_2H_4. Ini menunjukkan bahawa GTP adalah ejen penurunan yang lebih berkesan berbanding larutan N_2H_4 untuk penurunan GO. Kebanyakan aplikasi grafin terutamanya di dalam bidang bioperubatan memerlukan pertumbuhan lapisan grafin yang seragam di atas satu substrat dalam skala yang besar. Oleh itu, di dalam kajian ini, filem grafin (GFs) telah dibangunkan di atas substrat keluli tahan karat (SS) 316L menggunakan proses pemendapan elektroforetik (EPD). Didapati bahawa keseragaman, berat endapan dan ketebalan GFs dipengaruhi oleh voltan aplikasi dan tempoh pemendapan. Dijangkakan bahawa GFs yang dihasilkan melalui pemendapan zarah RGO di atas substrat SS mempunyai potensi yang besar untuk digunakan di dalam aplikasi bioperubatan.

THE SYNTHESIS OF GRAPHENE FILMS VIA GRAPHENE OXIDE REDUCTION USING GREEN TEA POLYPHENOL AND ELECTROPHORETIC DEPOSITION FOR BIOMEDICAL APPLICATION

ABSTRACT

In recent years, graphene has emerged as the most promising nanomaterial for various potential applications especially in biomedical field owing to its unique two dimensional (2D) nanostructure and intriguing physicochemical properties. A simple method to produce graphene was developed by reducing graphene oxide (GO) using green tea polyphenol (GTP) in a batch reactor. The aforementioned method was non-detrimental to the environment, cost effective and scalable for high-volume production. The product of the reduction process was referred as reduced GO (RGO). The effects of weight ratio of GTP/GO and reaction temperature on the reduction of GO were examined in details. The ultraviolet-visible (UV-Vis) spectroscopy, Fourier transform infrared (FTIR), thermogravimetric analysis (TGA) and the measurement of zeta potential as well as the electrophoretic mobility reveal that a successful reduction of GO and the preparation of stable RGO dispersion in aqueous media could be attained by performing the reduction reaction of GO with GTP at 90 ℃ using a weight ratio of GTP/GO=1. In addition, the UV-Vis spectroscopy and X-ray photoelectron spectroscopy (XPS) analysis show that the RGO prepared using GTP exhibits final position of absorption peak (271 nm) and intensity of sp^2 carbon that almost similar to the RGO produced using hydrazine (N_2H_4) solution. This observation indicates that the effective reduction property of GTP as compared to the N_2H_4 solution as a standard reducing agent. The

cytotoxicity testing reveals that the RGO possesses very low toxicity effects towards human colonic fibroblasts (CCD-18Co) cells lines as evidenced by <30 % inhibition of cell proliferation at low concentration of 6.25 µg/mL. On the other hand, the mechanism of the removal of epoxy group from GO via reduction reaction with GTP was investigated by implementing hybrid functional method of Becke-3-parameters-Lee-Yang-Parr (B3LYP) combined with 3-21G basis set, in which all calculations were computed using Gaussian 09 software. The energy and frequency calculations have revealed that the GO reduction using GTP has higher change of entropy (ΔS) (0.039 kcal/mol·K) and lower Gibbs free energy (G) barrier (52.880 kcal/mol) than the GO reduction using N_2H_4 solution. This shows that the GTP is a more efficient reducing agent than the N_2H_4 solution for the GO reduction. Most of the applications of graphene particularly in biomedical field require a uniform growth of graphene layers on a substrate in large scale. Thus, in this study, the graphene films (GFs) were developed on 316L stainless steel (SS) substrate using electrophoretic deposition (EPD) process. The uniformity, deposition weight and the thickness of the GFs were found to be influenced by the applied voltage and the deposition time. It is anticipated that the GFs produced by the deposition of RGO particles on SS substrate possess promising potential to be used in biomedical applications.

CHAPTER 1

INTRODUCTION

1.1   General Knowledge – Graphene-Based Nanomaterials

Nanomaterials have attracted enormous attention from both academia and industry as their unique and special properties have driven extensive researches to investigate their exciting potentials in a variety of applications such as in nanoelectronics, computer technology, biomedical field and health care (Moghimi et al., 2005; Rao and Cheetham, 2001; Roco, 2003; Sahoo et al., 2007). Nanomaterials are described as the organic or inorganic materials which possess one or more elements with a feature size less than 100 nanometers (nm) (Borm et al., 2006; Moghimi et al., 2005; Rao and Cheetham, 2001; Sahoo et al., 2007) including nanofibres (Jayakumar et al., 2010; Leung and Ko, 2011), nanoparticles (Fu et al., 2005; Li et al., 2012c), nanotubes (Sinha and Yeow, 2005; Yang et al., 2007), nanosheets (Liu et al., 2012; Turchanin et al., 2009), nanowires/nanorods (Choi et al., 2011), nanopatterns (McMurray et al., 2011), nano-structures surfaces and nanocomposites materials (Meng et al., 2011; Singh et al., 2008).

In the case of nanotubes, the size represents the diameter of the nanotubes while the size for thin films or multilayer coatings is indicated by the thickness of the films (Sundararajan and Rao, 2009). For comparison, an atom is smaller than 1 nm while most of the existing molecules including proteins are larger than 1 nm (Whitesides, 2003). The conceptual of nanomaterials was first emerged in 1959 when a physicist, Richard Feynman managed to explore the prospect of material

manipulation at atomic and molecular level (Mehra, 2002). Since then, tremendous works and researches have been carried out on nanomaterials mainly due to the availability of various methods to synthesize nanomaterials and the improving tools for the characterization of nanomaterials (Rao and Cheetham, 2001).

The ongoing trends of miniaturization in materials and technologies have led to the integration of material engineering with chemistry, physics and biology to produce the nanomaterials (Borm et al., 2006; Lehn, 2002). Many researchers have described nanomaterials as "small but special" as they have very different physical and chemical properties from those of the same materials in bulky form (Lavik and Von Recum, 2011). The exceptional properties of nanomaterials with well-controlled size and shape are very attractive especially in biomedical field, where the nanomaterials could be used for the treatment and diagnosis of infections and diseases at molecular level (Kim et al., 2010; Peer et al., 2007) or as a mimic structure for implants in the body (Borm et al., 2006).

Viruses or bacteria which cause infections are normally in nanometers size and they are possibly protected by nanometer-size barriers (Kim et al., 2010). Hence, by taking the advantage of the similarity in sizes of nanomaterials to biological molecules (Kim et al., 2010; West and Halas, 2003) as well as the ability for the modification of their chemical compositions and surface chemical characteristics (Kuila et al., 2012), nanomaterials could be designed to assist the transport of diagnostic agents through nanometer-size biological barrier in order to intervene the interaction of viruses and bacteria to human genes and cells (Kim et al., 2010; Liu et al., 2008; Peer et al., 2007).

Recent advancement of nanomaterials offers an exciting opportunity for further development of biomedical applications. Up to date, various nanomaterials have been studied extensively in biomedical field including carbon nanotubes (CNTs) (Emerich and Thanos, 2003; Ferrari, 2005; Lacerda et al., 2006), nanodiamonds (CNDs) (Huang and Chang, 2004), quantum dots (QDs) (Cai and Hong, 2012), carbon nanohorns (CNHs) (Iijima et al., 1999), paramagnetic nanoparticles (Thorek et al., 2006), nanoshells (Hirsch et al., 2006) and dendrimers (McCarthy et al., 2005; Svenson and Tomalia, 2005). Over the past few years, a future nanomaterial with enormous and exciting potential named graphene have received significant interests from researchers to be applied in various applications especially in biomedical field due to its unique structure and extraordinary mechanical, physical and chemical properties (Akhavan and Ghaderi, 2010; Shen et al., 2012; Zhang et al., 2012b).

Graphene is a single atomic planar sheet of sp^2-bonded carbon atoms tightly packed in a hexagonal lattice (Geim, 2009; Geim and Novoselov, 2007; Park and Ruoff, 2009; Rao et al., 2009), and it is known to be the "mother" of all other graphitic materials (Geim and Novoselov, 2007; Neto et al., 2006). One-dimensional (1D) CNTs are made of rolled-up layers of graphene, three-dimensional (3D) graphite is a stack of graphene sheets and zero-dimensional (0D) fullerenes are formed of wrapped-up sheets of graphene (Figure 1.1) (Geim and Novoselov, 2007). Graphene could be distinguished into three different types namely, single-layer, bi-layer and few-layers graphene (Choi et al., 2010b; Rao et al., 2009). Single layer graphene consists of one layer of two-dimensional (2D) hexagonal lattice of carbon atoms, while bi-layer and few-layers graphene consists of 2 and 3 to 10 sheets of such 2D hexagonal lattice. These 3 types of graphene received enormous and equal

attention from researchers, in contrast to thick graphene layers (more than 10 layers of graphene) which attract less scientific interest (Choi et al., 2010b; Rao et al., 2009).
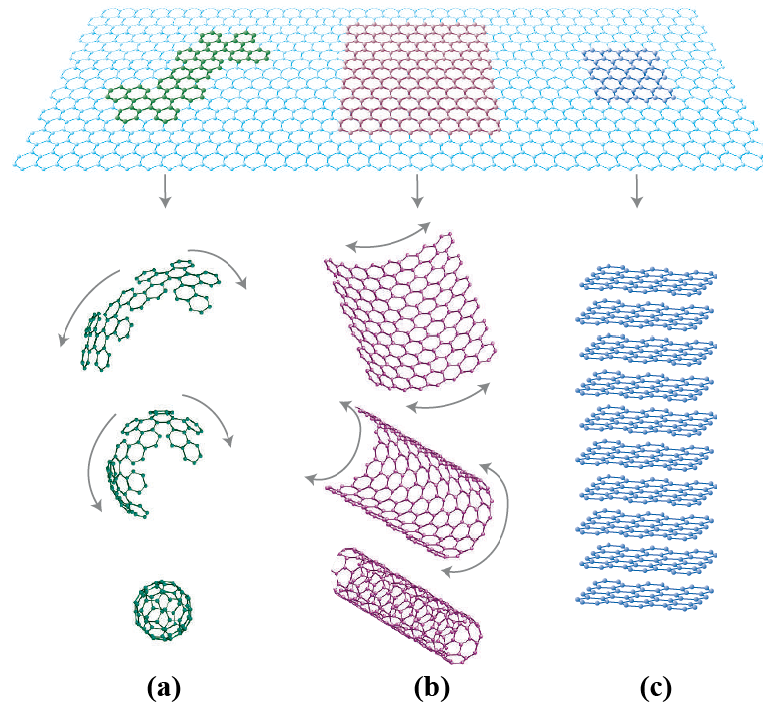
Figure 1.1: Graphene: "Mother" of all other graphitic materials, (a) fullerene (b) CNTs and (c) graphite (Geim and Novoselov, 2007).

The outstanding characteristics of graphene are fastening the development of various methods to produce graphene. Since its initial discovery, graphene has been demonstrated to be synthesized through a number of different techniques, most notably via the micromechanical cleavage of highly oriented pyrolytic graphite (HOPG) using adhesive tapes (Novoselov et al., 2004; Rao et al., 2009). This technique is also widely known as 'Scotch tape' or peel off technique with aims to achieve very thin platelets of graphite (Novoselov et al., 2004). The stacked layers of graphene sheets in graphite are bound together by weak van der Waals forces, where these bonds could be broken by simple mechanical cleavage to yield out the

4

individual graphene layers (Novoselov et al., 2004). Although single-layer graphene could be prepared by this method, the resulting yields are very low with only small quantities of graphene obtained were suitable for research purposes. In addition, micromechanical cleavage is a time-intensive process and it is highly difficult to scale-up for commercial applications (Choi et al., 2010b; Singh et al., 2011).

Alternatively, single and few-layers graphene also has been reported to be produced by chemical vapor deposition (CVD) technique such as the decomposition of hydrocarbon (e.g., ethylene) on transition metal (e.g., nickel (Ni), copper (Cu) and cobalt (Co)) surfaces (Kim et al., 2009a). In CVD process, carbon precursor will be dissolved into metal substrate at high temperature (700-850 ℃), which followed by natural cooling of the substrate to obtain few-layers graphene (Kim et al., 2009a). However, this technique still facing several issues which remain to be solved including the difficulty to obtain uniform growth of single-layer graphene and minimizing the folds of graphene (Choi et al., 2010b). Single-layer graphene also could be produced by thermal decomposition of silicon carbide (SiC) through high temperature annealing (Penuelas et al., 2009). Still, this method is impractical for large scale production of graphene due to very high temperature needed (>1100 ℃) and the complexity to produce large domains of graphene layer (Penuelas et al., 2009; Singh et al., 2011).

Graphene also has been demonstrated to be produced through the preparation of colloidal suspension of graphene oxide (GO), followed by the subsequent reduction of GO (Akhavan, 2010; Stankovich et al., 2007). Usually, GO is produced by the exfoliation of graphite oxide, which is prepared by the oxidation of graphite

in the presence of strong oxidizing agents (i.e., potassium permanganate ($KMnO_4$) (Hummers and Offeman, 1958), potassium chlorate ($KClO_3$) (Brodie, 1860)). GO is electrically insulating due to the disruption of its sp^2 bonding network, in which this bonding network could be restored through the reduction process (Dreyer et al., 2010; Stankovich et al., 2007). Owing to its hydrophilicity nature, GO possesses the ability to form stable aqueous suspension to facilitate the high volume production of reduced GO (RGO), which is very much desired in the research and the development of graphene (Pei and Cheng, 2012).

Apart from its well-known properties such as high Young's modulus (~1100 GPa) (Lee et al., 2008), remarkable intrinsic mobility (200,000 $cm^2v^{-1}s^{-1}$) (Bolotin et al., 2008), high fracture strength (125 GPa) (Lee et al., 2008), good thermal conductivity (~5000 $Wm^{-1}K^{-1}$) (Balandin et al., 2008) and excellent electrical conductivity (Cai et al., 2009), graphene also exhibits distinctive properties which are relevant to biological effects including large surface area, minimum number of layer, high purity, less toxicity and versatility for chemical modification (Sanchez et al., 2012; Zhang et al., 2010b). These excellent properties have lead graphene to become the forefront of present nanomaterials to be used in biomedical field. In fact, the biomedical applications of graphene are relatively still new with the first report emerged only in 2008 (Liu et al., 2008) due to short time span since its discovery in 2004 (Novoselov et al., 2004). Since then, numerous researches and works have been done to explore the potential of graphene to be used for biomedical applications such as gene/drug delivery (Chen et al., 2011; Liu et al., 2008), bioimaging (Eda et al., 2010), cancer therapy (Yang et al., 2010a), biosensors (Chang et al., 2010) and graphene-based scaffolds for tissue engineering (Fan et al., 2010).

1.2   Problem Statement

Since the first report of its discovery appeared in 2004, graphene has emerged as the most promising nanomaterial to be used in a wide variety of applications including nanoelectronics (Lam and Liang, 2012), nanocomposites (Mishra and Ramaprabhu, 2011; Santos et al., 2012), energy storage (Grande et al., 2012; Radich et al., 2011), sensors (Hill et al., 2011; Stine et al., 2012) and biomedical applications (Shen et al., 2012) owing to its intriguing and exceptional physicochemical properties. However, most of these exciting applications particularly the biomedical applications require uniform growth of single or few layers graphene on a substrate in large scale, which remains challenging and yet to be accomplished (Choi et al., 2010b; Park and Ruoff, 2009). Graphene and its derivatives have been widely reported to be prepared via a number of versatile techniques including the micromechanical cleavage of HOPG using adhesive tape (Novoselov et al., 2004; Rao et al., 2009), the decomposition of hydrocarbon on transition metal surfaces (e.g., Ni and Cu) using CVD technique (Kim et al., 2009a) and the thermal decomposition of SiC through high temperature annealing (Singh et al., 2011). Although single and few layers graphene could be prepared by the aforementioned methods, they are still surrounding with some problems and issues including low yield, high temperature needed (>1100 ℃) and the difficulty to obtain uniform growth of single-layer graphene (Choi et al., 2010b; Rao et al., 2009; Singh et al., 2011). Thus, the development of an alternative method to produce single and few layers graphene in large scale is in dire need.

The reduction of GO is known to be the most promising and efficient route to produce graphene owing to its cost effective, scalable for mass production, versatility for chemical functionalization, and requiring only simple equipment setup

as well as non-complex reaction procedures (Park and Ruoff, 2009; Pham et al., 2012). The chemical reduction of GO has attracted much attention from researchers with various chemical-based reducing agents such as hydrazine (N_2H_4) (Park et al., 2009; Stankovich et al., 2007), hydroquinone (Wang et al., 2008a) and sodium borohydride ($NaBH_4$) (Si and Samulski, 2008) have been used to remove the oxygen-functional groups (i.e., epoxide (–O–), hydroxyl (–OH), carbonyl (–C$=$O) and carboxyl (–COOH)) in GO. Although N_2H_4 is known to be the most widely used and effective reducing agent for the chemical reduction of GO, it is found to be highly corrosive and toxic (Akhavan et al., 2012; Powell and Gannett, 2002; Wang et al., 2011c). The environmentally detrimental properties of N_2H_4 have prompted research communities to substitute N_2H_4 with natural and more environmental-friendly reducing agents including vitamin C (Dua et al., 2010; Gao et al., 2010a; Zhu et al., 2012), bovine serum albumin (BSA) (Liu et al., 2010a) and melatonin (Esfandiar et al., 2011). However, these environmental-friendly reducing agents still facing some restrictions which hindered their effectiveness in reduction of GO. Thus, an environmental-friendly and effective reducing agent for the reduction of GO is very much desired (Wang et al., 2011c).

Since many decades, green tea has been utilized as a common beverage which brings enormous health benefits. However, only recently green tea attracts significant interest for its application in production of nanomaterials and nanocomposites (Chen et al., 2008a; Wang et al., 2011c). Green tea possesses the highest composition of polyphenolic compound in which this compound was regarded as an effective reducing agent due to its ability to donate hydrogen atom easily (Akhavan et al., 2012) and the capability to form π-π interaction with nanomaterial (Terao et al., 2009). With this regard, it is highly probable that the

environmental-friendly reduction of GO and the preparation of stable dispersion of RGO could be achieved by using green tea polyphenol (GTP). Although the reduction of GO by GTP has been reported by Wang et al. (2011c), the reduction mechanism of GO remains unclear due to complex structures of GTP. Liao et al. (2011b) have proposed that the epoxide groups in GO could be removed by S_N2 nucleophilic attack of epigallocatechin gallate (EGCG), the most potent catechin in GTP to produce RGO and galloyl-derived orthoquinone. Nevertheless, this proposed mechanism requires verification by experimental or computational study (Gao et al., 2010b).

Graphene nanostructures particularly graphene films (GFs) have attracted tremendous attention due to their promising applications especially in biomedical field (Akhavan and Ghaderi, 2010; Krishnamoorthy et al., 2012). In fact, GFs possess huge potential to be used as drug/gene delivery (Chen et al., 2011; Liu et al., 2008), cancer therapy (Yang et al., 2010a), antibacterial materials (Hu et al., 2010) and scaffolds for tissue engineering (Fan et al., 2010). Previously, it has been reported that GFs have been produced by reduction of GO, followed by subsequent filtration (Srinivas et al., 2010), spin coating (Fang et al., 2010) and micro-tip spreading of RGO suspension (Guo et al., 2009) on a substrate. However, it remains challenging and difficult to control the thickness of GFs for specific applications when employing these methods. In this regard, electrophoretic deposition (EPD) is proposed as the promising technique to fabricate GFs from RGO suspension. In recent years, EPD have attracted enormous attention from both academia and industry owing to its versatility, simple process, effective cost and the ability to produce uniform deposits on wide range of shape, 3D complex and porous structures

with controlled thickness (Boccaccini et al., 2006; Corni et al., 2008; Sarkar and Nicholson, 1996; Van der Biest and Vandeperre, 1999).

1.3   Research Objectives

The main aim of the undertaken research project is to produce RGO suspension through the reduction of GO by using GTP with views of potential applications in biomedical field. The present project has the following specific objectives:

i.   To prepare a stable RGO suspension from the reduction of GO by GTP.

ii.   To determine the effects of weight ratio of GTP/GO and reaction temperature on the reduction of GO.

iii. To evaluate the cytotoxicity of GO and RGO suspensions.

iv.   To determine the possible mechanism of GO reduction by GTP using computational study.

v.   To prepare GFs from RGO suspension using EPD process.

1.4   Research Scope

In the present work, GTP was employed as the reducing agent with aims to achieve successful reduction of GO and to yield a stable and well-dispersed RGO suspension in aqueous media. The effects of weight ratio of GTP/GO and reaction temperature on the reduction of GO and the stability of the as-produced RGO suspension were investigated in details. Then, the best reduction conditions were determined with aim to maximize the efficiency of the GO reduction, while at the same time yielding a stable RGO suspension for further processing. Accordingly,

the reduction mechanism of GO by EGCG, the most dominant and potent catechin in GTP (Chen et al., 2008a) was also investigated through computational study. One important aspect that is still in major discussion is the estimation of the reduction efficiency of the reducing agent. In this regard, the reduction efficiency of GTP was compared to the efficiency of N_2H_4 solution as a standard reducer. N_2H_4 is widely reported to be the most effective reducing agent for the reduction of GO, although its utilization in GO reduction has been deterred due to its environmentally detrimental properties (Powell and Gannett, 2002).

Apart from offering the non-detrimental route for the production of graphene, the employment of GTP as the reducing agent in the GO reduction may open up the possibilities for the preparation of non-toxic graphene with views of future applications in biomedical field. However, despite its huge potential to be applied in biomedical field, the toxicity behavior of graphene towards biological cells is yet to be fully understood and characterized (Sanchez et al., 2012). Therefore, in this work, the cytotoxicity of GO and RGO suspensions were investigated against human fibroblast cells. In addition, most of the applications in biomedical field may require the uniform growth of graphene layer on a substrate in large scale. Hence, the GFs were fabricated using EPD in which the effects of EPD parameters (i.e., applied voltage and deposition time) on the deposition weight, uniformity and thickness of GFs were investigated in details.

1.5   Organization of Thesis

Basically, the thesis was composed into five main chapters. In chapter one, the general knowledge related to the nanomaterials particularly the graphene-based nanomaterials were covered in the introduction. Problem statement presents a

11

discussion about the problems and issues faced by the current techniques to produce graphene in large scale. Then, the research objectives were revised with aims to solve and encounter those problems that have been addressed. In the last part of chapter one, the content of each chapter was highlighted in the organization of thesis.

The literature review of the topics related to the synthesis of graphene particularly the GO reduction technique was presented in chapter two. In addition, the compilation of the methods and materials used were also included, and the imperative discussions about the reduction of GO by other authors were also collected and compared. All the details information regarding the materials, chemicals and software used in this work were presented in chapter three. Besides, the methodology and the characterization techniques employed in this work were explained in detail in this chapter including the sample preparation, parameter investigated and the model of the instruments that have been used.

In chapter four, a complete and detail discussion on the results obtained in the present work was presented. Specifically, this chapter elucidates the effects of the weight ratio of GTP/GO and reaction temperature on the reduction of GO, the reduction efficiency of GTP in comparison to standard reducing agent, the stability and cytotoxicity of GO and RGO suspensions, the mechanism of GO reduction and the deposition of RGO particles on SS substrate. The overall of the statement discussed in chapter four was represented as a conclusion in chapter five. Additionally, the recommendations for future research based on the current findings were also included in this chapter.

CHAPTER TWO

LITERATURE REVIEW

2.1 Synthesis of Graphene

The initial work related to graphene has been carried out as early as in 1960s when the discovery of higher conductivity of graphite intercalation compounds was reported (Thompson et al., 1977; Ubbelohde and Lewis, 1960). This discovery has prompted researchers to synthesize single layer of graphite. In 1975, Lang (1975) has successfully reported the development of single and multi-layer graphite on platinum (Pt) by using thermal decomposition method. However, no further investigation has been carried out due to the inability to identify the useful applications of the product and the inconsistency of the properties of graphite sheets that have been developed on different Pt substrates (Choi et al., 2010b). Until late 20th century, the interests to thin graphite and graphene layers have grown steadily due to excellent electrical properties of the materials for nanoelectronics applications (Singh et al., 2011). During that time, it was widely believed that 2D crystals of graphite were thermodynamically unstable and unable to exist without 3D base (Geim and Novoselov, 2007; Singh et al., 2011). This has been supported by theoretical study which revealed the instability of graphene sheets when the size was reduced below 20 nm (or about 6000 atoms) (Shenderova et al., 2002). In addition, Mermin (1968) has reported that there was rapid decreasing of melting temperature of thin films which resulted in instability of graphene films at very low thickness (few atomic layers). With this regard, 2D materials of graphite were presumed to be impossible to exist until the historic discovery of graphene by Novoselov et al.

(2004) in 2004. Since then, tremendous researches and works have been done to develop new methods for large scale production of graphene and to explore the potential applications of this exciting nanomaterial in various fields.

2.1.1 Exfoliation and Cleavage of Graphite

Graphite is formed by stacked layers of graphene sheets, which are bonded by weak interlayer energy. Hence, in principal, single and few-layer graphene could be produced by simply break-off these bonds using mechanical or chemical energy (Choi et al., 2010b). In 1998, the first attempt to synthesize few-layer graphene using mechanical cleavage has been reported where atomic force microscope (AFM) tips have been used to rip graphene sheets from HOPG (Lu et al., 1999; Roy et al., 1998). In this process, the weak van der Waals forces between graphene layers have been overcome by adequate energy produced from the interaction between AFM tips and HOPG surfaces. Afterwards, Viculis et al. (2003) have formed the dispersion of carbon nanoscrolls in ethanol by intercalation and exfoliation of pure graphite using potassium metal. Although this technique requires modification to produce few-layer graphene, it has shown that it is highly possible to separate graphene layers from pure graphite. Single-layer graphene has been successfully produced only in 2004 by Novoselov et al. (2004) through mechanical exfoliation of HOPG using adhesive tapes (this technique is widely known as "Scotch tape" method). In this method, the commercially available HOPG was first been dry etched in oxygen plasma to produce 5 μm deep mesas. Mesas are the squares with various sizes ranging from 20 μm to 2 mm. The mesas were separated from the rest of the HOPG sample by attaching them to a photoresist layer. Only then, the layers were peeled-off from graphite sheet repeatedly using scotch tape as shown in Plate 2.1. The thin

14

flakes which remained on the photoresist were released in acetone and then, were transferred onto a silicon (Si) wafer to produce single and few-layer graphene (Novoselov et al., 2004).

Plate 2.1: Mechanical exfoliation of HOPG using scotch tape (Singh et al., 2011).

On the other hand, the physical exfoliation methods are attractive when there is necessity to preserve the graphene structure. In order to fabricate defects-free single layer graphene, a number of exfoliation approaches have been reported including electrolytic exfoliation of graphite (Wang et al., 2009a), exfoliation of graphite in water aided by surfactants (i.e., sodium dodecylbenzene sulfonate (SDBS) (Lotya et al., 2009) and sodium cholate (SC) (Green and Hersam, 2009)) and graphite exfoliation in ionic liquids (ILs) (Nuvoli et al., 2011) and specific solvents (i.e., N-methylpyrrolidone (NMP) (Hernandez et al., 2008) and dimethylformamide (DMF) (Blake et al., 2008)). Wang et al. (2009a) have demonstrated the production of graphene by the electrolytic exfoliation of graphite. In their work, stable graphene suspension was produced by using simple electrolysis

process which involved the use of graphite rods as electrodes and poly(sodium-4-styrenesulfonate) (PSS) as electrolyte. It is suggested that the electrolytic exfoliation of graphite rod was resulted from the interaction between aromatic rings in PSS and graphite surface. Meanwhile, Lotya et al. (2009) have successfully produced monolayer graphene from graphite exfoliation in water aided by SDBS which acts as a surfactant. The stability of graphene suspension could be appreciated with larger graphene flakes only tend to precipitate after 6 weeks while smaller flakes were remained stably dispersed in solution. This stability is contributed by huge potential barrier which is originated from the Coulomb repulsion between surfactant and coated sheets (Lotya et al., 2009). In another work by Green and Hersam (2009), SC was used as surfactant to exfoliate graphite in aqueous solution. Subsequently, the exfoliated-graphene flakes with controlled thickness were isolated by employing density gradient ultracentrifugation (DGU) technique. It has been proposed that a stable graphene suspension was formed due to amphiphilic nature of SC molecules, in which the hydrophobic faces interact with the graphene sheets and hydrophilic faces were leaved to interrelate with the aqueous environment.

In the meantime, Hernandez et al. (2008) and Blake et al. (2008) have reported direct exfoliation of graphite in NMP and DMF respectively. Such exfoliation took places due to the interaction between graphite sidewalls and those solvents, in which this interaction was occurred because of the dispersive, polar and H-bonding components of the surface energy (Bergin et al., 2009) associated with the solvents. Although this approach could provide the opportunity for direct exfoliation of graphite into graphene, the solvents required in this process were expensive and it might be difficult to deposit graphene on a substrate due to high boiling point of the solvents (Singh et al., 2011). It has been reported as well that

few-layer graphene have been produced by direct exfoliation of graphite in ILs (Nuvoli et al., 2011). Briefly, graphite was grounded and sonicated in an IL, 1-hexyl-3-methylimidazolium hexafluorophosphate (HMIH) to yield stable graphene suspension. Interestingly, high concentration of graphene could be obtained and no chemical modification of graphite was required when employing this method.

2.1.2 Chemical Vapor Deposition (CVD)

Apart from the mechanical exfoliation method, single and few layers graphene also have been reported to be produced through CVD technique. Although the CVD technique is promising for large scale production of graphene (Choi et al., 2010b; Singh et al., 2011), it is relatively quite new and still facing several issues which remain to be solved including the difficulty to obtain uniform growth of graphene and minimizing the folds of graphene (Singh et al., 2011).

2.1.2 (a) Thermal Chemical Vapor Deposition (CVD)

The first report on the production of few layers graphene using thermal CVD method was emerged in 2006 (Somani et al., 2006). In this study, a low cost precursor, camphor was utilized to produce graphene films on Ni foils. Initially, the camphor precursor was evaporated at 180 ºC and subsequently pyrolyzed at 700 ºC-850 ºC in another chamber of the CVD furnace. Then, few layers graphene films were observed on the Ni foils upon natural cooling of the pyrolyzed-camphor to the room temperature. Since then, substantial works have been carried out to obtain graphene films on other types of metal substrates with controlled thickness (Cao et al., 2010; Kim et al., 2009a; Lee et al., 2010; Li et al., 2009). It is imperative to fully understand the mechanism of the growth of graphene on the metal substrates in

order to improve the efficiency of the CVD technique for high volume production of graphene films (Obraztsov, 2009). The growth mechanism of graphene on metal substrates was suggested to be based on the diffusion of the carbon atoms into the metal film (at growth temperature) and the segregation of the carbon atoms out of the bulk metal onto the metal surface upon cooling (Kim et al., 2009a; Reina et al., 2009). In 2008, Yu et al. (2008) have reported the formation of four layers graphene on polycrystalline Ni foils via CVD technique. From the high resolution transmission electron microscope (HRTEM) and Raman spectroscopic analyses, the formation of graphene on Ni foils was taken place only at moderate cooling rate whereas the high and low cooling rates were found to be detrimental to the formation of the graphene layers. This observation was suggested to be due to the carbon solubility and the kinetics of carbon segregation in Ni (Yu et al., 2008). At low cooling rate, the carbon atoms possess adequate time to diffuse in the bulk Ni and thus, no segregation was occurred on the Ni surface. In contrast, the carbon atoms segregate and form graphene layers at moderate cooling rate. Although the carbon atoms also segregate out of Ni at high cooling rate, the as-produced graphene layers possess defective and less crystalline structure. This study by Yu and his coworkers has generated important information to further understand the growth mechanism of graphene on metal substrates in CVD process (Yu et al., 2008).

Wang et al. (2009c) have proposed an attractive method to produce substrate-free few layers graphene. The graphene was produced in a ceramic boat using magnesium oxide (MgO)-supported Co as the catalyst. The graphene was prepared at 1000 ºC for 30 minutes under a gas envelope of methane and argon with volume ratio of 1:4 (total flow rate is 375 mL/minute). The product of the reaction was washed with the concentrated hydrochloric acid (HCl) to remove the excess

MgO and Co. Subsequently, the product was rinsed with abundant distilled water and dried at 70 ºC. The scanning electron microscopy (SEM), HRTEM and Raman spectroscopic analyses have revealed that at least five layers of rippled graphene sheets are produced (Wang et al., 2009c). Meanwhile, Reina et al. (2009) have demonstrated the formation of single and few layers graphene on polycrystalline Ni film by using thermal CVD technique. The Ni film was evaporated on a silicon dioxide (SiO_2)/Si substrate and annealed at 900 ºC-1000 ºC in argon/hydrogen atmosphere for 10-20 minutes. The Ni grains with size of 5-20 μm were created through the annealing step. The graphene layer was observed to form on the Ni film with the size of the graphene was restricted by the grain size of the Ni. In addition, the as-produced graphene layer could be transferred to any substrate while keeping the electrical properties of the graphene unchanged, making it suitable to be applied in electronics or as energy storage (Reina et al., 2009). Meanwhile, Bae et al. (2010) have reported the roll-to-roll preparation of graphene films using CVD method. Plate 2.2 illustrates the fabrication process of the graphene layer through roll-to-roll technique. The fabrication steps include the preparation of graphene layers on Cu substrate, the adhesion of polymer supports to the graphene on Cu foil, etching of Cu foil and the transfer of graphene layers onto a target substrate. The as-obtained graphene monolayer has resistance as low as ~125 Ω/square with 97.4 % of the optical transmittance, indicating its promising potential to replace the current commercial transparent electrodes such as indium tin oxide (ITO) (Bae et al., 2010). The recent progress in graphene growth through thermal CVD has assured the reproducibility of high quality graphene on centimeter (cm) scale substrate and the successful transfer of the graphene layer to the other substrates (Choi et al., 2010b;

Singh et al., 2011). These achievements have created pathways for the application of graphene in various fields especially in electronics and biomedical field.
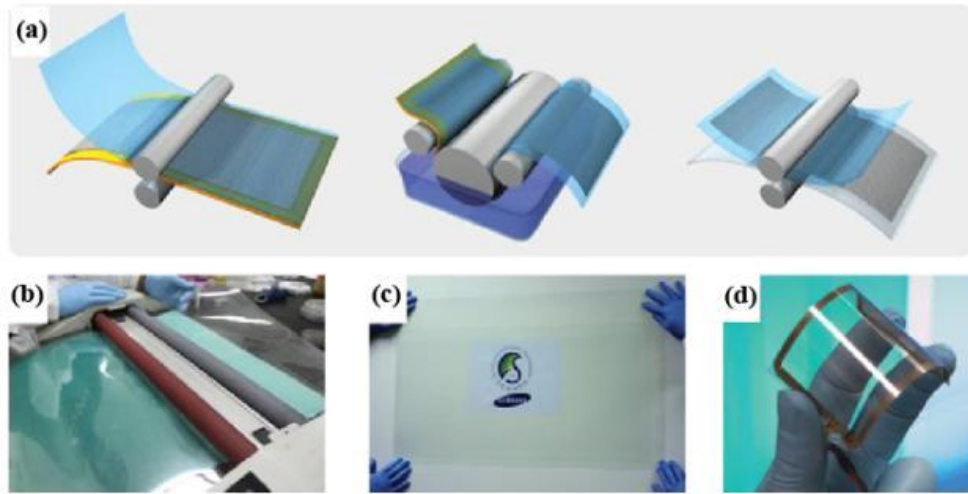
Plate 2.2: (a) Illustration for the fabrication of graphene films on Cu foils through roll-to-roll CVD technique. Optical images of (b) roll-to-roll transfer of graphene films onto a polyethylene terephthalate (PET) film at 120 ºC, (c) transparent graphene film after transferred to a PET film and (d) the assembled graphene/PET touch panel (Bae et al., 2010).

2.1.2 (b) Plasma Enhanced Chemical Vapor Deposition (CVD)

Plasma enhanced CVD offers the alternative route for the production of graphene at a lower temperature than the thermal CVD. In 2003, Obraztsov et al. (2003) has produced nanostructure graphite-like carbon by using direct current (DC) discharge plasma enhanced CVD method. Obraztsov and his co-workers used Si wafer and some metal sheets (e.g., Ni, molybdenum (Mo) and tungsten (W)) as the substrate in which a gas mixture of methane and hydrogen was also utilized in the process. The as-produced nanostructure graphite-like carbon films look thicker except at some twisted fragment (Obraztsov et al., 2003). The first report on the production of single and few layers graphene using plasma enhanced CVD method was emerged in 2004 (Wang et al., 2004a; Wang et al., 2004b). The graphene films

were synthesized on a variety of substrates (e.g., Si, W, Mo, titanium (Ti) and chromium (Cr)) using a radio frequency plasma enhanced CVD technique. This process was carried out in a gas mixture of methane and hydrogen at a temperature of 680 ºC (Wang et al., 2004a; Wang et al., 2004b). Since then, extensive works have been performed in order to fully understand the mechanism of the graphene growth in plasma enhanced CVD and to optimize the operating conditions to control the thickness of the graphene films (Malesevic et al., 2008; Vitchev et al., 2010). Zhu et al. (2007) have suggested the mechanism of the graphene growth in plasma enhanced CVD chamber. According to them, the GFs were synthesized through a balance between deposition (via surface diffusion of carbon-bearing growth species from precursor gas) and etching caused by the atomic hydrogen. In addition, they also suggest that the verticality of the GFs was caused by the plasma electric field direction (Zhu et al., 2007). The plasma enhanced CVD method possesses great advantages in term of short deposition time (less than 5 minutes), lower growth temperature (less than 650 ºC) and versatility to synthesize graphene on any substrate as compared to the thermal CVD approach (Choi et al., 2010b; Obraztsov, 2009; Singh et al., 2011). It is expected that future developments of plasma enhanced CVD technique will result in a better control of the thickness of the graphene films for high volume production.

2.1.3   Thermal Decomposition of Silicon Carbide (SiC)

Another alternative method to produce graphene is through thermal decomposition of SiC. Graphene sheets were formed when the hydrogen-etched surface of SiC was heated to temperature of 1250 ºC-1450 ºC. Once heated, the Si atoms sublimate from the substrate and the removal of the Si atoms will leave the

surface carbon atoms to rearrange into graphene layers (Choi et al., 2010b; Hass et al., 2008; Singh et al., 2011). The thickness of the layers depends on the temperature and the heating time (Singh et al., 2011). Penuelas et al. (2009) have suggested that in order to produce few layers graphene, the surface of the SiC must be heated at temperature around 1200 ℃ for a few minutes. Juang et al. (2009) have reported a significant improvement of this technique in which graphene was successfully synthesized on a Ni coated SiC substrate at a lower temperature (750 ℃). In addition, this process is favorable for future industrial application due to its promising potential to produce graphene in large scale.

Although the thermal decomposition of SiC is an attractive method to produce graphene, this technique still facing several issues that remain to be solved including the difficulty to control the thickness of the graphene films and to fully understand the relationship between the electrical properties and the structures of the interface layers between the graphene film and the substrate (Choi et al., 2010b; Singh et al., 2011). Additionally, the epitaxial growth pattern on different polar face of the SiC (i.e., Si-face or C-face) was yet to be fully understood (Hass et al., 2008; Sprinkle et al., 2009). The unusual rotational graphene stacking were observed in few layers graphene grown on the C-face surface while no unusual graphene stacking were observed on the Si-face surface. Such disparity of the growth pattern has profound effects on the physicochemical and the electrical properties of the as-produced graphene. On the C-face, the unusual graphene stacking leads to the decoupling between the graphene layers, in which each of the layers behaves as a single layer (Sprinkle et al., 2009). However, the electrical properties of the graphene layers on the Si-face remain debatable (Hass et al., 2008). In future research, extensive works will need to be carried out in order to understand the

mechanism of the graphene growth on both the Si-face and C-face surfaces. This method has huge potential to be used for high scale production of graphene once the growth mechanism and the interface effects were fully understood and the thickness of the graphene films could be controlled effectively (Choi et al., 2010b; Rao et al., 2009; Singh et al., 2011).

2.1.4 Reduction of Graphene Oxide (GO)

The discovery of graphene has been reported for the first time in 2004 by Novoselov et al. (2004), where the single layer of graphene has been successfully synthesized by using "Scotch tape" method. Since then, a number of techniques have been explored in order to prepare high quality graphene including CVD technique (Kim et al., 2009a), thermal decomposition of SiC (Penuelas et al., 2009), and reduction of GO (Stankovich et al., 2007). Among these methods, the reduction of GO is considered to be the most efficient route to produce graphene in large scale at a reduced cost (Akhavan et al., 2012; Liao et al., 2011b; Pei and Cheng, 2012; Stankovich et al., 2007; Wang et al., 2011c). GO is obtained from the exfoliation of graphite oxide, in which the graphite oxide is prepared by the oxidation of graphite precursor. Graphite oxide possesses similar stacked structure as graphite. However, the carbon atoms plane of graphite oxide contains myriad of oxygen functional groups which resulted in hydrophilicity and expansion of its interlayer spacing (Dreyer et al., 2010). In addition, the presence of numerous oxygen functionalities has disrupted the sp^2 bonding networks of graphite oxide and GO, which resulted in electrical insulation of both of these materials (Dreyer et al., 2010; Stankovich et al., 2007). This is where the reduction has become the most important reaction of GO as the electrical conductivity of graphite oxide and GO can be restored by removing the

oxygen functional groups by reduction process (Dreyer et al., 2010; Pei and Cheng, 2012; Stankovich et al., 2007). The product of reduction of GO has been identified with various names such as RGO, chemically modified graphene (CMG), chemically reduced graphene oxide (CRGO), chemically reduced graphene (CRG) or reduced graphene (RG) (Dreyer et al., 2010). It is inappropriate to refer RGO as pristine graphene since the properties and structure of both of these materials could differ to a varying degrees. However, it is worthy to note that the reduction of GO is the most efficient route to produce large amount of graphene-like material that possesses physicochemical properties and structure almost similar to pristine graphene (Dreyer et al., 2010; Pei and Cheng, 2012).

2.1.4 (a) Preparation of Graphene Oxide (GO) and its Structural Characteristics

GO has attracted enormous attention from researchers due to its role as a precursor for the production of graphene-like materials in large quantities. The earliest works related to GO have been reported for the first time in 1840 and 1859 by Schafhaeutl (1840) and Brodie (1859), respectively. Up to date, the chemical structure and the synthesis process of GO have been reviewed extensively by Dreyer et al. (2010), Compton and Nguyen (2010), Mao et al. (2012) and recently by Pei and Cheng (2012). GO could be synthesized by using a number of methods that have been proposed by Brodie (1859), Staudenmaier (1898) and Hummers and Offeman (1958). Initially, Brodie has performed the oxidation reaction of graphite by reacting a slurry of flake graphite with $KClO_3$ in nitric acid (HNO_3). Brodie has confirmed that his proposed oxidation treatment could increase the oxygen content in the resulting product. However, he was unable to measure the interfacial angles of

the lattice of the crystal product (Brodie, 1859). In 1898, Staudenmaier has improved Brodie's method by introducing concentrated sulfuric acid (H_2SO_4) in the mixture as well as adding $KClO_3$ in multiple additions over the course of the oxidation reaction. This improvement has enabled the highly oxidized GO to be produced more practically in a single reactor (Staudenmaier, 1898). Whilst in 1958, Hummers and Offeman have proposed alternative oxidation technique by mixing flake graphite with $KMnO_4$ and sodium nitrate ($NaNO_3$) in concentrated H_2SO_4 solution (Hummers and Offeman, 1958). Some researchers have developed the modified version of the Hummers method in which it has emerged as the most common technique that has been used to prepare GO nowadays (Hirata et al., 2004; Kovtyukhova, 1999; Wu et al., 2009b; Zhao et al., 2010). The representation of the improved and modified versions of the Hummers method has been outlined as in Figure 2.1. Meanwhile, it has been demonstrated that the quality of the products of the oxidation reaction is varies significantly depending on the reaction conditions, the type of the oxidants used and the source of the natural graphite (Dreyer et al., 2010).
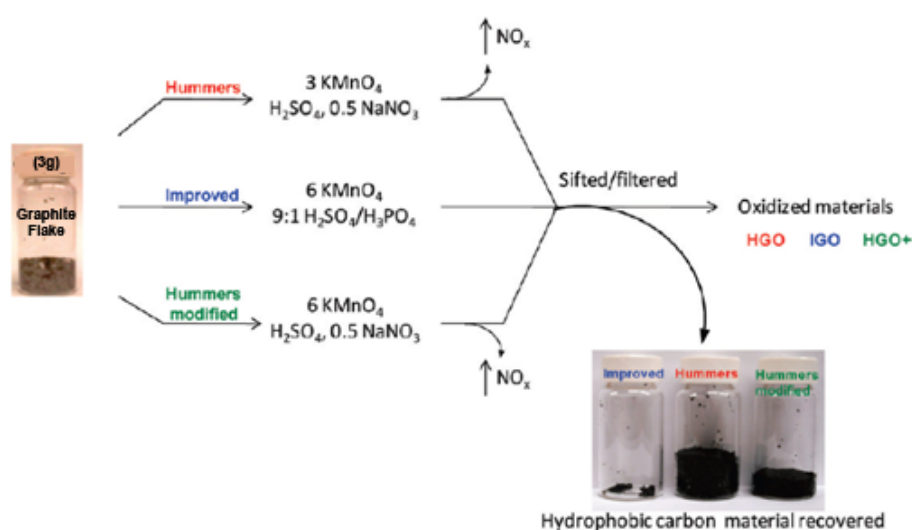
Figure 2.1: Representation of improved and modified versions of Hummers method with starting material of graphite flake (Marcano et al., 2010).

Although GO has been prepared successfully since many decades, its precise chemical structure is still unclear and remains debatable for many years. Even up today, there is no unambiguous model of GO structure that exists due to the amorphous nature which resulted in complexity of the material, non-stoichiometric atomic composition and lack of definite analytical methods available that can be used to characterize such materials (Dreyer et al., 2010). However, since recent years, enormous works have been carried out in order to further understand the chemical structure of GO in which incredible results have been produced from most of these efforts (Dreyer et al., 2010; Mao et al., 2012). It is very crucial to understand the atomic structure and physical properties of GO in order to enhance the yield and improving the unique properties of graphene-like material.

In most of the earliest investigation of structural model of GO, the regular lattices are suggested to be composed with distinct repeating units as illustrated in Figure 2.2. The earliest structural model of GO has been proposed by Hofmann and Holst (1939) in 1939, where their suggested GO model consisted only epoxy groups that are randomly distributed across the graphite's basal plane. In 1947, Ruess (1947) has suggested the presence of hydrogen content in the basal plane of GO by incorporating the hydroxyl groups in his model. In addition, Ruess also has proposed that the oxygen atoms in epoxy groups are connecting to the 1,3 sites of the carbon atoms (1,3-ether) rather than to 1,2 sites (1,2-ether). As a result, the basal plane of graphite is distorted into 3D system due to the presence of these 1,3-ethers and hydroxyl groups. In 1969, Scholz and Boehm (1969) have eliminated the epoxy and ether groups from their suggested model, while at the same time, replacing the quinoidal species in the conjugated carbon backbone. In another model suggested by Nakajima and Matsuo (1994), the adjacent layers were linked by the oxygen atoms

26

in the epoxy groups while the carbon lattices were presumed to be similar to those of poly(dicarbon monofluoride) $(C_2F)_m$. Meanwhile, Szabó et al. (2006) have proposed a GO model which incorporated the characteristics from Ruess and Scholz's models by including the random distribution of trans-linked cyclohexane species and corrugated hexagonal ribbons as portrayed in Figure 2.3.
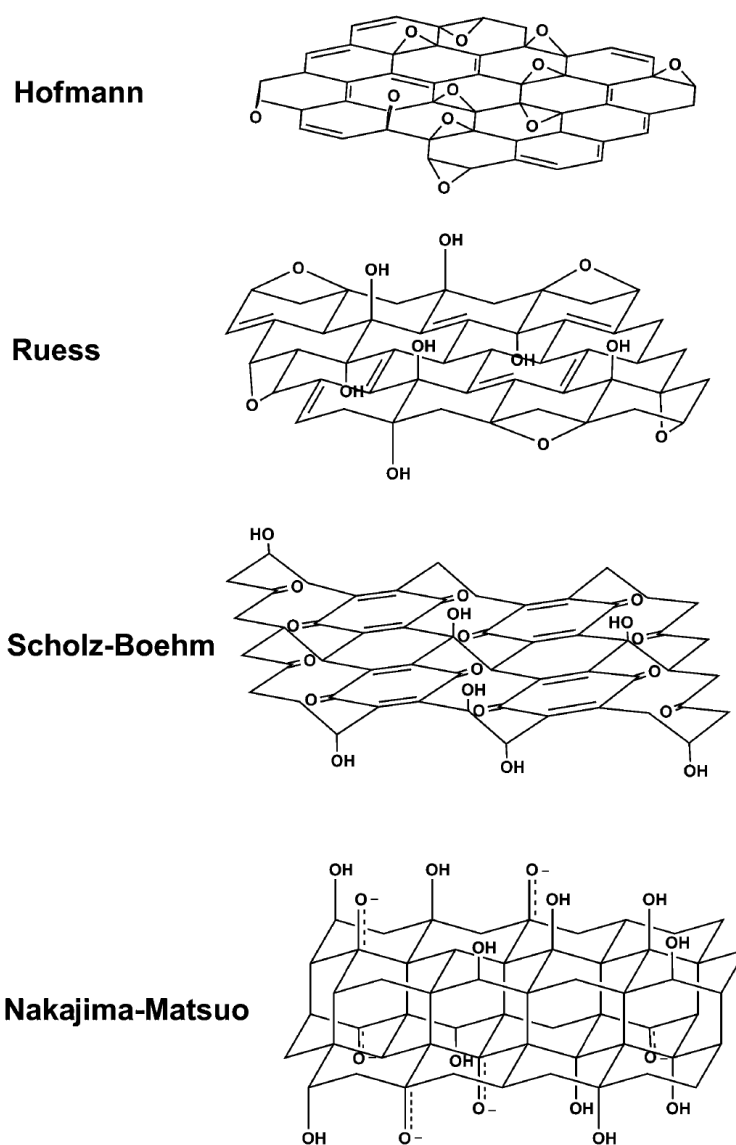
Figure 2.2: Several earliest structural models of GO (Szabó et al., 2006).

27
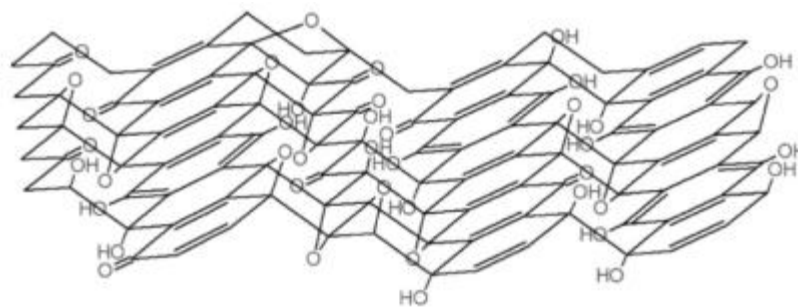
Figure 2.3: Structural model of GO as proposed by Szabo and his colleagues (Szabó et al., 2006).

In contrast to the earlier models of GO which were largely focusing on lattice-based model, the recent structural model of GO was proposed based on the non-stoichiometric and amorphous model. In 1998, Lerf et al. (1998) have proposed a non-stoichiometric based model of GO that incorporating the random distribution of major components; epoxy and hydroxyl groups across the basal plane and the allocation of minor components; carboxyls, lactones and carbonyls at the edge of GO's plane as depicted in Figure 2.4. Nowadays, the Lerf-Klinowski model is the most well-known GO model and it is widely accepted by most researchers. In their initial study, Lerf and his colleagues have prepared GO by using Hummers method and for the first time, the GO has been characterized by using nuclear magnetic resonance (NMR) spectroscopy (Lerf et al., 1998). In earlier studies of GO model, the characterization of GO has been made primarily via elemental components, X-ray diffraction (XRD) and reactivity studies (Dreyer et al., 2010). From ^{13}C NMR spectra, Lerf et al. (1998) have allocated the chemical shift line at 60 ppm to 1,2-ethers (epoxy groups) rather than to 1,3-ethers as per initially been suggested by Mermoux et al. (1991). In addition, Lerf et al. (1998) also have assigned the shift line at 70 ppm to hydroxyl groups and the peak at 130 ppm to conjugated double bonds and aromatic units. In order to obtain a clearer picture of the complexity of

GO, Lerf and his co-workers have revised their initial model by reacting the GO with a number of reactive reagents (i.e. potassium iodide (KI), triethyl phosphate ($P(OEt)_3$), dimethylsulfoxide (DMSO), acetic acid anhydride (Ac_2O), pentylamine (C_5NH_2), ethylenediamine (EDA), etc). As a result, the double bonds in GO were determined to be likely either conjugated or aromatic as they were unlikely to persevere in strong oxidation conditions (Lerf et al., 1998). In addition, the revised model also included the presence of very low amount of carboxylic acid groups at the edge of the carbon plane (Rodríguez and Jiménez, 1986; Scholz and Boehm, 1969).
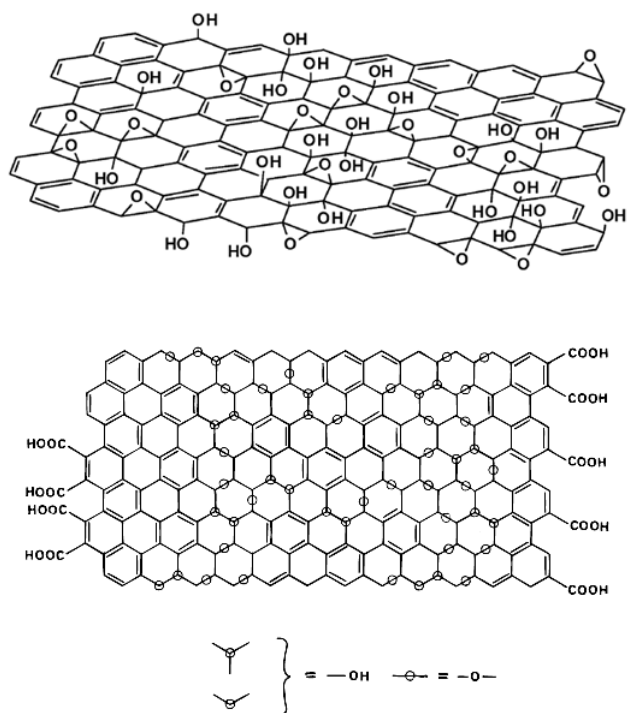
Figure 2.4: Nonstoichiometric-based model of GO as proposed by Lerf and Klinowski with the absence (top) (He et al., 1998) and the presence (bottom) (Lerf et al., 1998) of carboxyl groups on the edge of carbon backbone.

Since its first report appeared in 1998, the Lerf-Klinowski model of GO remained unchanged even until today. However, some researchers have suggested

minor modifications to the GO structure. Gao et al. (2009) have proposed the distribution of five- and six-membered lactols at the edge of the graphitic flakes while Cai et al. (2008) have successfully revealed the ability to label the ^{13}C solid-state NMR spectra of GO as shown in Figure 2.5. The variation of the properties and structure of GO depends mainly to the graphite source and the oxidation procedure. In order to acquire clearer insight of GO structure, the experimental observations have been compared to the theoretical characterization technique (density functional theory (DFT) calculations) (Barone et al., 2011; Boukhvalov et al., 2012; Gao et al., 2010b; Kim et al., 2009b; Tang and Cao, 2012; Yu et al., 2011).
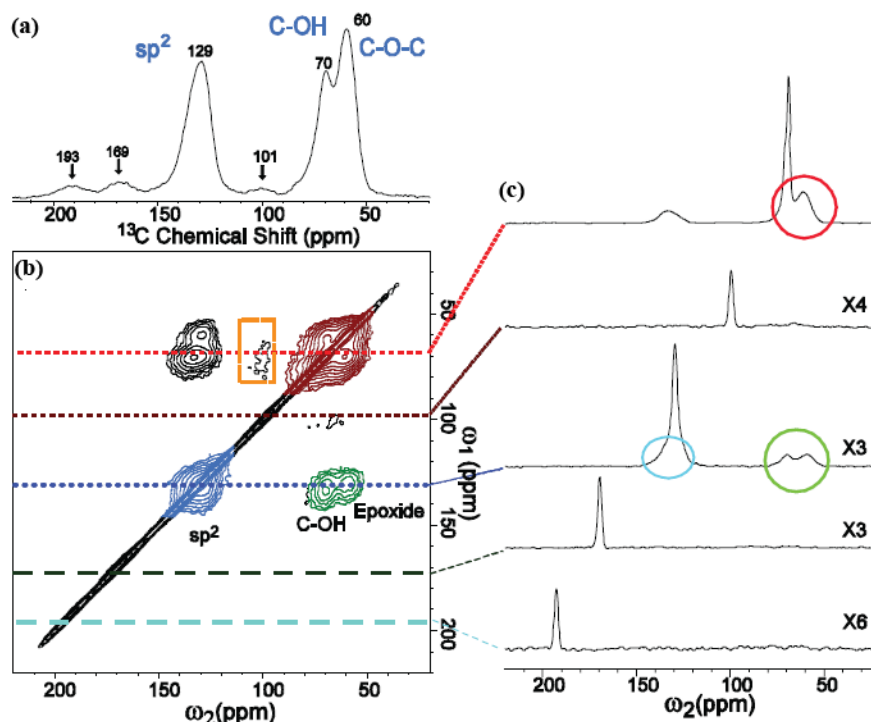
Figure 2.5: (a) 1D ^{13}C magic angle spinning (MAS) and (b) 2D ^{13}C/^{13}C chemical-shift correlation solid-state NMR spectra of ^{13}C-labeled graphite oxide with (c) slices selected from 2D spectrum at the indicated positions (70, 101, 130, 169 and 193 ppm) in the ω_1 dimension. The green, red and blue areas in (b) and circles in (c) represent cross peaks between sp^2 and hydroxyl/epoxide (green), those between hydroxyl and epoxide (red) and those within sp^2 groups (blue), respectively (Cai et al., 2008).

30

2.1.4 (b) Reduction Methods

The reestablishment of the sp^2 bonding network of GO and the restoration of its electrical conductivity could be achieved by removing the oxygen functionalities in GO through reduction process. The reduction process could be categorized into chemical reduction, thermal reduction and multi-step reduction.

2.1.4 (b)(i) Chemical Reduction

The chemical reduction of GO has been performed by using various reducing agents including N_2H_4 (Park et al., 2009; Stankovich et al., 2007), hydroquinone (Wang et al., 2008a), $NaBH_4$ (Muszynski et al., 2008; Si and Samulski, 2008), sulfur containing compounds (Chen et al., 2010a) and hydroiodic (HI) acid (Moon et al., 2010; Pei et al., 2010). Usually, the chemical reduction of GO could be achieved at room temperature or by moderate heating. Hence, the requirement for the equipment and environment was not that critical as compared to the thermal reduction, in which this makes the chemical reduction a cheaper, simpler and easier route to produce graphene in large scale as compared to the thermal reduction (the discussion on thermal reduction will be presented in section 2.1.4 (b)(ii)).

The preparation of chemically derived graphene using N_2H_4 was first reported by Stankovich et al. (2007) in 2007. Post the reduction reaction of GO with N_2H_4, the brown colour dispersion of GO in water was changed to black colour and the RGO sheets were observed to be aggregated and precipitated (Stankovich et al., 2007). Stankovich and his coworkers have suggested that the RGO dispersion became less hydrophilic due to the removal of the oxygen functionalities, in which this resulted in the aggregation and the precipitation of the RGO sheets. From the

^{13}C NMR spectra of GO and RGO, significant structural change was observed to be induced by the reduction process as illustrated in Figure 2.6 (Stankovich et al., 2007). This structural change indicates that the successful removal of the oxygen functionalities from GO has been attained. This report has opened-up the possibility to produce graphene in large scale. Since then, substantial works have been reported on the GO reduction using N_2H_4 and its derivatives (e.g., N_2H_4 hydrate and dimethyl-N_2H_4) (Gómez-Navarro et al., 2007; Li et al., 2008; Mattevi et al., 2009). As a result, N_2H_4 was accepted and widely known to be the most effective reducing agent for the GO reduction.

Although the GO has been demonstrated to be successfully reduced, the agglomeration and the precipitation of the as-produced RGO sheets have prevented the RGO dispersion from further processing for applications in various fields. Hence, extensive efforts have been made to produce stable RGO suspension by including surface functionalization step in the reduction reaction (Veerapandian et al., 2012; Xu et al., 2008) or by adding soluble polymers as stabilizer (Hasan et al., 2011; Stankovich et al., 2006a) and ammonia to alter the charge state of the RGO sheets (Li et al., 2008). Simple process such as filtration could then be used to assemble the macroscopic structures of the RGO sheets for wide range of applications (Li et al., 2008; Pei and Cheng, 2012). Despite its effectiveness in GO reduction, N_2H_4 was found to be highly toxic and corrosive (Akhavan et al., 2012; Powell and Gannett, 2002). Thus, the utilization of N_2H_4 in GO reduction has been deterred due to its environmentally detrimental properties.
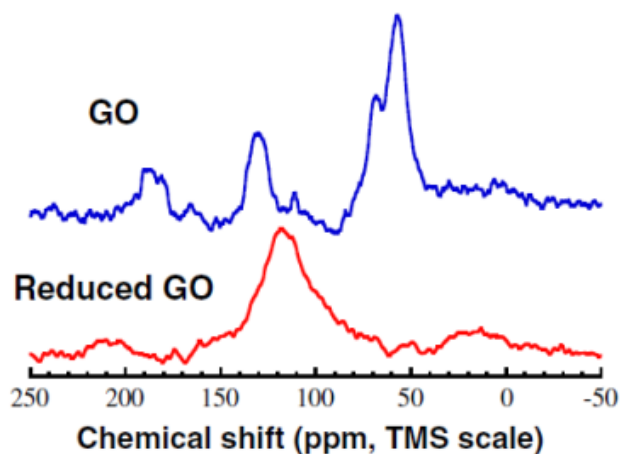
Figure 2.6: ^{13}C NMR spectra of GO (top) and RGO (bottom) (Stankovich et al., 2007).

Apart from N_2H_4 and its derivatives, metal hydrides (e.g., sodium hydride (NaH), $NaBH_4$ and lithium aluminium hydride) also have been accepted as the effective reducing agent for the reduction of GO (Pei and Cheng, 2012; Shin et al., 2009). The GO reduction by using $NaBH_4$ was demonstrated to be more efficient than the reduction using N_2H_4 (Shin et al., 2009). Although $NaBH_4$ is able to remove the carbonyl groups effectively, it has low efficiency to eradicate epoxy and carboxyl groups. In order to further enhance the reduction efficiency of $NaBH_4$, Gao et al. (2009) have added an additional dehydration process at 180 ºC using concentrated H_2SO_4 after the reduction with $NaBH_4$. Meanwhile, Chen et al. (2010a) have reported the successful reduction of GO by using sulfur containing compounds including sodium bisulfite ($NaHSO_3$), thionyl chloride ($SOCl_2$) and sulfur dioxide (SO_2). Raman spectroscopy, elemental analysis and thermogravimetric analysis (TGA) have confirmed that the reducing ability of $NaHSO_3$ is comparable to that of N_2H_4. Chen and his coworkers also has proposed the reduction mechanism of GO by $NaHSO_3$ in which the $NaHSO_3$ was oxidized to sodium sulfate (Na_2SO_4) after the reduction reaction (Chen et al., 2010a). On the other hand, the GO was also reported

to be reduced using hydroquinone (Wang et al., 2008a). The graphene nanosheets were observed to corrugate into ripples, like wavy silk as illustrated from the low magnification of TEM images in Figure 2.7 (Wang et al., 2008a). Pei et al. (2010) have reported the employment of another reducing agent, HI acid in the GO reduction. Pei and his coworkers have demonstrated that the GO reduction using HI acid resulted in very high C/O ratio of RGO of 15 and conductivity of 300 S/cm. In addition, the as-produced RGO films were observed to have good flexibility and improved tensile strength (Pei et al., 2010).
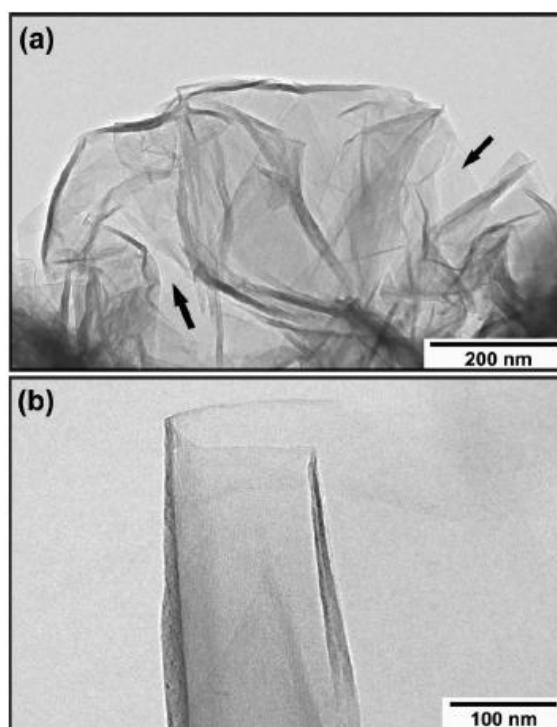
Figure 2.7: TEM images of (a) graphene nanosheets which resembling the crumpled silk and (b) a scrolled graphene nanosheets (Wang et al., 2008a).

It has also been demonstrated that efficient reduction of GO could be achieved by using NaBH$_4$, hydroquinone, sulfur containing compounds and HI acid (Chen et al., 2010a; Pei et al., 2010; Shin et al., 2009; Wang et al., 2008a). However, most of these reducing agents possess certain level of toxicity towards human and

environment (Paredes et al., 2011) similar to that of N_2H_4 as been discussed earlier. Therefore, the safer and more environmentally-friendly approaches toward the high volume production of graphene through GO reduction are very much desired. Significant works in this area have been made with the aims of the researches were directed to replace the hazardous chemical reducing agents with natural and more environmental-friendly reducing agents and to develop sustainable and environmental-friendly methods to reduce GO that circumvent the use of the reducing agent (Paredes et al., 2011). Among the natural reducing agents that have been reported to be used in GO reduction are vitamin C (Gao et al., 2010a), BSA (Liu et al., 2010a), reducing sugar (Zhu et al., 2010a), melatonin (Esfandiar et al., 2011) and green tea (Liao et al., 2011b; Wang et al., 2011c).

Gao et al. (2010a) have reported the employment of ascorbic acid (vitamin C) in the reduction of GO. Each molecule of ascorbic acid can release two protons to form dehydroascorbic acid (Gao et al., 2010a). These protons have a high binding affinity for oxygen functionalities such as epoxy and hydroxyl groups. During the GO reduction reaction with ascorbic acid, these protons were bound to the aforementioned oxygen functional groups to form RGO and water molecule. Although the reduction using ascorbic acid generally took long reaction time (from 8 to 48 hours), the effective removal of oxygen functionalities was achieved as evidenced from the elemental analyses (Gao et al., 2010a). However, the eradication of oxygen functionalities resulted in the instability of the RGO dispersion. Gao et al. (2010a) have reported that the stability of the RGO suspension could be increased by the addition of amino acid in the dispersion. Gao and his co-workers have suggested that the amino acid molecules were adsorbs on both sides of the RGO sheets through π-π stacking interactions which resulted in the improvement of the

electrostatic stabilization of the RGO dispersion (Gao et al., 2010a). On the other hand, Fernández-Merino et al. (2010) have also reported the successful reduction of GO by using vitamin C. In addition, Fernández-Merino and his coworkers have compared the reduction efficiency of vitamin C to the efficiency of other reducing agents including $NaBH_4$, pyrogallol and N_2H_4. The results from the ultraviolet-visible (UV-Vis) spectroscopy, TGA, Fourier transform infrared (FTIR) and X-ray photoelectron spectroscopy (XPS) analyses have revealed that the effective reduction of GO was achieved when the vitamin C was used as the reducing agent, in which its reduction property was almost comparable to that of N_2H_4 (Fernández-Merino et al., 2010). The employment of vitamin C in the GO reduction also resulted in the preparation of a stable RGO suspension in water and in common organic solvents such as DMF and NMP (Fernández-Merino et al., 2010) as depicted in Plate 2.3. These results have opened-up the perspective of replacing N_2H_4 with an innocuous reducing agent of similar reduction efficiency, thus, facilitating the employment of non-toxic graphene-based materials for wide range of applications.
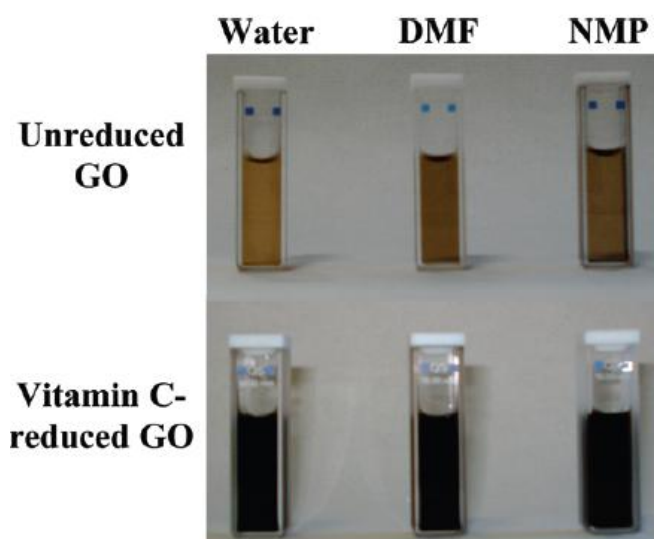
Plate 2.3: Optical images of GO (top row) and RGO after reduction with vitamin C (bottom row) in water, DMF and NMP (Fernández-Merino et al., 2010).

Meanwhile, it has been demonstrated that the effective reduction of GO in aqueous media was also achieved when the GO was reduced by BSA (Liu et al., 2010a) and reducing sugar such as glucose, fructose and sucrose (Zhu et al., 2010a). For the case of BSA, the successful reduction was attained under basic conditions. The BSA molecules were suggested to be adsorbed onto the RGO sheets, in which this resulted in the formation of stable RGO suspension (Liu et al., 2010a). On the other hand, the graphene nanosheets with improved conductivity were reported to be produced via the GO reduction reaction with glucose (Zhu et al., 2010a). Glassy carbon electrodes coated with the as-produced graphene nanosheets show greater electrochemical response towards dopamine as compared to that of bare electrode. This observation indicates that the graphene nanosheets obtained via GO reduction with glucose have huge potential to be used as the electrochemical sensing platform for the detection of biomolecules (Zhu et al., 2010a). In another work, Esfandiar et al. (2011) have reported the reduction of GO by using melatonin. In this work, the GO suspension was reduced by melatonin in an alkaline condition for 3 hours at temperature of 40 ℃-80 ℃. The results from the XPS analysis, current-voltage measurement and optical observation have revealed that the reduction efficiency of melatonin was comparable to that of N_2H_4 (Esfandiar et al., 2011). The XPS spectra have also revealed that the melatonin-RGO sheets possess higher amount of nitrogen than the N_2H_4-RGO sheets. Esfandiar et al. (2011) have suggested that the high amount of nitrogen in melatonin-RGO sheets was due to the π-π adsorption of the oxidized-melatonin on the RGO sheets, in which this resulted in the preparation of a stable melatonin-RGO dispersion.

A stable dispersion of RGO suspension also has been reported to be produced through GO reduction in tea solution (Liao et al., 2011b; Wang et al.,

2011c). Tea has been consumed for centuries and it is known to be the most widely consumed beverage in the world next to water (Chen et al., 2008a; Kanwar et al., 2012; Matthews, 2010). Tea particularly green tea possesses substantial health benefits including cancer and heart disease prevention, reduction of hypertension and insulin resistance as well as reducing the potential of plaque and gingivitis (Matthews, 2010; Mukhtar and Ahmad, 2000). Green tea contains significant amount of polyphenolic constituents which possess high anti-inflammatory, antioxidant and antimutagenic properties in various biological systems. Major class of polyphenolic compound is catechins. Four main types of catechins were occurred naturally in green tea extract including epicatechin (EC), epigallocatechin (EGC), epicatechin gallate (ECG) and EGCG (Babu and Liu, 2008; Chen et al., 2008a; Kanwar et al., 2012; Mukhtar and Ahmad, 2000). The structures of these catechins were shown in Figure 2.8 (Babu and Liu, 2008). EGCG is the most dominant and potent catechins in which it comprises approximately 50-75 % of the total catechins in green tea extracts (Babu and Liu, 2008; Chen et al., 2008a; Kanwar et al., 2012).
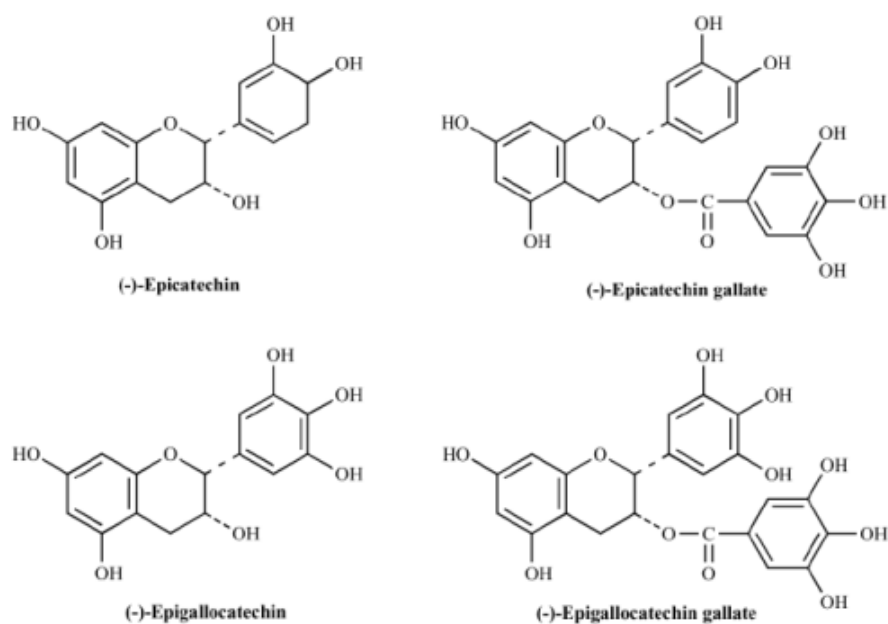
Figure 2.8: Structures of major catechins in green tea (Babu and Liu, 2008).

Although green tea has been consumed for many decades, only recently it attracts significant attention for its application in preparation of nanomaterials and nanocomposites. Green tea has been reported to be used for the synthesis of metal nanoparticles including palladium (Pd), silver (Ag), gold (Au) and iron (Fe) (Moulton et al., 2010; Nadagouda and Varma, 2008; Nune et al., 2009) and for the production of stable dispersion of SWCNTs in water (Chen et al., 2010b). Chen et al. (2010b) have suggested that the green tea possesses the ability to form π-π stacking interaction with the graphitic lattice of the SWCNTs. Chen et al. (2010b) also have further suggested that the non-covalent interaction between the green tea and SWCNTs leads to the disaggregation of SWCNTs particles and resulting in the preparation of a stable dispersion of SWCNTs in water. SWCNTs is the nearest analogue to graphene (Sanchez et al., 2012), hence, it is expected that the preparation of stable graphene dispersion also can be attained by using green tea.

Wang et al. (2011c) have demonstrated that soluble graphene could be synthesized through GO reduction in green tea solution. The results from the UV-Vis spectra, TGA, FTIR, XPS and XRD analyses have revealed that the oxygen functionalities in GO were eradicated effectively in the GO reduction reaction with green tea solution. Wang et al. (2011c) have suggested that the high stability of RGO dispersion in aqueous and organic solvents was due to the strong interactions between the aromatic GTP and the RGO sheets. Liao et al. (2011b) also have reported the preparation of stable dispersion of RGO in a wide range of solvents (e.g., butyl methacrylate, ethyl acetate, dichloromethane, acetone, DMF and NMP) through the reduction of GO with GTP. The high stability of the RGO dispersion was suggested to be due to the steric effects provided by the adsorption of oxidized GTP onto the RGO sheets, in addition to the strong π-π interactions between GTP

and RGO sheets. GTP possesses a myriad of hydroxyl groups in which these groups can form strong hydrogen bonding interactions (π-π interactions) with epoxy and hydroxyl groups in RGO (Yang et al., 2008). GTP is highly soluble and stable in water (Zhao et al., 2001), thus the strong π-π interactions between GTP and RGO will render the high stability of RGO suspension in aqueous media. The incorporation of GTP in the RGO suspension also provides the steric effect in which this effect prevents the agglomeration of the RGO sheets (Kajiya et al., 2001; Yu and Xie, 2012) and ensuring the high stability of the RGO dispersion in water. In their work, Liao et al. (2011b) have proposed the reduction mechanism of GO by GTP as illustrated in Figure 2.9. However, this mechanism requires further verification either through experimental work or computational study.

Figure 2.9: The proposed reduction mechanism of GO by GTP (Liao et al., 2011b).

Apart from using natural and more environmental-friendly reducing agents, the reduction of GO can also be achieved through sustainable and environmentally-friendly method that circumvent the use of the reducing agent. The first environmentally-friendly method to produce RGO is through the electrochemical

reduction (An et al., 2010; Ramesha and Sampath, 2009; Zhou et al., 2009a). The electrochemical reduction of GO could be carried out using a normal electrochemical cell in an aqueous electrolyte at room temperature. In addition, no chemical agent was used in the electrochemical reduction in which the reduction was occurred mainly due to the electron exchange between the GO and the electrodes (Pei and Cheng, 2012). Zhou et al. (2009a) have demonstrated that the efficient reduction of GO was achieved through the electrochemical reduction. The elemental analyses have revealed that the as-produced RGO films possess high C/O ratio of 23.9 and conductivity of 85 S/cm. In their work, Zhou et al. (2009a) have observed that the efficiency of the reduction was influenced by the pH value of the buffer solution in which the efficient reduction of GO was taken place at low pH value. Thus, due to this observation, Zhou et al. (2009a) have suggested that H^+ ions were participated in the reduction reaction. On the other hand, Ramesha and Sampath (2009) have deposited a thin film of GO on an ITO substrate. Then, an inert electrode is placed opposite to the thin film in an electrochemical cell using a 0.1 M potassium nitrate (KNO_3) solution as the electrolyte. Ramesha and Sampath (2009) have found that the successful reduction of GO was achieved when cyclic voltammetric scanning in the range of -0.60 V to -0.87 V was applied. In another work by An et al. (2010), the GO sheets were found to be successfully reduced during EPD process. An and his co-workers were intended to develop GO film using EPD process. However, they have observed that the as-deposited GO film has significantly lower oxygen content after the EPD process. Further analyses have revealed that the oxygen functional groups in GO were successfully eradicated by the EPD process and the as-deposited GO film shows improved electrical conductivity (An et al., 2010). Although the reduction mechanism is unclear, the

simultaneous film fabrication and reduction might be favorable for some electrochemical applications.

Another sustainable and environmental-friendly method for the reduction of GO is solvothermal reduction (Fan et al., 2008; Wang et al., 2009b; Zhou et al., 2009b). Usually, solvothermal process was carried out in a sealed container, hence, the temperature of the solvent could be elevated well above its boiling point by the increase of the pressure resulting from the heating process (Demazeau, 1999). In hydrothermal process, supercritical water behaves like a strong electrolyte with high dielectric constant and diffusion coefficient. Such properties will facilitate the removal of oxygen functionalities through dehydration reaction (Paredes et al., 2011; Zhou et al., 2009b). Zhou et al. (2009b) have reported the reduction of GO by hydrothermal treatment. The results have revealed that the supercritical water was not only able to eradicate the oxygen functionalities but also can recover the aromatic structures in the carbon lattice (Zhou et al., 2009b). In another work by Wang et al. (2009b), the reduction of GO has been achieved through solvothermal reduction in which DMF was used as the solvent. The solvothermal reduction was performed for 12 hours at temperature of 180 ºC. Post solvothermal reaction, the C/O ratio of the as-produced RGO was determined to be around 14.3, which is significantly higher than that of the RGO produced by N_2H_4 reduction at normal pressure (Wang et al., 2009b). Meanwhile, Fan et al. (2008) have demonstrated that the oxygen functionalities in strongly alkaline GO dispersion could be removed just through heating at temperature of 50 ºC-90 ºC. The results from ^{13}C NMR and XPS analyses have revealed that the amount of the oxygen functionalities was decreased after the treatment process (Fan et al., 2008). Although this simple method is very attractive, recent studies have shown that the strong alkaline condition leads to only

limited reduction in which the as-produced RGO sheets possess considerably low C/O ratio and conductivity as compared to the RGO produced through N_2H_4 reduction (Paredes et al., 2011).

2.1.4 (b)(ii) Thermal Reduction

Apart from chemical reduction, the oxygen functionalities in GO can also be removed through thermal reduction (Cote et al., 2009; McAllister et al., 2007; Schniepp et al., 2006; Zhang et al., 2010c; Zhu et al., 2010b). At the initial stage of the graphene research, the graphite oxide was reduced through thermal annealing in which the oxygen functional groups were eradicated by rapid heating (higher than 2000 °C/minute) (McAllister et al., 2007; Schniepp et al., 2006; Wu et al., 2009b). The oxygen functionalities that attached to the carbon plane were decomposed into carbon monoxide and carbon dioxide gases due to the rapid increase of the temperature. This resulted in the generation of huge pressure between the stacked layers (McAllister et al., 2007; Schniepp et al., 2006). From the evaluation of the Hamaker constants, it is predicted that two stacked graphite oxide layers could be separated by a pressure of only 2.5 MPa (McAllister et al., 2007). Based on the state equation, it is suggested that the temperature of 300 °C could generate pressure of 40 MPa whereas the pressure of 130 MPa could be generated at temperature of 1000 °C (McAllister et al., 2007).

Nevertheless, the thermal annealing process was found to produce only small size and wrinkled graphene sheets as depicted in Figure 2.10 (Schniepp et al., 2006). The carbon atoms were observed to be removed during the decomposition of oxygen functionalities in which this resulted in the separation of graphene sheets into smaller fraction and the distortion of the carbon plane. In addition, thermal

annealing process also resulted in the structural damage to the graphene sheets due to the release of carbon dioxide (Kudin et al., 2008). Alternatively, the exfoliation of graphite oxide was performed in liquid phase in order to produce large lateral size of graphene sheets (Zhao et al., 2010). The thermal annealing reduction was performed after the exfoliated graphite oxide was converted into films or powders. Wang et al. (2008b) have annealed the thin films of GO at different temperatures. The conductivity measurement have revealed that the electrical conductivity of the RGO films depends on the annealing temperature in which the film obtained at annealing temperature of 500 ºC possesses conductivity of 50 S/cm, while annealing at 700 ºC and 1100 ºC resulted in the formation of RGO films with conductivity of 100 S/cm and 550 S/cm, respectively (Wang et al., 2008b). Apart from the annealing temperature, annealing atmosphere also plays an important role in the thermal annealing reduction of GO. Oxygen gas should be excluded during the annealing process since the etching of oxygen will be significantly increased at high temperature. Hence, usually, the annealing process was carried out in vacuum or in an inert atmosphere (Becerril et al., 2008; Wang et al., 2008b).
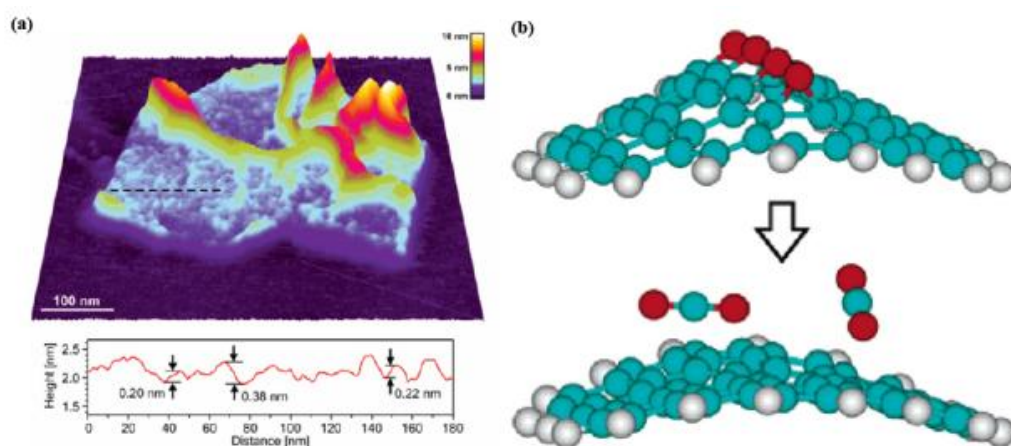
Figure 2.10: (a) AFM spectrum of an individual graphene sheet showing the rough and wrinkled surface structure. (b) Atomic model represents the transition of graphite oxide to graphene sheet (Schniepp et al., 2006).

Thermal reduction of GO can also be performed by using microwave (Zhu et al., 2010b), photo (Cote et al., 2009) and laser irradiation (Zhang et al., 2010c). Zhu et al. (2010b) have demonstrated that the RGO powder could be obtained simply by heating the graphite oxide powder in a microwave oven for 1 minute at ambient conditions. Elemental analyses have revealed that the as-prepared RGO powder consisted of crumpled, few-layers thick and conductive graphitic sheets (Zhu et al., 2010b). Meanwhile, Cote et al. (2009) have reported the reduction of GO film by using single flash from a xenon lamp. At a close distance (less than 1 mm), the photo energy released from the flash lamp is 9 times higher than the thermal energy needed for heating GO film (thickness ~1 μm) over 100 ºC. This suggests that there is more than enough energy to induce the deoxygenation reaction. The RGO films with conductivity of 10 S/cm were obtained after treatment with photo irradiation (Cote et al., 2009). On the other hand, Zhang et al. (2010c) have proposed the reduction of GO by using laser irradiation. The focused laser beam with laser pulse of 790 nm wavelength and 80 MHz repetition rate has higher energy density than a xenon lamp flash. The heated area in GO film is highly localized with the line width was ranged between 10^{-1}-10 μm (Zhang et al., 2010c). As a result, RGO film with much higher conductivity of 256 S/cm could be obtained from the GO reduction by laser irradiation.

2.1.4 (c) Reduction Mechanism

The reduction of GO has been demonstrated to be achieved through numerous strategies (An et al., 2010; McAllister et al., 2007; Schniepp et al., 2006; Wang et al., 2009b; Wang et al., 2011c). However, there are still a number of questions regarding the GO reduction that are yet to be answered. For example, are

the oxygen functionalities in GO could be fully eradicated? What is the dominant mechanism of the oxygen removal? How the reduction efficiency can be improved? The answers of these questions and further improvements in the GO reduction will depend on the improved understandings of the reduction mechanism. So far, very few works that have been carried out to investigate the reduction mechanism of GO possibly due to the amorphous nature of RGO, the lack of definite tools to directly monitor the reduction reaction and the complexity of the reduction reaction (Pei and Cheng, 2012). As a result, most of the works on the reduction mechanism were carried out using computational study (Pei and Cheng, 2012).

A computational chemistry can simulate the chemical structures and their reactions numerically based on the fundamental laws of physics. In other word, a chemical reaction can be investigated by executing calculations on computers instead of examining it experimentally (Foresman and Frisch, 1996). In addition, computational simulation can also be used to model not only stable molecules, but also the unstable intermediates and even the transition state (TS) (Foresman and Frisch, 1996). The computational calculation can be performed using three methods namely molecular mechanics, electronic structure method and DFT method (Foresman and Frisch, 1996). Molecular mechanics method uses the laws of classical physics to predict the structures and properties of the molecules while the electronic structure method employs the laws of quantum mechanics as the basis for its computations. On the other hand, the DFT method is similar to the electronic structure method in many ways. However, the DFT method is significantly attractive because it includes the effects of electron correlation in its model (Becke, 1993; Foresman and Frisch, 1996; Lee et al., 1988). There are numerous computational programs available commercially such as Gaussian 09, Spartan, CASTEP, DMol3,

Siesta, and GAMESS, to name a few (Foresman and Frisch, 1996). Most of the programs contain a hierarchy of procedures corresponding to different approximation methods which were commonly referred to as the different level of theory. Among the common level of theories are Hartree-Fock (HF), Becke-3-Parameter-Lee-Yang-Parr (B3LYP), Moller-Plesset 2nd Order (MP2) and Moller-Plesset 4th Order (MP4) (Becke, 1993; Frisch et al., 1990; Lee et al., 1988; McWeeny and Dierksen, 1968; Raghavachari and Pople, 1978). In every computation, the level of theory must be applied with a basis set. Basis set is the mathematical representation of the molecular orbitals within a molecule. The basis set can be interpreted as restricting each electron to a particular region of space. Larger basis set will impose fewer restrictions on the electron and hence, increases the accuracy of the approximation of the molecular orbitals (Foresman and Frisch, 1996).

The main aim of the GO reduction reaction is to eradicate the oxygen functionalities from the GO in order to reestablish the sp^2 bonding network of GO and to restore the electrical conjugation of GO. However, the mechanisms of the GO reduction reaction are still unclear and are mostly proposed, with only a few works have reported the mechanism of the reduction using computational simulation. The first mechanism of the GO reduction using N_2H_4 has been proposed by Stankovich et al. (2007). The proposed reduction pathway was shown in Figure 2.11. Stankovich et al. (2007) have proposed that during the GO reduction reaction with N_2H_4, the hydrazino alcohols were formed due to the ring opening of the epoxy groups. The hydrazino alcohols then react with aminoaziridine moiety to eliminate diimide and form a double bond, which resulted in the restoration of the conjugated graphene network (Stankovich et al., 2007). Meanwhile, Kim et al. (2009b) have

reported the mechanism of epoxide reduction by N_2H_4 using DFT method. The results from the computational study have revealed that the epoxide reduction was governed by ring opening of epoxide which was initiated through hydrogen transfer from the N_2H_4. Kim et al. (2009b) also have reported that the formation of derivatives such as aminoaziridine during the reaction can facilitate the removal of epoxide by reducing the energy barrier of the ring opening reaction. In another work by Gao et al. (2010b), the effect of N_2H_4 on the removal of epoxy, hydroxyl, carbonyl and carboxyl groups from GO was further investigated through DFT simulation. Gao et al. (2010b) have revealed that the GO reduction by N_2H_4 resulted only in the removal of epoxy groups while no reduction path was found for the removal of hydroxyl, carbonyl and carboxyl groups. Computational simulation offers huge opportunity for the researchers to further understand the mechanism of the GO reduction. However, extensive works on the computational simulation are needed to be performed before the reduction mechanism of GO could be fully understood.
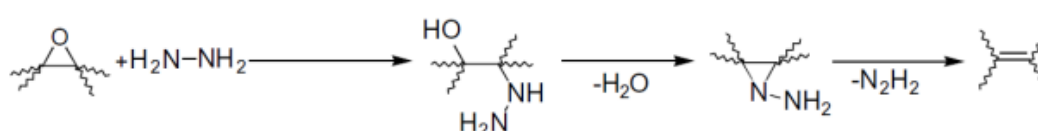
Figure 2.11: Suggested reaction pathway of epoxide reduction by N_2H_4 (Stankovich et al., 2007).

2.2 Graphene Films (GFs)

Graphene nanostructures especially GFs have gained substantial attention owing to their promising potential to be used in wide range of applications particularly in nanoelectronics and biomedical applications. In the initial stage of the

graphene research, GFs were reported to be developed through filtration, spin coating and micro-tip spreading techniques. Xu et al. (2008) have reported the preparation of GFs via GO reduction with N_2H_4 monohydrate, followed by subsequent filtration through a cellulose acetate membrane. They have demonstrated that free-standing and flexible GFs could be obtained by the filtration of the RGO dispersion through a membrane filter (Xu et al., 2008). In addition, Xu et al. (2008) also have suggested that the GFs with varying thickness could be obtained by simply adjusting the volume and the concentration of the dispersion. In another work by Wang et al. (2010), the GFs were produced on a cellulous ester filter membrane through vacuum filtration. Similarly, the thickness of the GFs was suggested to be controlled by adjusting the concentration and volume of the suspension (Wang et al., 2010). Meanwhile, Zhang et al. (2013) have reported the preparation of GFs on quartz slides using spin coating. The substrate was completely covered with the graphene particles after performing spin coating for 10 s at 600 rpm. In their work, Zhang et al. (2013) have proposed that the thicker GFs could be fabricated through repeated spin coating using suspension with higher concentration.

On the other hand, Guo et al. (2009) have prepared GFs through micro-tip spreading of RGO suspension on a glassy carbon electrode, followed by drying process in a vacuum desiccator. They have suggested that the GFs-coated glassy carbon electrodes could be used for further applications in electrocatalysis and biosensors (Guo et al., 2009). In the aforementioned techniques for the fabrication of GFs, the thickness of the GFs was suggested to be controlled by adjusting the volume and the concentration of the suspension (Guo et al., 2009; Wang et al., 2010; Xu et al., 2008; Zhang et al., 2013). However, it remains challenging and difficult to control the thickness of GFs for specific applications that require the thickness of the

films in micrometer or in nanometer sizes. Hence, the EPD was proposed as the promising technique to fabricate GFs with controlled-thickness on a wide range of shapes, 3D complex and porous structures. The EPD technique will be further discussed in the next section (section 2.2.1).

2.2.1 Electrophoretic Deposition (EPD)

EPD is a unique particulate forming technique that uses an electric field to move the charged particles in suspension into desired arrangement on a conductive electrode surface (Van Tassel and Randall, 2006). EPD is a two-steps process. In the first step, the particles acquired the electric charge in the liquid in which they are suspended. These charged particles were forced to move towards one of the electrodes after the electric field was applied. This step was known as electrophoresis. In the second step, the charged particles precipitated and formed coherent deposit on one of the electrodes (deposition) (Fukada et al., 2004; Van der Biest and Vandeperre, 1999; Zhitomirsky, 2002). The EPD can be applied to any solid that is available as a fine powder (particle size ~30 μm) or as a colloidal suspension including metals, polymers, ceramics and glasses (Corni et al., 2008; Van der Biest and Vandeperre, 1999).

In order to achieve the successful deposition of the particles using EPD, a stable suspension with high zeta potential and low ionic conductivity must be prepared (Fukada et al., 2004; Van der Biest and Vandeperre, 1999). In previous EPD studies, the suspensions that been used are water-based (Van der Biest and Vandeperre, 1999; Zhitomirsky, 2000; Zhitomirsky, 2002) and organic-based suspensions (Yamashita et al., 1997; Zhao et al., 2005). Water has been widely used for the preparation of the suspension mainly due to its cost effective and non-

detrimental properties to the environment (Van der Biest and Vandeperre, 1999). However, the used of water-based suspensions may lead to the generation of gas bubbles due to the electrolysis of water (Ammam, 2012; Neirinck et al., 2009; Van der Biest and Vandeperre, 1999). The electrolysis of water can occur at voltage as low as 5 V (Van der Biest and Vandeperre, 1999). The formation of gas bubbles at the electrodes will prevent the deposition of a uniform adherent layer and resulted in the production of pinholes, voids and pores (Zhitomirsky, 2002). Nevertheless, the reports describing the success of EPD using aqueous suspension were continued to be published (Neirinck et al., 2009; Zhitomirsky, 2002). The organic solvents are less preferred to be used for the preparation of the suspension due to their lower dielectric constant in which this will limits the charge on the particles (Van der Biest and Vandeperre, 1999).

In 20th century, only limited works on the applications of EPD were reported in which most of the works were focused on the applications of the ceramic processing (e.g., EPD was used to produce traditional ceramics such as porcelain) (Gani, 1994). However, since the last 2 decades, EPD has gained increasing attention as an attractive technique for the fabrication of thin film (Besra and Liu, 2007; Boccaccini et al., 2010). The main driving forces that lead EPD to be one of the preferred techniques for the fabrication of thin film are its cost effectiveness, simplicity and ability to produce uniform deposits with high microstructural homogeneity as well as providing the adequate control of the thickness of the thin films (Boccaccini et al., 2010; Corni et al., 2008; Sarkar and Nicholson, 1996; Van der Biest and Vandeperre, 1999). Due to these reasons, numerous works on the applications of EPD in the processing of composite, ceramics, thin films and nanomaterials have been reported (Besra and Liu, 2007; Boccaccini et al., 2010;

Boccaccini and Zhitomirsky, 2002; Gani, 1994; Sarkar and Nicholson, 1996; Van der Biest and Vandeperre, 1999). Recently, the enormous works on EPD of graphene and graphene-based materials have been reported in which this indicates the increasing interest to find the processing routes that might help to exploit the unique properties of graphene (Chavez-Valdez et al., 2013). In general, the GFs could be developed by EPD process using two methods. In the first method, the GO films were produced using EPD and they were subsequently transform into GFs through reduction process. While in the second method, the GO was first reduced and then followed by the EPD of the RGO suspension to produce GFs. The overview of the EPD parameters used to fabricate GFs and its respective application was shown in Table 2.1.

Table 2.1: Overview of the EPD parameters used to fabricate GFs and its respective application.

Materials		Suspension medium	EPD parameters		Application	Reference
Coating	Substrate		Applied voltage	Deposition time		
GO	ITO	Water	150 V	45 s	Supercapacitor electrodes	(Liu et al., 2011)
PPD-modified graphene	Ni foam	Ethanol	50 V	-	Electrochemical electrode	(Chen et al., 2010c)
GO	SS	Water	3-15 V	3-10 minutes	Electrodes	(Hasan et al., 2010)
GO-NiO	Ni foam	Isopropyl alcohol	100 V	20 s	Supercapacitor electrodes	(Xia et al., 2011)
Graphene-Pt	Carbon paper	Tetrahydrofuran	75 V/cm	-	Electro catalyst support for fuel cells	(Seger and Kamat, 2009)
Graphene-Pt	ITO	DMF	4-5 V	30-600 s	Solar cells/hydrogen generation device	(Chartarrayawadee et al., 2012)

Table 2.1: Continued.

Materials		Suspension medium	EPD parameters		Application	Reference
Coating	Substrate		Applied voltage	Deposition time		
Graphene -Pt	ITO	Water	150 V	45 s	Support structure in fuel cell	(Liu et al., 2010b)
Graphene	ITO	Isopropyl alcohol	160 V	1 minute	Field emitter	(Wu et al., 2009a)
Graphene	SS, Ni, Al and Si	Water	10 V	1-10 minutes	Conductive material	(An et al., 2010)
GO	SiO$_2$- coated Si	Water	1-30 V	1-30 minutes	Transparent conductive material	(Ishikawa et al., 2012)
Graphene -Ti	Si	Isopropyl alcohol	300 V	5 minutes	Field emitter	(Jun et al., 2012)
Graphene -CNTs	Graphite paper	Ethanol- acetone	30 V	30 minutes	Solar cells	(Zhu et al., 2011)
Graphene -CNTS	Ni foils	Isopropyl alcohol	100 V	10 minutes	Lithium-ion battery	(Seo et al., 2012)
Graphene -TiO2	ITO	Ethanol	30 V	3 minutes	Photovoltaic device	(Tang et al., 2010b)
Graphene	Glassy carbon	DMF	120 V	3 minutes	Sensors	(Tang et al., 2010a)
Graphene	SS	Isopropyl alcohol	150 V	2 minutes	Biocompatible material	(Akhavan and Ghaderi, 2010)

2.2.2 Applications of Graphene Films (GFs)

2.2.2 (a) Nanoelectronics

The EPD process has been demonstrated to be a useful technique to develop GFs on conductive substrates for nanoelectronics applications particularly as electrochemical electrodes, conductors and field emission devices. In most of the electronic devices such as batteries, supercapacitors and fuel cells, the

electrochemical electrodes were fabricated using conventional carbonaceous materials (e.g., SWCNTs and graphite). Graphene possesses large surface area and high conductivity which makes graphene as an attractive potential substitute or addition to the conventional systems. Liu et al. (2011) have reported the preparation of GFs through EPD of GO, followed by in situ electrochemical reduction. Initially, the GO films were developed on ITO electrodes by using applied voltage of 150 V and deposition time of 45 s. Then, the prepared films were electrochemically reduced by a constant potential reduction step to yield the GFs. Further analyses have revealed that the as-produced GFs possess low contact resistance and high capacitance, making GFs as the suitable candidate for supercapacitor electrodes (Liu et al., 2011).

Meanwhile, Chen et al. (2010c) have reported the fabrication of GFs on Ni foams. The graphene suspension was first prepared using p-phenylene diamine (PPD) in ethanol. The EPD process was subsequently performed using applied voltage of 50 V to deposit the graphene particles on the 3D Ni foam. This was followed by the annealing process at 400 ºC for 3 hours. The SEM images of the bare Ni foam and the as-produced GFs were shown in Figure 2.12. The GFs were revealed to possess high capacitance indicating their ability to store energy with potential application as electrochemical electrodes for capacitors (Chen et al., 2010c). On the other hand, An et al. (2010) have developed the GFs for the application as transparent conductor. In their work, the GFs were obtained without the addition of any chemical agent or high temperature treatment. The GO were deposited on the SS meshes and other substrates such as Cu and Ni. The conductivity value of the as-deposited films ($1.43x10^4$ S/m) was higher than the value for GO paper produced using filtration method ($0.53x10^{-3}$ S/m) (An et al.,

2010). The oxygen functionalities of the GO films were suggested to be removed during the EPD process. An et al. (2010) have also reported the formation of films with wide range of thickness ranging from hundreds nanometers to tens of micrometer by varying the deposition time.
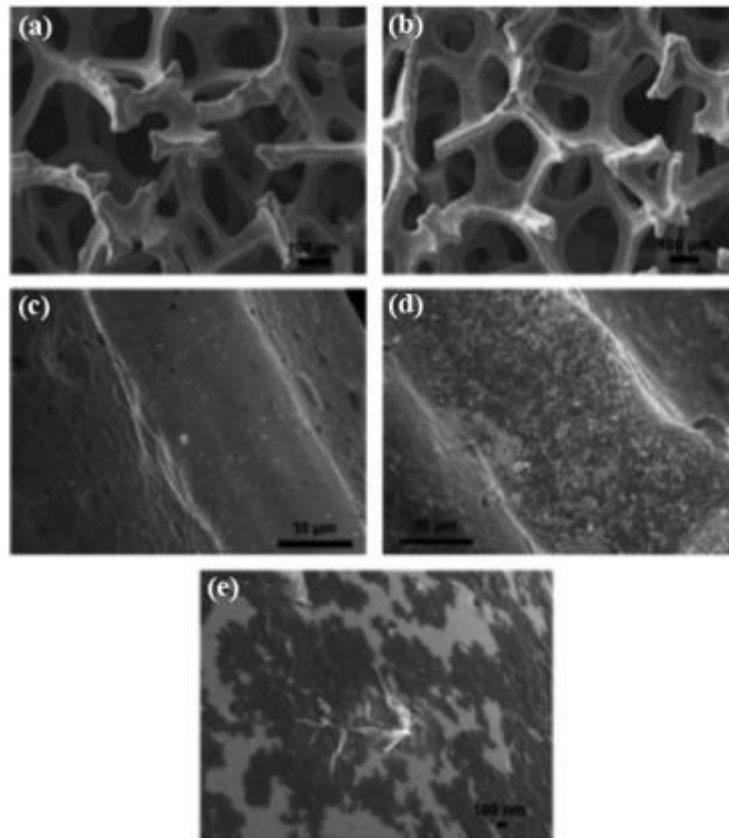
Figure 2.12: SEM images of (a, c) bare Ni foam and (b, d, e) GFs fabricated on Ni foam by EPD (Chen et al., 2010c).

The GFs also have been proposed to be used in field emission devices. Wu et al. (2009a) have prepared GFs through EPD for application in field emission devices. In their investigation, Wu et al. (2009a) have added magnesium nitrate to increase the stability of the graphene suspension. The EPD process was carried out for 1 minute using voltage ranging from 100-160 V. GFs with homogeneous planar structure were obtained post EPD process. Further analysis has revealed that the GFs

possess high electric conductivity of ~1000 S/cm which indicates the potential of the GFs to be used in field emission devices (Wu et al., 2009a). In another work by Maiti et al. (2011), GFs were fabricated on 3D carbon fabric substrates with view for potential application as flexible field emitter. The EPD process was performed for 5-600 s using constant current of 2.4 mA/cm. It can be observed that the graphene was distributed uniformly on single carbon fibers within the woven geometry of the carbon fabric. Maiti et al. (2011) have revealed that flat GFs were obtained at short deposition time while thicker films with wrinkles were obtained at higher deposition time. After the EPD process, the GFs were plasma-etched to generate a structure of isolated graphene nanocones. This structure minimized the threshold field and increases the apparent field enhancement, in which these properties are very much desired in a field emission device (Maiti et al., 2011). On the other hand, Li et al. (2012b) have reported that the addition of Ti layer at the interface between the GFs and the Si substrate could improve the field emission properties of the GFs. Hundred nm of Ti layer was deposited on the substrate using ion-beam sputtering before the EPD of GO was performed. The as-produced GFs were annealed at different temperatures between 600 ℃-900 ℃ for 1 hour in argon atmosphere (Li et al., 2012b). The GFs prepared by EPD may have practical relevance to the development of large area and low cost field emitters in the future.

2.2.2 (b) Biomedical Applications

Apart from the application in nanoelectronics, graphene also attracts enormous attention from researchers to investigate its potential in biomedical applications. Biomedical applications of graphene is relatively still at the nascent stage. The first report of the biomedical application of graphene was emerged in

2008 (Liu et al., 2008), in which the GO was investigated to be used as a nanocarrier for drug delivery. Since then, extensive works have been carried out to explore the potential of graphene for wide range of biomedical applications particularly as biosensors and scaffolds for tissue engineering.

Biosensors were developed in order to detect any biological responses of chemical biomatrix such as antibodies, enzymes or nucleic acid and then convert those responses into electric signal (Fisher et al., 2012; Wu et al., 2010). Biosensors consist of two parts namely transducer and receptor. The receptor interacts with the analyte while the transducer processes the response and translates it into a useable signal (Fisher et al., 2012; Wu et al., 2010). Graphene has attracted enormous attention for biosensing application due to its remarkable electrochemical properties and large surface area (Fisher et al., 2012). In addition, the versatility of graphene enables it to be used either as receptor or transducer. Srivastava et al. (2013) have reported the formation of GFs on ITO-coated glass substrate by EPD process. The as-produced GFs were utilized for covalent attachment of aflatoxin antibodies for the detection of food toxin. The electrochemical sensing analyses reveal that the GFs/ITO-based electrode exhibits high sensitivity (68 uAng^{-1}mLcm^{-2}) and improved detection limit (0.12 ng/mL) (Srivastava et al., 2013). In another work, Akhavan and Ghaderi (2010) have reported the preparation of GFs on SS substrate using EPD process. They have investigated the toxicity of the GFs in order to determine whether the electrode has resistance to fouling. The GFs were produced through deposition of GO on SS substrate using EPD, followed by subsequent reduction by N$_2$H$_4$ vapor for 1 hour. The EPD was performed for 5 minutes using applied voltage of 150 V. The toxicity of the as-produced GFs was tested against Escherichia coli and Staphylococcus aureus bacteria. High antibacterial activity was observed for the

57

GFs due to the high charge transfer between the sharp edges of the GFs and the bacteria (Akhavan and Ghaderi, 2010). Meanwhile, Chang et al. (2010) have developed highly sensitive aptasensor for thrombin detection by combining GFs with SDBS. The addition of SDBS was suggested to be able to increase the biocompatibility of the GFs. Further analysis has revealed that the GFs/SDBS aptasensor was highly sensitive to the thrombin detection with high specificity in buffer and blood serum (Chang et al., 2010). In addition to its remarkable electrochemical properties, graphene also possesses unique ability to interact with biological entities including enzyme and antibodies. These attractive properties of graphene make it as the most promising nanomaterial to be applied in biosensors (Fisher et al., 2012).

Apart from the biosensors, GFs have also been investigated to be used as scaffolds for tissue engineering. Fan et al. (2010) have developed graphene/chitosan film with view to use it as the scaffolds for tissue engineering. The cell adhesion results have revealed that the human mesenchymal stem cells can adhere on the surface of the film suggesting good biocompatibility of the graphene/chitosan film. In fact, the film has been revealed to accelerate the interaction between the stem cells and the bone cells indicating the potential of the film to be used for proliferation and transplantation of stem cells into muscles and bones (Fan et al., 2010). In another work by Kalbacova et al. (2010), the GFs were shown to be biocompatible toward human osteoblasts and human mesenchymal stem cells and the films were revealed to stimulate the growth and the proliferation of the cells. Motivated by the work of Kalbacova et al. (2010), Li et al. (2011) have investigated the potential of GFs to be used as the substrate for neurites. Neurites are the key structures for neural functions during the development in mouse hippocampal

culture model (Li et al., 2011). Li et al. (2011) have observed that the neurites average length on GFs was significantly increased after 7 days of cell seeding. This observation indicates that the GFs possess huge potential to be used as scaffold for cell culture and as a novel material for neural interfacing.

2.3   Attractive Features of Graphene

Graphene is known to be the basic building block for other graphitic materials including fullerenes, carbon nanotubes and graphite (Geim and Novoselov, 2007). However, graphene possesses unique structural characteristics and exceptional physicochemical properties that are relevant to biological effects which make graphene a special nanomaterial compared to other forms of carbon-based materials (Sreeprasad and Pradeep, 2012). Intriguing properties of graphene such as large planar surface area (Sanchez et al., 2012; Singh et al., 2011; Sreeprasad and Pradeep, 2012), versatility for chemical modification (Georgakilas et al., 2012; Sanchez et al., 2012) and low toxicity (Fisher et al., 2012; Sanchez et al., 2012; Wang et al., 2011a) are very attractive for wide range of applications especially for biomedical applications. Although the biomedical applications of graphene are still at nascent stage, the remarkable properties of graphene have drawn tremendous attention from researchers to investigate its interactions with microorganisms and biological cells (Hu et al., 2010). In order to fulfill the exciting potential of graphene in biomedical applications, it is vital to fully understand the association of these physicochemical properties to biological interactions of graphene (Albanese et al., 2012).

2.3.1 Large Planar Surface Area

The interactions of nanomaterial with biological cells were known to be greatly influenced by the surface properties of nanomaterial such as the porosity, shape, surface crystallinity and functionalization, roughness and most notably, the surface area of the nanomaterial (Albanese et al., 2012; Nel et al., 2009). For the case of single layer graphene, every carbon atom on two surface sides is exposed to the surrounding which resulted in large theoretical surface area (~2600 m^2/g) of the monolayer graphene sheet (Sanchez et al., 2012; Singh et al., 2011; Sreeprasad and Pradeep, 2012). The large surface area and flexible surface chemistry of monolayer graphene are essential to provide continuous and stable platform for the interactions between graphene and biological cells (Nguyen and Berry, 2012; Sanchez et al., 2012). In addition, it is anticipated that the biological response of graphene will be highly dictated by its surface phenomena including physical adsorption and chemical surface modification due to large surface area of single layer graphene (Sanchez et al., 2012). Although there is very limited studies that have been conducted to investigate surface phenomena of graphene, its adsorptive interferences could be foreseen by drawing comparison to SWCNTs, the nearest analogue of graphene. SWCNTs is highly hydrophobic and has large theoretical surface area of ~1300 m^2/g. Worle-Knirsch et al. (2006) and Casey et al. (2007) have reported the adsorption of probe dyes and human lung epithelial-like cells onto large surface area of SWCNTs. In another work by Guo et al. (2008), it is reported that the micronutrients from cell culture medium could be modified through the adsorption of micromolecules onto surface area of SWCNTs, which could potentially inhibit the cell growth. In short, the similar adsorption behavior is predicted for other materials which have large surface area including graphene.

60

2.3.2 Versatility for Biological and Chemical Modification

Graphene and its derivatives possess varying surface chemistry mainly due to the different processing routes during the synthesis process (Sanchez et al., 2012). GO is hydrophilic due to the presence of oxygen functionalities including hydroxyl and carboxyl decorated at its basal plane (Stankovich et al., 2006a). In contrast, pristine graphene is hydrophobic and the biochemical reactions occurred primarily at the edge or defect sites. On the other hand, RGO is intermediate in hydrophilicity and basal reactivity due to the presence of basal defects produced during the oxygen removal process (Bagri et al., 2010). Sanchez et al. (2012) have reported that most of the biomedical works have been carried out for GO due to its higher dispersibility in aqueous media. Pristine graphene is poorly dispersible in water and it requires the addition of stabilizer or surfactant for any application requiring dispersion in biological solution (Sanchez et al., 2012). The stability of the graphene suspension can also be improved through functionalization step (Georgakilas et al., 2012). The main purpose of the functionalization is to enhance the dispersibility of graphene in organic solvents in which this will result in the easiness of further processing for the applications process.

Liao et al. (2011b) have reported the functionalization of RGO with dodecyl mercaptan in order to improve the solubility of RGO in organic solvents. Post functionalization step, the RGO was observed to be stably dispersed in various organic solvents including DMF, NMP, acetone, dichloromethane and all of the esters. The high stability of the functionalized graphene was confirmed as no precipitation occurs even after 1 month (Liao et al., 2011b). In another work, Georgakilas et al. (2010) have reported the decoration of graphene with dihydroxyl phenyl groups through the addition of azomethine ylide precursor. The azomethine

ylide precursor is formed through condensation of 3,4-dihydroxybenzaldeyde and sarcosin. It has been observed that the dispersibility of the functionalized graphene was increased in polar solvents such as ethanol and DMF (Georgakilas et al., 2010). Meanwhile, Sinitskii et al. (2010) have reported the functionalization of graphene with nitrophenyls upon reaction with diazonium salt. When the diazonium salt was heated, highly reactive free radical is produced. The free radical attacks the sp^2 carbon atoms of graphene to form a covalent bond. The conductivity measurement has revealed that the conductivity of the functionalized graphene was significantly reduced due to the disruption of the aromatic system by the transformation of sp^2 carbon atom to sp^3 hybridization (Sinitskii et al., 2010).

Apart from chemical functionalization, extensive works have also been carried out on the biological functionalization of graphene (Park et al., 2010; Wang et al., 2011b). The biological functionalization improves the biocompatibility, selectivity and solubility of graphene (Wang et al., 2011b). Most of the biological functionalization of graphene has been focused on the functionalization with deoxyribonucleic acid (DNA) and protein. Mohanty and Berry (2008) have demonstrated that the hole-density in the graphene layer was increased upon functionalization with DNA. The resultant DNA/graphene biointerface was used in a field-effect transistor (FET) for the detection of the complementary DNA (Mohanty and Berry, 2008). In another work, horseradish peroxidase (HRP) has been immobilized on DNA/graphene sheets to form HRP/DNA/graphene-coated electrode (Zhang et al., 2010a). This electrode was used as a biosensor for the detection of hydrogen peroxide. Further measurements have revealed that the biosensor possesses high sensitivity and wide linear relationship of hydrogen peroxide sensing (Zhang et al., 2010a). Apart from its remarkable properties,

graphene also possesses another significant advantage in term of its versatility for surface modification. The intriguing properties of graphene will be beneficial for biotechnological applications particularly in areas of biosensors, medicine and bioelectronics (Wang et al., 2011b).

2.3.3 Toxicity and Biocompatibility

The increasing number of potential applications of graphene in biomedical field has raised concern over its toxicity behavior when exposed to the biological system, especially for in vivo applications (Fisher et al., 2012; Singh et al., 2011). In contrast to well characterized-toxicity behavior of CNTs, the potential toxicity (Sanchez et al., 2012), biocompatibility (Wojtoniszak et al., 2012) and interactions of graphene with living cells (Chen et al., 2008b; Sun et al., 2008) in biological system are yet to be fully understood. It has been suggested that a number of parameters including concentration (Wang et al., 2011a; Wojtoniszak et al., 2012; Yan et al., 2011), composition (Zhang et al., 2010b), shape (Zhang et al., 2010b), size (Liao et al., 2011a) and type of dispersant (Wojtoniszak et al., 2012) could greatly affect the toxicity behavior of GO and graphene toward bacteria, mammalian cells and other living cells in biological system (Zhang et al., 2010b; Zhang et al., 2012b). Ang et al. (2008) and Park et al. (2010) have reported that reduced-GO paper was non-toxic towards mouse fibroblast cells (L929), Vero cells, embryonic bovine cells and Crandell-Rees feline kidney (CRFK) cells. From live-dead test, those cells have been observed to proliferate and grow consistently on RGO paper, which indicates the non-toxicity of the paper. In addition, a number of research studies also have demonstrated the non-toxicity of GO and graphene toward human living cells including human fibroblasts (Liao et al., 2011a; Wang et al., 2011a), human hepatoma cells (Yuan et al., 2012), human lung cancer cells (A549) (Chang

et al., 2011) and HeLa cells (Lu et al., 2010). However, in contrast to these reports, Akhavan and Ghaderi (2010) have demonstrated that GO and reduced-GO nanowalls are toxic toward Escherichia coli and Staphylococcus aureus bacteria. The damage of the cell membrane of the bacteria could be observed, which attributed by strong interaction of the bacterial cell to sharp edges of GO and reduced-GO nanowalls (Akhavan and Ghaderi, 2010). Meanwhile, Hu et al. (2010) have reported the mild toxicity of GO and reduced-GO nanosheets toward Escherichia coli bacteria. The metabolic activity of Escherichia coli was dropped to 13 % and 24 % within 2 hours post-interaction with GO and reduced-GO nanosheets of 85 μg/mL at 37 ℃, respectively (Hu et al., 2010).

In the meantime, Zhang et al. (2010b) have reported the comparison of cytotoxicity level of graphene and CNTs toward neuronal cells (PC12). It has been concluded that in general, graphene possesses lower cytotoxicity as compared to CNTs. In addition, they also reported that the cytotoxicity behavior of graphene was significantly dependent on the composition and shape of graphene (Zhang et al., 2010b). However, astonishingly, the toxicity of graphene was found to be inversely proportional to the concentration, where graphene exhibits higher toxicity as compared to CNTs at low concentration and vice versa (Yan et al., 2011). Apart from composition, shape and concentration, the effect of size of GO nanosheets toward cytotoxicity behavior also have been demonstrated. Chang et al. (2011) have reported that smaller size of GO (s-GO) (160 ± 90 nm) possesses higher cytotoxicity than the medium (m-GO) (430 ± 300 nm) and large size of GO (l-GO) nanosheets (780 ± 410 nm). The cytotoxicity behavior of GO nanosheets was estimated quantitatively by measuring the viability of A549 cells on GO surface. Post 24 hours exposure, higher loss of cell viability was observed for s-GO as compared to m-GO

and l-GO nanosheets. It has been reported that the generation of oxidative stress and reactive oxygen species (ROS) by GO nanosheets have induced the decrease in cells viability (Chang et al., 2011). However, further investigation has revealed that the oxidative stress which induced the reduction in cell viability is most probably originated from external ROS (Chang et al., 2011). This conclusion has been made when the proliferation of A549 cells on GO surface was discovered to be similar as control cells and there is no cellular internalization of GO nanosheets that has been observed (Chang et al., 2011). The effects of size and concentration of GO nanosheets for their in vitro cytotoxicity evaluation were summarized as in Table 2.2.

Table 2.2: Effects of size and concentration to the cytotoxicity level of GO nanosheets.

Size range	Concentration (µg/mL)	Intra-cellular localization	Cell	Cytotoxicity concentration (µg/mL)	Reference
1-2 µm	5-100	Lysosomes, mitochondrion, endoplasm and nucleus	Human fibroblast cell, MGC803, MCF-7, MDA-MB-435 and HepG2 cell lines	50	(Wang et al., 2011a)
3-5 nm	0.1-100	-	PC12 cells	100	(Zhang et al., 2010b)
70-250 nm	10-200	Hardly localized inside the cell	A549	50	(Chang et al., 2011)
130-730 nm	10-200	Hardly localized inside the cell	A549	200	(Chang et al., 2011)
370-1190 nm	10-200	Hardly localized inside the cell	A549	50	(Chang et al., 2011)
100-700 nm	20-85	Endosome	A549	85	(Hu et al., 2010)
100-700 nm	20-85	-	Escherichia coli	85	(Hu et al., 2010)

Apart from its cytotoxicity behavior, the biocompatibility of graphene also plays a critical role in determining the acceptance of graphene to be used in biomedical applications. Wang et al. (2011a) have revealed that the cytotoxicity of GO was dose-dependent where there is no toxicological effect that has been observed in mice for low dose of GO ($\leq$0.25 mg per mouse). However, 4 mice were found to be dead within 1-7 days after been injected with 0.4 mg GO per mouse. Further histopathological analysis has shown that the dose-dependent lung inflammatory response has been induced by the pulmonary exposures to GO. The severity of inflammation cells in mice's lungs has been observed to increase when higher dose of GO have been used as illustrated in Figure 2.13 (Wang et al., 2011a). In addition, they also have reported that higher dose of GO ($>$50 µg/mL) could induce severe toxicological effects (i.e. reduction in cell adhesion, cell apoptosis and the entrance of GO into mitochondrion, lysosomes, endoplasm and cell nucleus) to human fibroblast cells and other cell lines such as human breast cancer (MCF-7), liver cancer (HepG2) and human gastric cancer (MGC803) cell lines. Although extensive studies have been carried out to investigate the potential of GO as gene/drug delivery and in cellular imaging, its long term stay in kidney may provide huge obstacles for GO to be used for in vivo applications (Sanchez et al., 2012). In order to reduce the toxicological effects of GO and RGO as well as to enhance their biocompatibility behavior, GO and RGO have been conjugated with biocompatible materials including polyethylene glycol (PEG) (Liu et al., 2008; Yang et al., 2011; Yang et al., 2010a), perylene tetracarboxylic acid (PTCA) (Feng et al., 2011a), chitosan (Yang et al., 2010b) and polyethylenimine (PEI) (Feng et al., 2011b).

For in vitro application of drug delivery, it has been reported that the PEG-functionalized GO (PEG-fGO) was non-toxic towards human colon carcinoma (HCT-116) cells (Liu et al., 2008). In addition, there is no toxicological effect that has been observed in injected mice when PEG-fGO was used for in vivo application of photothermal therapy for tumor uptake (Yang et al., 2010a). Meanwhile, Yang et al. (2011) have investigated the bio-distribution and the potential of long term toxicity of PEG-fGO in female Balb/c mice. It has been revealed that the PEG-fGO was accumulated primarily in the liver, kidneys and spleen. However, the accumulated PEG-fGO has been cleared-out gradually from the organs through renal and fecal excretion. Additionally, any potential toxic effects were not observed within 3 months after the introduction of PEG-fGO in female mice, as been confirmed by blood biochemistry, hematological and histological analysis (Yang et al., 2011). Apart from PEG-fGO studies, PTCA-functionalized graphene (PTCA-fG) also have been studied for cancer cell detection application. It has been demonstrated that PTCA-fG and aptamer sensor could successfully differentiate normal and cancer cells. In addition, PTCA-fG was found to be non-toxic towards HeLa cells (Feng et al., 2011a). PEI-functionalized graphene (PEI-fG) also has been revealed to have lower toxicological effects towards HeLa cells as compared to pristine graphene (Feng et al., 2011b). Yang et al. (2010b) have reported the biocompatibility of chitosan-graphene nanocomposites and demonstrated their application in tissue engineering.
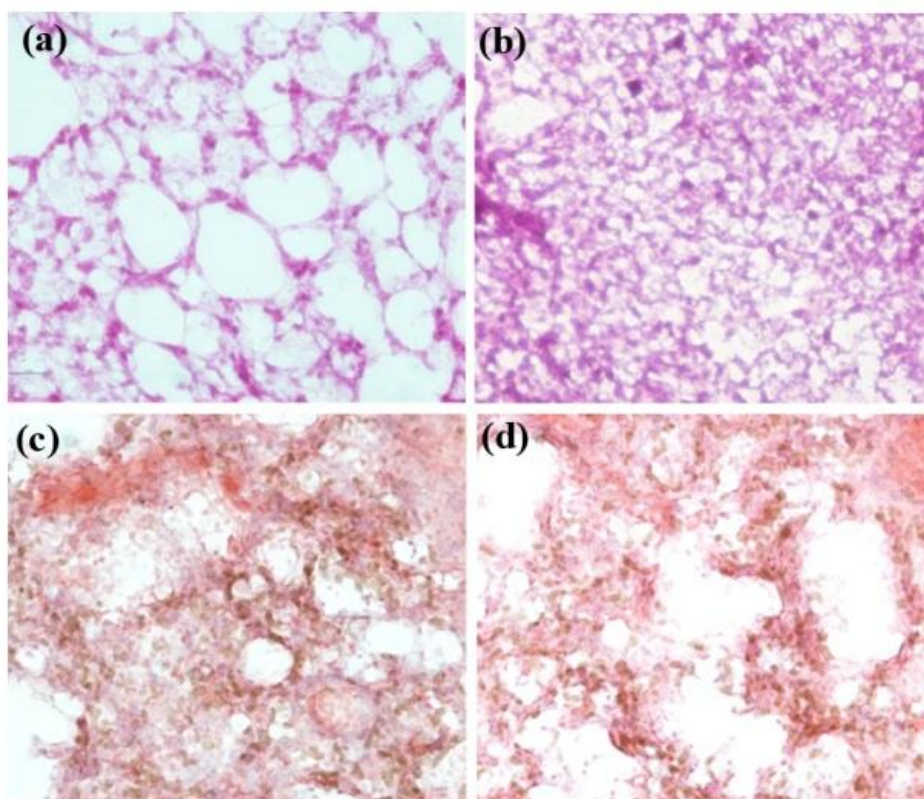
Figure 2.13: Micrograph of tissues in mice's lungs exposed to different dose of GO for 7 days (a) 0 mg (b) 0.10 mg (c) 0.25 mg and (d) 0.40 mg (Wang et al., 2011a).

2.4   Summary

Graphene is a unique 2D nanostructure with promising and exciting potential to be used in a wide variety of applications. Graphene was first synthesized in 2004 through mechanical exfoliation of HOPG. Since then, tremendous works have been carried out to develop alternative methods for the high volume production of graphene including CVD, thermal decomposition of SiC and the reduction of GO. Among these methods, the reduction of GO is the most attractive route to produce graphene owing to its cost effectiveness, scalable for mass production and requiring only simple equipment setup. In early stage of the investigation of the GO reduction, various chemical-based reducing agents have been used to reduce the GO. However,

these chemical-based reducing agents were later found to be highly corrosive and toxic. This has prompted research communities to substitute the hazardous chemical-based reducing agents with more environmental-friendly reducing agents and to develop sustainable methods to reduce GO that circumvent the use of the reducing agent. The efficiency of the GO reduction process can be improved by understanding the structure of RGO sheets and the reduction mechanism of GO. The improved understandings of the reduction mechanism can be achieved through investigation using computational study. Graphene nanostructures particularly GFs have drawn increasing attention from researchers to be applied in various applications especially in biomedical field. Hence, it is anticipated that the research and development of graphene will continue to progress in order to further enhance the properties of graphene and to discover more sustainable and environmental-friendly routes to produce graphene.

CHAPTER 3

MATERIALS AND METHODOLOGY

3.1 Materials and Chemicals

The specification of all materials and chemicals as well as the software that have been used in this research project was summarized as in Table 3.1 and Table 3.2, respectively.

Table 3.1: Specification of the materials and chemicals used in the research work.

No.	Materials/ Chemicals	Specification		Manufacturer/ Supplier
1.	Graphite oxide	Product code	: TNSOG	Chengdu Organic
		Purity	: >99 wt%	Chemicals Co., Ltd,
		Thickness	: ~0.55-1.20 nm	Chinese Academy
		Diameter	: 2-5 µm	of Sciences, China
2.	Green tea leaves extract powder	Appearance	: Brown-red powder	
		Total tea polyphenols	: 99.50 %	
		Total catechins	: 78.20 %	
		Epigallocatechin gallate	: 48.60 %	Guangzhou New
		Caffeine	: 2.87 %	Sino Biotech Co.,
		Loss on drying	: 2.30 %	Ltd, China
		Mesh size	: 80 mesh (100 %)	
		Heavy metals (Lead)	: $\leq$10.0 ppm	
		Ash	: $\leq$0.3 %	
		Total bacterial	: $\leq$1000 cfu/g	
3.	Hydrazine (N_2H_4) solution	Appearance	: Colourless liquid	
		Concentration	: 35 wt% in water	
		Molecular weight	: 32.05 g/mol	Sigma Aldrich,
		Relative density	: 1.011 g/cm^3 (25 ºC)	Malaysia
		Vapor pressure	: 5 mmHg (25 ºC)	

Table 3.1: Continued.

No.	Materials/ Chemicals	Specification		Manufacturer/ Supplier
4.	Stainless steel (SS) type 316L	Thickness Purity Description	: 0.2 mm : AISI 316L Fe/Cr18/Ni10/Mo3 : Temper annealed	Advent Research Materials, Oxford, England
5.	Deionized (DI) water	Resistivity	: 18.2 MΩcm	ELGA Purelab Option-Q Water Purification System (Model: DV25)
6.	Human colonic fibroblasts (CCD-18Co) cells line	Organism Tissue Morphology Culture properties Disease Age	: Human : Colon : Fibroblasts : Adherent : Normal : 2.5 months	American Type Culture Collection (ATCC), Manassas, United State of America (USA)
7.	Dulbecco's Modified Eagle's Medium (DMEM)	Form Volume Glucose Glutamine HEPES buffer Phenol red indicator Serum supplementation Additive	: Liquid : 500 mL : Low : No : No : No : Standard : Sodium pyruvate	Invitrogen Life Technologies, Karlsruhe, Germany
8.	MTT (3-(4,5-dimethyl-thiazol-2-yl)-2,5-diphenyltetrazolium bromide) salt solution	Form Indicator properties	: Solid : Colourimetric reagent-based	Invitrogen Life Technologies, Karlsruhe, Germany

Table 3.2: Specification of the software used in the research work.

No.	Software	Specification		Manufacturer/ Supplier
1.	Gaussian 09 & GaussView 5	Version	: 32-bit	Gaussian, Inc., Wallingford, United State of America (USA)
		Processor	: Intel Pentium 4, AMD Athlon, and later	
		Operating system	: Windows XP, Vista, Windows 7	
		Memory (RAM)	: 1 GB	
		Disk	: 1 GB (storage)	

3.2 Research Methodology

3.2.1 Preparation of Graphene Oxide (GO) Suspension

The aqueous suspension of GO consisted of 0.3 mg/mL commercially available graphite oxide powder in deionized (DI) water was prepared. The graphite oxide were dispersed ultrasonically in DI water for 200 s using an ultrasonic processor (Telsonic Ultrasonix Model SG-20kHz-500P & Converter SE-26/20-4) in order to exfoliate them into GO. Then, the GO suspensions were centrifuged (Eppendorf Centrifuge 5702R) at 4000 rpm for 30 minutes to remove the unexfoliated graphite oxide sheets. The as-prepared GO suspensions were directly used for the reduction reaction with GTP.

3.2.2 Preparation of Reduced Graphene Oxide (RGO) Suspension

The reduction reaction of GO with GTP was carried out in a 50 mL batch reactor-closed system as demonstrated schematically in Figure 3.1. Typically, GTP (weight ratio of GTP/GO=1) was added to 30 mL of GO suspension and the mixture was sonicated for 5 minutes. Subsequently, the reduction of GO was performed in the reactor for 8 hours at 80 ℃ while the GO-GTP mixture was stirred continuously

at 200 rpm during the reduction reaction. Then, the suspension of the final products was filtered through a nylon membrane (0.22 μm) and washed repeatedly with DI water in order to collect the resultant RGO sheets and to remove the residual GTP. A stable suspension of RGO was prepared by dispersing the resultant RGO sheets in DI water through sonication while maintaining its concentration at 0.3 mg/mL. In order to exclude the thermal effects on the reduction of GO, a similar heat treatment (at 80 ºC) was applied to GO without the presence of GTP (weight ratio of GTP/GO=0). The product of this treatment was referred as control-GO (c-GO) and was subjected for further analysis. Meanwhile, the effects of weight ratio of GTP/GO and reaction temperature on the reduction of GO were investigated by varying the weight ratio of GTP/GO from 0.5-5 and reduction temperature from 60-97 ºC. The designation of the RGO samples prepared using different weight ratio of GTP/GO and reaction temperature was shown as in Table 3.3 and Table 3.4, respectively. Then, the effects of these two parameters on the reduction of GO were evaluated by employing UV-Vis spectroscopy, FTIR and TGA analyses. In addition, the effects of weight ratio of GTP/GO and reduction temperature on the stability of the as-produced RGO suspension were also examined by performing zeta potential and electrophoretic mobility measurements. The best reduction conditions (weight ratio of GTP/GO and reduction temperature) for the GO reduction using GTP was determined from the aforementioned measurements and analyses. Thus, in order to compare the reduction efficiency of GTP with the efficiency of N_2H_4 solution as a standard reducer, the GO suspension was also reduced using N_2H_4 solution for 8 hours at similar reduction conditions. The reduction efficiency of GTP and N_2H_4 solution was evaluated by employing UV-Vis spectroscopy and XPS analyses.
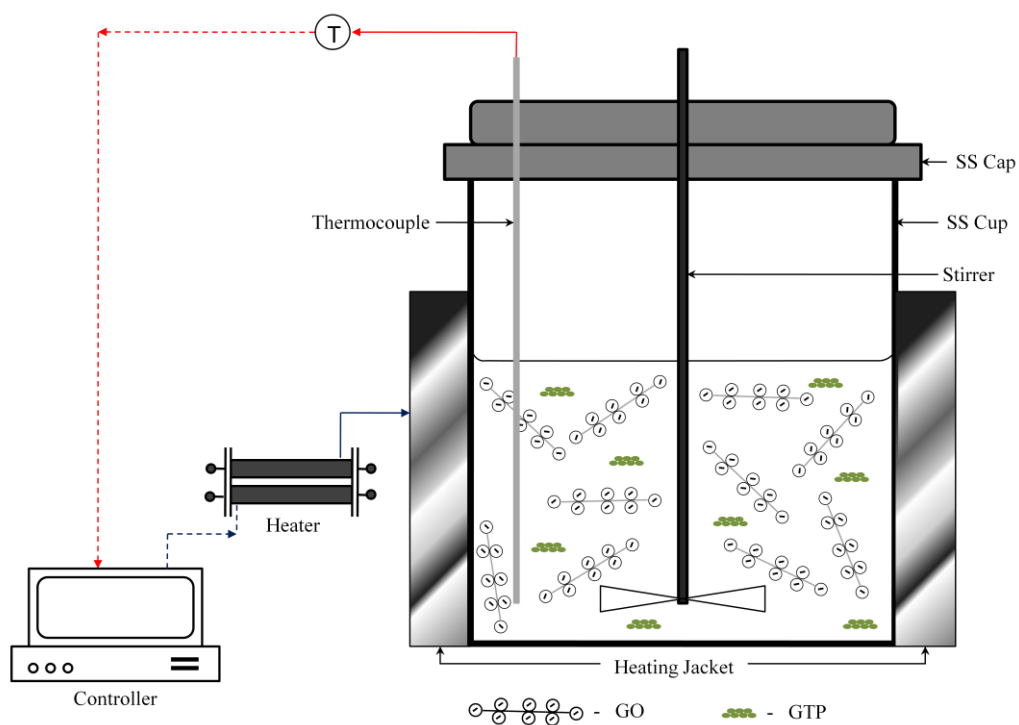
Figure 3.1: Schematic diagram of batch reactor-closed system setup for the reduction of GO by GTP.

Table 3.3: Samples designation and the reduction conditions using different weight ratio of GTP/GO.

Sample	Operating parameters	
	Temperature (ºC)	Weight ratio of GTP/GO (g/g)
RGO-1	80	0.5
RGO-2	80	1.0
RGO-3	80	2.0
RGO-4	80	3.0
RGO-5	80	5.0

Table 3.4: Samples designation and the reduction conditions using different reaction temperature.

Sample	Operating parameters	
	Temperature (ºC)	Weight ratio of GTP/GO (g/g)
RGO-6	60	1.0
RGO-7	70	1.0
RGO-8	80	1.0
RGO-9	90	1.0
RGO-10	95	1.0
RGO-11	97	1.0

3.2.3 Fabrication of Graphene Films (GFs)

GFs were prepared by the deposition of RGO particles on type 316L SS plates (Advent Research Materials Ltd.) with dimension of 10 mm × 10 mm × 2 mm by using EPD process as illustrated schematically in Figure 3.2. Prior to the EPD process, the SS plates were washed thoroughly with running DI water, ultrasonically degreased with acetone in a sonicator bath and again, rinsed thoroughly with DI water followed by drying in furnace at 60 ºC for 2 hours. Both SS plates (anode and cathode) were immersed in a stable RGO suspension inside a 50 mL borosilicate glass beaker. The EPD process was conducted by applying voltage ranging from 10-50 V and deposition time ranging from 100-500 s with electrodes distance of 10 mm for all experiments. Post deposition process of RGO particles, the anode was taken out immediately from the suspension and was dried in a desiccator at room temperature for 24 hours. After that, the deposition weight of the GFs was measured by using accurate analytical balance (Shimadzu AUW220D) with resolution of 0.1 mg. The Hamaker equation was used to express the relation between the deposition weight per unit area, m/S (g/cm^2) and the suspension properties (e.g., solid loading, C_s (g/cm^3) and electrophoretic mobility, μ (cm^{2}s^{-1}V^{-1})), in conjunction with the

electrical and physical parameters of the EPD system (e.g., electric field, E (V/cm) and deposition time, t (s)). The Hamaker equation (Eq. (3.1)) was given as:

Deposition weight of GFs per unit area, $\frac{m}{S} = (C_s)(\mu)(E)(t)$ (3.1)

In the meantime, the thickness of the GFs was measured from the cross-section view of the SEM images by using the measurement tool in SEM. The cross-section view was taken by tilting the SEM stage at 45°. Thus, the Eq. (3.2) was used to determine the actual value of the thickness of the GFs.

Thickness $_{actual}$ = Thickness $_{measured} \times \cos45°$ (3.2)
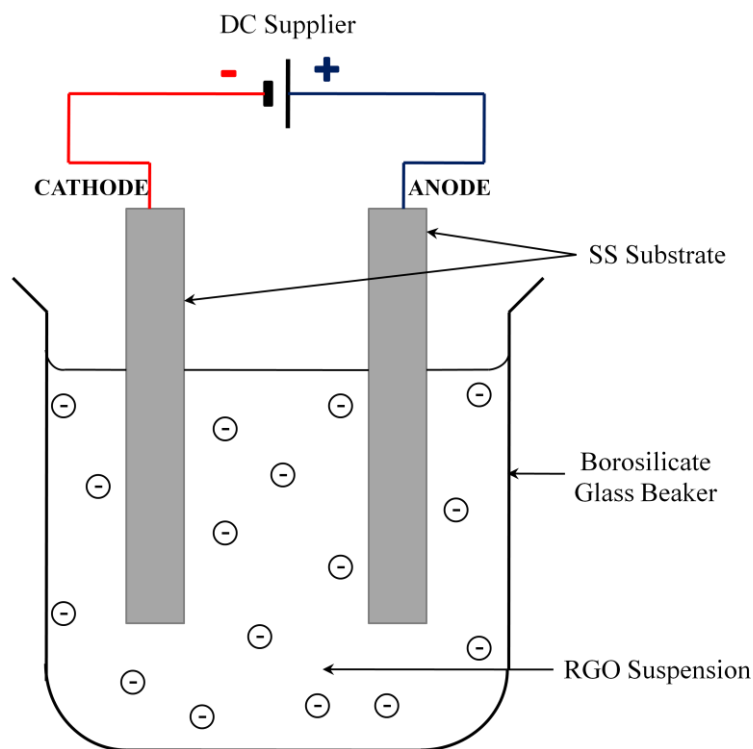
Figure 3.2: Schematic diagram of an EPD cell used for the deposition of RGO particles on SS substrate.

3.3   Characterization Techniques

3.3.1   Ultraviolet-Visible (UV-Vis) Spectroscopy

The measurement of the light absorption by a specific specimen was conducted by using a UV-Vis spectrophotometer. In order to monitor the reduction reaction of GO, the UV-Vis absorption spectra of RGO were recorded by using Agilent Technologies Cary-60 UV-Vis spectrophotometer. Additionally, the UV-Vis absorption spectroscopy also has been used to monitor the effects of weight ratio of GTP/GO and reaction temperature on the reduction of GO. Prior to the UV-Vis spectroscopy measurement, a fraction of RGO solution (0.5 mL) was extracted-out from the reactor, filtered and washed with abundant DI water. The as-filtered RGO sheets were then re-dispersed and diluted in DI water. The GO and GTP samples were directly diluted in DI water without further filtration. The diluted sample was contained in a quartz cuvette and was used directly for the UV-Vis spectroscopy measurement. The UV-Vis spectra were plotted as plots of absorbance versus wavelength.

3.3.2   Fourier Transform Infrared (FTIR) Spectroscopy

FTIR analysis was conducted in order to determine the presence of specific oxygen functional groups in GO and RGO. This analysis will determine the successful removal of oxygen functionalities from GO by reduction reaction using GTP. FTIR samples were prepared by directly drying the GO and RGO suspension in a vacuum oven to yield bulk powders of GO and RGO. The diamond crystal area of the FTIR spectrophotometer was cleaned using ethanol and the background spectrum was collected prior to the FTIR analysis. The solid powders of GO and

RGO were placed onto the diamond crystal top-plate. Once the samples have been placed on the crystal area, the pressure arm is put over the crystal/samples area and locked into a precise position above the diamond crystal to ensure direct contact of the samples and the crystal area. The FTIR spectra were recorded over frequency range of 600 to 4000 cm^{-1} by using Shimadzu IR Prestige-21 FTIR spectrophotometer.

3.3.3 Thermogravimetric Analysis (TGA)

TGA was performed in order to evaluate the thermal stability of GO and RGO samples. In this analysis, the change in the mass of the sample was measured while subjecting to a controlled temperature program. TGA was carried out under air atmosphere with heating rate of 10 ºC/minute using a simultaneous thermal analysis TGA7 Perkin Elmer Pyris instrument.

3.3.4 X-ray Photoelectron Spectroscopy (XPS)

The variation of chemical states of GO and RGO samples were examined by XPS analysis. The XPS spectra of GO and RGO samples were recorded using a high resolution multi techniques X-ray spectrometer (Axis Ultra DLD XPS Model Kratos) with Al Kα radiation of 1486.6 eV. XPS works by irradiating atoms of the surface of a sample with X-ray photons (Al Kα), in which the irradiation causing the ejection of core electrons (e^{-}). The core electrons are close to the nucleus and they carry information in term of binding energies characteristics of their particular element. In addition, core electrons also possess higher probability to match the energy of Al Kα. However, the useful signal from core electrons is obtained only from a depth less than 10 nm from the surface of the sample. For the irradiation

using Al Kα (1486.6 eV), the ejected electrons from depth more than 10 nm may undergone higher loss of energy and thus, they will contribute to the background signal instead of the primary photoelectric peaks. The XPS analysis was performed in ultrahigh vacuum (UHV) environment in order to eradicate excessive surface contamination and to increase the accuracy of the analysis. The kinetic energy (KE) of the ejected electrons was measured by cylindrical mirror analyzer (CMA) in which the analyzer signal was used by the control computer to plot the XPS spectrum. The XPS spectra were plotted as plots of intensity versus binding energy (BE).

3.3.5 Measurement of Zeta Potential and Electrophoretic Mobility

The stability of GO suspension is a key factor to facilitate the successful generation of mono and few-layer RGO sheets as the extraordinary properties of graphene are associated only to the individual sheets (Che et al., 2010). In the meantime, a stable RGO suspension is a prerequisite to obtain successful deposition of RGO particles on SS substrate using EPD. Hence, the parameters which are associated to the stability of GO and RGO suspension such as zeta potential and electrophoretic mobility were measured using Malvern Instruments Nano Series Zetasizer (model ZEN 3600). The electrophoretic mobility is associated to the zeta potential as been demonstrated by Eq. (3.3) (Hanaor et al., 2011):

$$\text{Electrophoretic mobility, } \mu = \frac{2\varepsilon_0 \varepsilon_r \zeta}{3\eta} f(\kappa r) \qquad (3.3)$$

where, ε_0 and ε_r are the permittivity of free space and the suspension medium, respectively, η is the viscosity of suspension medium, ζ is the zeta potential of particles in the suspension and $f(\kappa r)$ is the Henry coefficient, which relates the

thickness of double layer ($1/\kappa$) to the core radius (r) of the suspended particle. The value of Henry coefficient is 3/2 for a point charge or 1 for a flat surface (Ferrari and Moreno, 2010; Hanaor et al., 2011). Both of the zeta potential and the electrophoretic mobility are important characteristics of EPD which will determine the successfulness of the deposition of RGO particles on SS substrate using EPD (Ammam, 2012).

The GO and RGO suspensions subjected to these stability tests were prepared according to the experimental procedures of section 3.2.1 and 3.2.2, respectively. Subsequently, the prepared sample of GO and RGO suspension was injected into a sample cell (folded capillary cell typed DTS 1060) by using a syringe. The sample cell was tapped gently to dislodge any bubbles that might be trapped in the cell before each port of the sample cell was closed using a cell stopper. Then, the sample cell was inserted to the instrument and the required parameters were measured by running a standard order procedure (SOP) measurement as provided in the zetasizer software. The zeta potential and electrophoretic mobility measurements were repeated in triplicate (n = 3).

3.3.6 Scanning Electron Microscopy (SEM)

SEM analysis was performed in order to examine the surface morphology and to determine the thickness of the as-prepared GFs. SEM analysis was conducted using Zeis Supra 35VP microscope by applying accelerating voltage of 5 kV. The images (top and cross-section view) of the selected samples of GNSs were taken at magnification of 5,000 to 30,000 times the original sizes. In addition, the chemical elements in the samples were determined by using energy dispersion spectroscopy (EDS) analysis which was incorporated within the SEM.

80

3.4   Cytotoxicity Testing

3.4.1   Cells Culture

The cytotoxicity of GO and RGO suspensions were examined against human colonic fibroblasts (CCD-18Co) cells by inoculating and exposing the cells to different concentrations of GO and RGO suspensions ranging from 6.25-200 µg/mL. Prior to the cytotoxicity testing, all glassware was sterilized in an autoclave for 10 minutes at 120 ºC. The human fibroblasts cells were cultured in Dulbecco's Modified Eagle's Medium (DMEM) supplemented with 10 % fetal bovine serum (FBS). The cells were incubated in a humidified incubator (5 % CO_2, 37 ºC) until the cells reach to 70 % confluency in flask (Gholami et al., 2013; Wang et al., 2011a).

3.4.2   Cells Seeding and Their Treatment with Graphene Oxide (GO) and Reduced Graphene Oxide (RGO) Suspension

The cultured cells were seeded in 96-well plate (1.5×10^5 cells per well) and allowed to attach for 24 hours before further treatment was made. The initial GO and RGO suspensions (0.3 mg/mL) were diluted using cell culture medium to achieve the desired concentrations of 6.25, 12.5, 25, 50, 100 and 200 µg/mL. Next, 100 µL of the medium containing GO and RGO particles with different concentrations were added into each well of the 96-well plate. For comparison, only 100 µL of cell culture medium with no particles was added to the control well (untreated cells).

3.4.3 MTT Viability Assay

The viability of the human fibroblasts cells treated with different concentration of GO and RGO suspensions was evaluated colourimetrically using MTT (3-(4,5-dimethyl-thiazol-2-yl)-2,5-diphenyltetrazolium bromide) assay. The colourimetric MTT assay was first introduced by Mosmann (Mosmann, 1983) in 1983, as a sensitive, reliable and quantitative measure of the viability, proliferation and activation of the mammalian cells. The MTT salt solution was added 4 hours before the end of the 72 hours sample incubation. Then, the cell culture medium and the MTT solution were aspirated while the formazan solubilization buffer was added into the wells. The plate was incubated at 37 ºC for another 5 minutes. The absorbance was measured at a wavelength of 570 nm with reference wavelength of 620 nm using Ascent Multiskan ELISA microplate reader. For every different concentration, the GO and RGO samples were examined in triplicate (n = 3). The cytotoxicity results were reported as the percentage of cell inhibition and were expressed in the form of mean ± standard deviation. The percentage of the cell inhibition was determined using the optical density (O.D.) values by employing Eq. (3.4) (Gholami et al., 2013; Wang et al., 2011a):

$$\% \text{ Cell inhibition} = \frac{\text{O.D. value (control cell)} - \text{O.D. value (treated cell)}}{\text{O.D. value (control cell)}} \times 100 \qquad (3.4)$$

3.5 Mechanism of Graphene Oxide (GO) Reduction by Green Tea Polyphenol (GTP)

3.5.1 Computational Models

The structural model of GO was suggested to be based on the nonstoichiometric and amorphous nature (Lerf et al., 1998). Its structure varies

depending on the reaction conditions and the techniques used to prepare it. Solid state ^{13}C NMR (Cai et al., 2008; Lerf et al., 1998) and Raman spectra (Kudin et al., 2008) have shown that a large fraction of oxygen functionalities in GO occurred in form of epoxy and hydroxyl groups. In addition, a number of theoretical studies (Jelea et al., 2004; Kim et al., 2009b; Li et al., 2006) have demonstrated that during the oxidation of graphite, most of the oxygen atoms were adsorbed above the C-C bond across the basal plane of graphite which resulted in the formation of epoxy structure. Thus, the GO was modeled as a fragment of graphene sheets decorated with epoxy groups. Meanwhile, EGCG was the most dominant and potent catechin in GTP (Akhavan et al., 2012; Chen et al., 2008a; Wang et al., 2011c). Hence, the structure of EGCG was used to represent GTP in this computational study.

3.5.2   Computational Method

The DFT method was used to investigate the possible mechanism of epoxy group removal from GO via reduction reaction with GTP. This method was based on the electronic structure theory which uses the laws of quantum mechanics as the basis for its computation (Calais, 1990; Szabo and Ostlund, 1982). According to the quantum mechanics law, the energy and other related properties of a molecule could be obtained by solving the Schrödinger equation for Ψ in an appropriate boundary condition. The Schrödinger equation (Eq. (3.5)) was given as (Schrödinger, 1926):

$$\left\{ \frac{-h^2}{8\pi^2 m} \nabla^2 + V \right\} \Psi\,(r, t) = \frac{ih}{2\pi} \frac{\partial \Psi\,(r, t)}{\partial t} \tag{3.5}$$

where Ψ is the wavefunction, m is the mass of particle, h is Planck's constant, V is the potential field in which the particle is moving, ∇ is the operator del and it is equivalent to partial differentiation with respect to x, y and z components, and (r, t)

is the spatial and time functions. However, the exact solution to the Schrödinger equation is practically very difficult to be attained except for the smallest systems (Foresman and Frisch, 1996). For any other systems, the Schrödinger equation was solved through the mathematical approximations to its solution.

All calculations involving the structures and energies were computed using Gaussian 09 program (Frisch et al., 2009). Initially, all of the geometrical structures were modeled with GaussView 5 program (Dennington et al., 2009) before they were optimized by locating the minima on the potential energy surface (PES) using hybrid functional theory of B3LYP (Becke, 1993; Lee et al., 1988) combined with the 3-21G basis set (Binkley et al., 1980; Gordon et al., 1982; Pietro et al., 1982). Subsequently, the thermodynamic quantities including the change of enthalpy (ΔH), the change of entropy (ΔS) and the change of Gibbs free energy (ΔG) were calculated by performing frequency analysis using the same level of functional theory (B3LYP/3-21G). Enthalpy (H) is a state function (i.e., the property of H does not depends on the path of the reaction) and it could be defined as the heat transferred during a constant-pressure process (Keszei, 2012; Müller and Müller, 2009). ΔH of a reaction could be determined by subtracting the H of the reactants from the H of the products as given by Eq. (3.6) (Keszei, 2012; Müller and Müller, 2009):

$$\Delta H = H_{product} - H_{reactant} \tag{3.6}$$

Meanwhile, entropy (S) is a measure of molecular disorder or randomness of a system (Keszei, 2012; Müller and Müller, 2009). The ΔS for a system could be defined as (Eq. (3.7)) (Keszei, 2012):

$$\Delta S = S_{product} - S_{reactant} \tag{3.7}$$

On the other hand, Gibbs free energy (G) is a thermodynamic property that was used to predict whether a reaction or process will occur spontaneously at constant pressure and temperature (Müller and Müller, 2009). The G is associated to the H and the S in which their association was demonstrated by Eq. (3.8):

$$G = H - TS \qquad\qquad (3.8)$$

The TS structures were located by using Synchronous Transit-Guided Quasi Newton (STQN) method (Peng and Schlegel, 1993) incorporated within the Gaussian 09 program. The STQN facility was initiated by selecting QST3 option in optimization setup. For QST3 option, geometrical specifications of reactant, product and a guess structure for the TS were need to be provided in its input file. The corresponding atoms within the three molecule specifications were ensured to appear in the same order by applying connection editor tool. A singlet spin-restricted B3LYP method was applied in all of the optimization and frequency calculations. Indeed, it has been reported that the employment of hybrid functional theory of B3LYP has resulted in more accurate and well-converged results for the carbon-based structure particularly for graphene material (Denis and Iribarne, 2012; Zhang et al., 2012a; Zhang and Xia, 2011).

CHAPTER 4

RESULTS AND DISCUSSIONS

4.1 Overall Scheme - Synthesis of Graphene Films (GFs) from Graphite Oxide

The route for the preparation of GFs from graphite oxide precursor is illustrated as in Figure 4.1. Graphite oxide is referred as the product of the oxidation of graphite and it is used as starting material in this work. As been illustrated in Figure 4.1(a), graphite oxide still retained the stacked structure similar to 3D graphite although it contained numerous groups of oxygen functionalities (e.g., epoxide, hydroxyl, carboxyl and carbonyl) as a result of the oxidation process. Then, GO is prepared by the exfoliation of graphite oxide through ultrasonication treatment in DI water as been depicted in Figure 4.1(b). The graphite oxide was sonicated in DI water for 200 s to yield a stable yellow-brownish dispersion of GO. The stability of the GO suspension is confirmed by its high absolute zeta potential value (-57.43 mV) and no precipitation occurred even after several months (>6 months). The stability of the GO suspension is vital as it provides an appropriate medium to prepare a stable RGO suspension. GO is chemically similar to graphite oxide but both of them are very different structurally. Instead of preserving the stacked structure as graphite oxide, GO is exfoliated to form monolayer and few-layers stacks that are stably dispersed in aqueous media. The schematic illustration of the monolayer and few-layers stacks of GO is portrayed at the top side of Figure 4.1(b). In the next step, the GO was subjected to reduction reaction using GTP in order to remove the oxygen functionalities and to restore the sp^2 bonding network of

GO, resulted in the production of RGO suspension as been shown in Figure 4.1(c). The schematic illustration of the RGO particles is shown at the top side of Figure 4.1(c). This reduction step will be further discussed in section 4.2. In the final step of the synthesis process, the RGO particles were deposited on SS substrate using EPD to yield GFs with wide range of coating thickness for specific applications as been illustrated in Figure 4.1(d). The fabrication of GFs using EPD will be discussed in details in section 4.6.
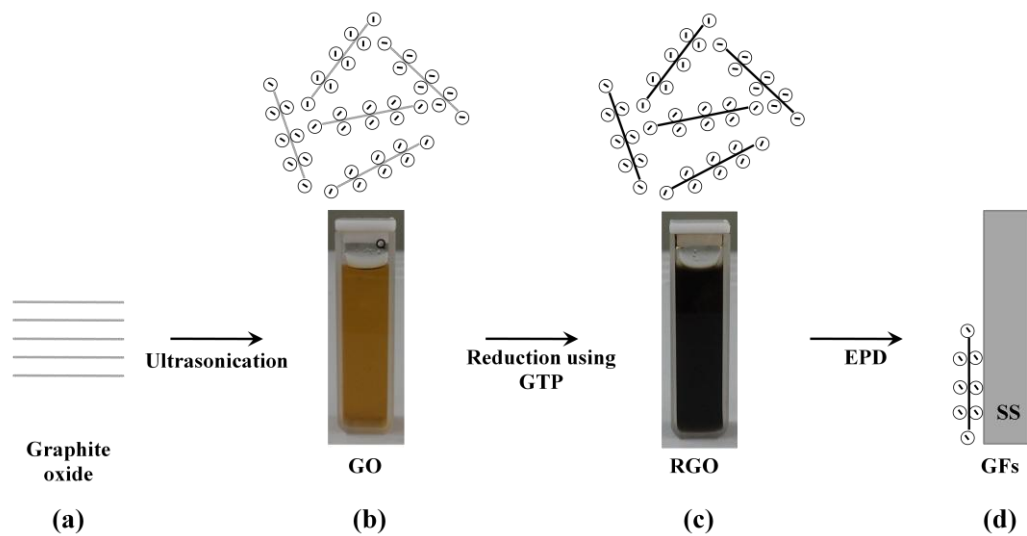
Figure 4.1: Scheme demonstrating the route for the synthesis of GFs from graphite oxide. (a) Graphite oxide as the starting material, (b) exfoliation of graphite oxide in DI water by ultrasonication treatment to yield stable dispersion of GO, (c) reduction of GO to produce stable RGO suspension via deoxygenation by using GTP, (d) fabrication of GFs through deposition of RGO particles on SS substrate using EPD.

4.2 Reduction of Graphene Oxide (GO) using Green Tea Polyphenol (GTP)

4.2.1 Monitoring the Reduction Reaction of Graphene Oxide (GO) with Green Tea Polyphenol (GTP)

The physical observation is the first indication and direct way to determine the successful reduction of GO. Post reduction reaction at 80 ºC using weight ratio

of GTP/GO=1, the colour of GO suspension was observed to change from yellow-brownish to black colour as shown in Figure 4.1(b) and Figure 4.1(c), respectively. This observation was presumably due to the partial re-graphitization of GO and the increased concentration of the RGO suspension as a result of the eradication of oxygen functionalities (Bourlinos et al., 2003; Stankovich et al., 2006a). In order to monitor the reduction reaction of GO with GTP, the UV-Vis absorption spectra of RGO were recorded as a function of reaction time (Figure 4.2).
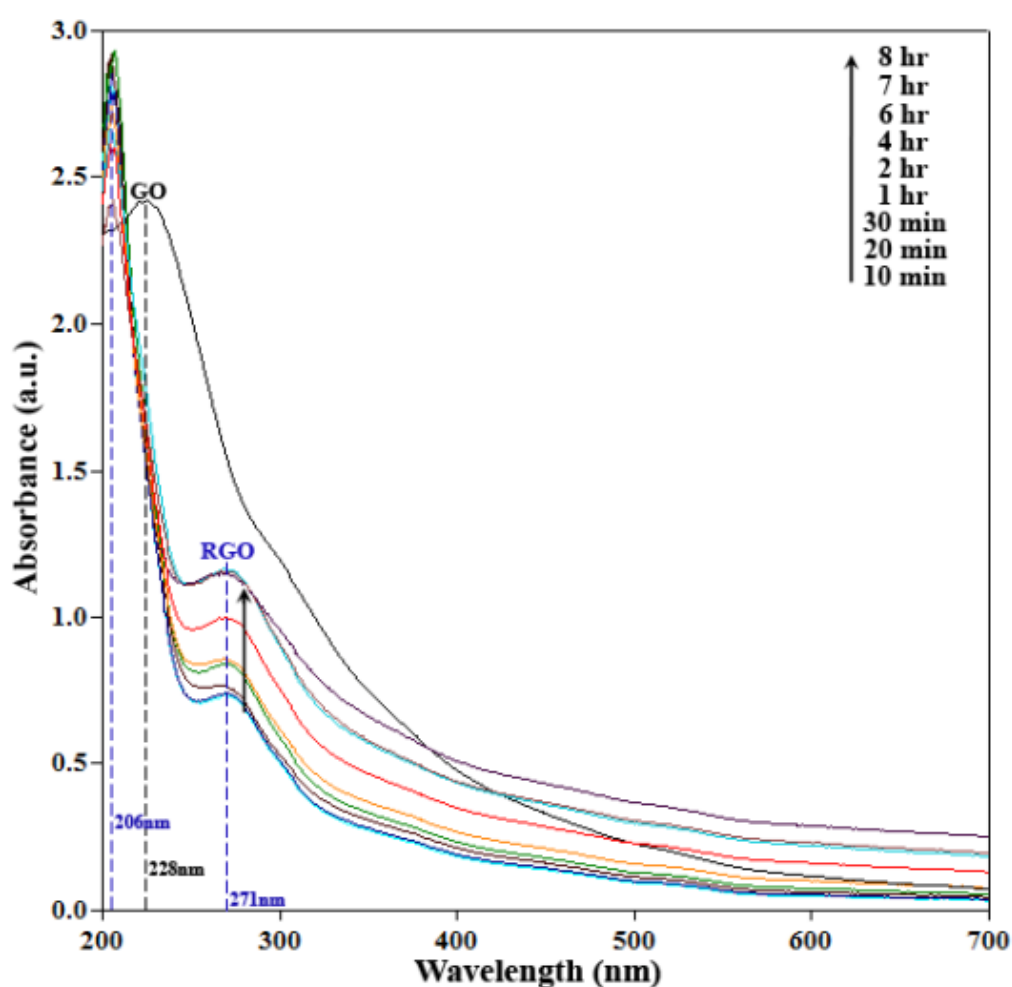
Figure 4.2: UV-Vis absorption spectra of RGO suspension as a function of reaction time (the arrow indicates the spectra of the as-produced RGO when the reaction time increases from 10 minutes to 8 hours) and the spectrum of GO suspension (black colour line).

The RGO samples for UV-Vis spectroscopy testing were prepared by pipetting-out a fraction of reaction solution (0.5 mL) from the reactor at a proposed time interval, filtered and washed for 3-5 times before they were re-dispersed and diluted in DI water. As been shown in Figure 4.2, a maximum peak at 228 nm was observed from the absorption spectrum of GO. The absorption peak at 228 nm could be assigned to the π-π* transitions of aromatic C=C bonds and C=O bonds (Liao et al., 2011b). As the reaction progressed, the absorption peak of GO was shifted to 271 nm which indicates that the GO has been reduced and the sp^2 bonding network of GO has been re-established. Apart from the absorption peaks at 271 nm, the RGO samples also exhibit strong UV-Vis absorption peaks at 206 nm. These peaks were corresponded to the structure of benzene ring in EGCG, the most potent catechin in GTP (Liao et al., 2011b; Zhao et al., 2012). The absorption peaks at 206 nm were observed in all of the UV-Vis spectra of RGO samples even after those samples went through repeated washing which signify the strong adsorption between GTP and RGO. The strong interaction between GTP and RGO may be the key factor that influences the stability of RGO suspension (this will be further discussed in section 4.3).

In addition, the UV-Vis absorption intensity of the resulted RGO suspension was observed to increase with the increasing reaction time. According to Beer's law, there is linear correlation between the absorption intensity and the concentration of an absorbing species (Lee et al., 2011; Yi et al., 2013). When the reaction time increases, the number of oxygen functional groups that have been eliminated from GO was multiplied. This led to the increase of the concentration of the resulted RGO suspension, which may explain the increase of the absorption intensity of RGO suspension at increasing reaction time. However, nearly constant absorption

intensity of RGO suspension was observed at a reaction time of 6 to 8 hours. At a longer reaction time (>6 hours), most of the oxygen functionalities of GO including epoxy and hydroxyl groups at basal plane and even carboxyl and carbonyl groups on the edges may already have been removed. Thus, there is no further or very little increase of the concentration of RGO that occurred, resulting in almost similar absorption intensity of RGO samples reduced at 6 to 8 hours.

4.2.2 Effect of Weight Ratio of GTP/GO on the Reduction of Graphene Oxide (GO)

Among the factors that have an enormous impact on the reduction of GO are weight ratios of GTP/GO and reaction temperature. The effects of these two factors on the reduction of GO were examined by using UV-Vis spectroscopy, FTIR and TGA analyses. Initially, the effect of weight ratio of GTP/GO was investigated by reducing GO at fixed temperature (80 °C) using different weight ratios of GTP/GO ranging from 0.5 to 5. Figure 4.3 shows the UV-Vis absorption spectra of RGO suspension prepared using different weight ratio of GTP/GO varying from 0.5 to 5 as assigned as RGO-1 to RGO-5, respectively. From Figure 4.3, almost no absorption peak of RGO was observed at 271 nm when the weight ratio of GTP/GO was 0.5 which suggests that possibly the amount of GTP used was not enough to reduce GO completely. When the weight ratio of GTP/GO was increased to 1, an absorption peak of RGO was established at 271 nm. This shows that a minimum weight ratio of GTP/GO equal to 1 (GTP/GO=1) was required to complete the reduction of GO. Although the weight ratio of GTP/GO was further increased to 5, the absorption peak of RGO was still remained at 271 nm albeit with much higher absorption intensity as compared to when weight ratio of GTP/GO=1 was used. The

final position of absorption peak at 271 nm was often regarded as the end of the reduction reaction (Guo et al., 2012; Wang et al., 2011c). Hence, the weight ratio of GTP/GO=1 was the minimum weight ratio required to achieve the establishment of RGO absorption peak at 271 nm. Meanwhile, in order to exclude the thermal effects on the reduction of GO, the GO was subjected to similar heat treatment at 80 ℃ without the presence of GTP (i.e., the weight ratio of GTP/GO=0) and the product was referred as c-GO. The UV-Vis absorption spectrum of c-GO shows that the absorption peak was un-shifted and remained at 228 nm which indicates that the reduction of GO was not occurred. Therefore, it can be concluded that a minimum amount of GTP aided with heat treatment was required in order to achieve successful reduction of GO, rather than solely due to thermal effects.
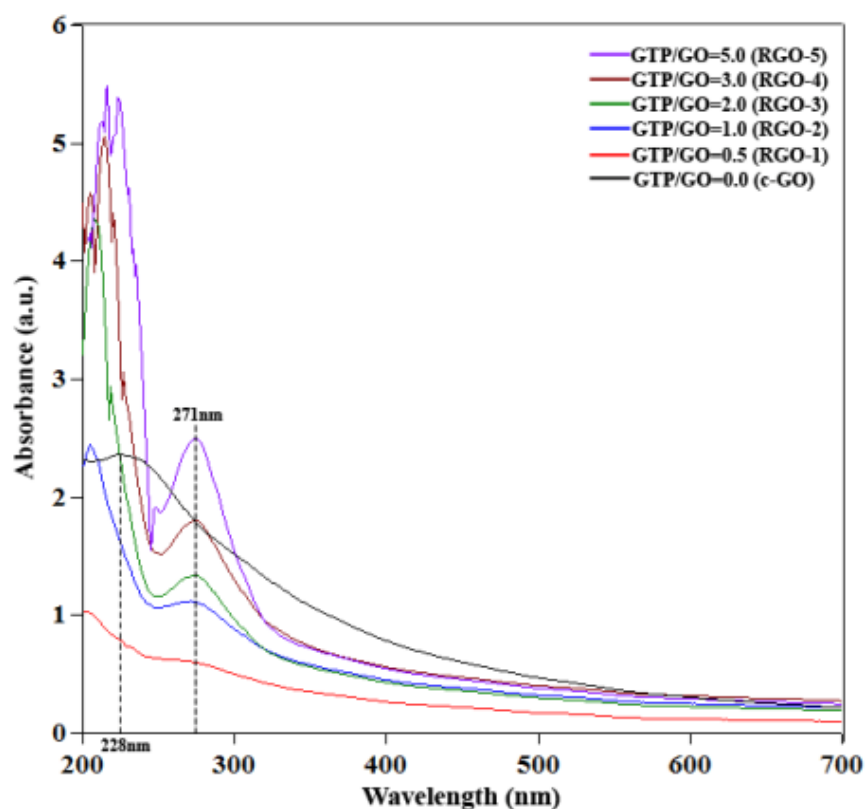
Figure 4.3: UV-Vis absorption spectra of RGO suspension prepared using different weight ratio of GTP/GO ranging from 0.5-5. All samples were reduced at 80 ℃ for 8 hours.

91

From Figure 4.3, it has been shown that the weight ratio of GTP/GO=1 (RGO-2) was the minimum weight ratio required to complete the reduction of GO. Hence, RGO-2 was selected for further analysis using FTIR and TGA in order to determine the efficiency of the removal of oxygen functionalities using weight ratio of GTP/GO=1. In addition, the efficiency of the eradication of oxygen functionalities was also investigated when very low weight ratio of GTP/GO=0.5 (RGO-1) and excessive weight ratio of GTP/GO=5 (RGO-5) were used for the GO reduction. Then, the removal efficiency of oxygen functionalities in RGO-2 was compared to those in RGO-1 and RGO-5. Figure 4.4(a-d) shows the FTIR spectra of GO, RGO-1, RGO-2 and RGO-5, respectively.
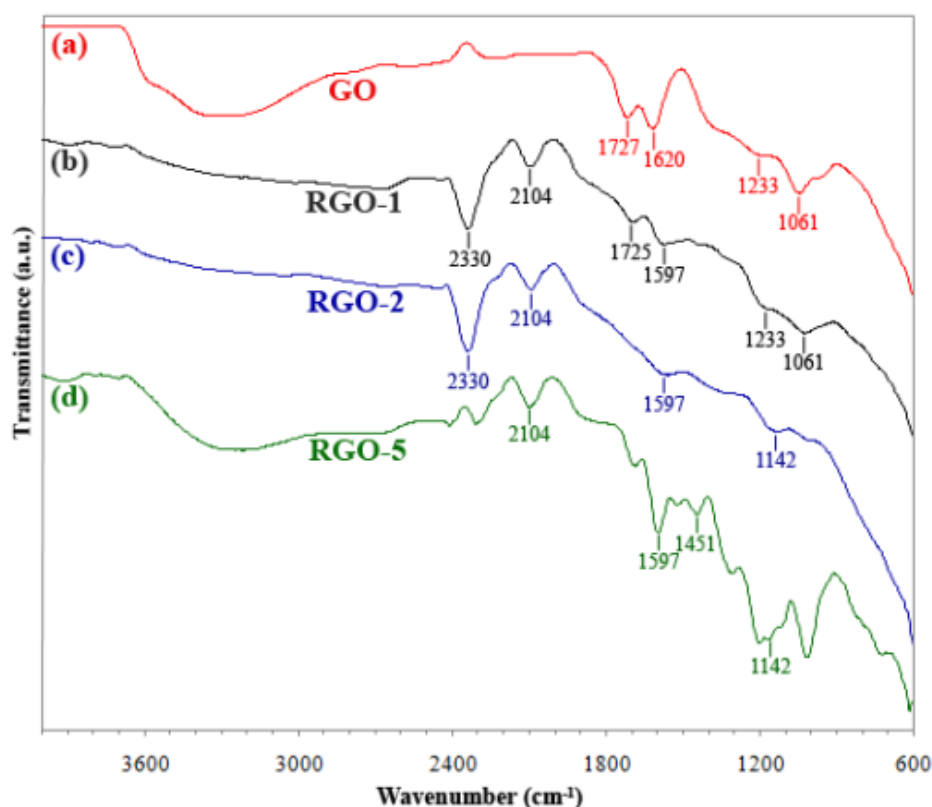
Figure 4.4: FTIR spectra of (a) GO, (b) RGO-1, (c) RGO-2 and (d) RGO-5. All RGO samples were reduced at 80 ℃ for 8 hours.

The GO sample possesses multiple peaks between 1000 cm^{-1} to 1800 cm^{-1} in which these peaks could be allocated to a variety of functional groups including

hydroxyl (1061 cm^{-1}), epoxy (1233 cm^{-1}) and carboxyl groups (1727 cm^{-1}) (Li et al., 2012a; Wang et al., 2011c). In addition, another peak was also observed at 1620 cm^{-1} as this peak could be assigned to the skeletal vibration of unoxidized graphitic domains (Choi et al., 2010a; Li et al., 2012a). Post reduction of GO using weight ratio of GTP/GO=0.5, the peaks that belong to the hydroxyl, epoxy and carboxyl groups were only slightly reduced, as illustrated from the FTIR spectrum of RGO-1. This observation indicates that the amount of GTP used may not enough to reduce GO completely, in agreement with the observation of the UV-Vis spectra as in Figure 4.3. However, new characteristic peaks were emerged at 1597 cm^{-1} and 2104 cm^{-1} in which these peaks could be assigned to the cumulative double bond due to the incorporation of GTP (Liao et al., 2011b). Additionally, there is another peak that has been observed at 2330 cm^{-1}. This peak could be assigned to the carbon dioxide that been trapped in the RGO-1 sample (Matranga et al., 2003), most probably during the drying process for the preparation of the sample for FTIR analysis.

In contrast, when the reduction of GO was performed using weight ratio of GTP/GO=1, the peaks that belong to the hydroxyl, epoxy and carboxyl groups as well as the peak of the vibration of unoxidized graphitic domains were significantly reduced and disappeared, as can be observed from the FTIR spectrum of RGO-2. This demonstrates that an efficient removal of oxygen functionalities could be achieved by using weight ratio of GTP/GO=1. Additionally, new peaks were observed at 1142 cm^{-1}, 1597 cm^{-1} and 2104 cm^{-1}; these peaks were allocated to the cumulative double bond of the oxidized GTP that was strongly adsorbed onto the structure of RGO sheets (Chen et al., 2010b; Liao et al., 2011b). A similar result was observed when the GO was reduced using weight ratio of GTP/GO=5 (RGO-5). The

peaks that been assigned to the hydroxyl, epoxy and carboxyl groups were disappeared and new peaks (e.g., 1142 cm^{-1}, 1451 cm^{-1}, 1597 cm^{-1} and 2104 cm^{-1}) (Chen et al., 2010b; Liao et al., 2011b) that belonged to the oxidized GTP were emerged, albeit with much higher intensity than those observed in RGO-2. This shows that the use of weight ratio of GTP/GO=1 was enough to eradicate most of the oxygen functionalities from GO without the needs to utilize excessive amount of GTP. Hence, in this study, the weight ratio of GTP/GO=1 was concluded to be the minimum weight ratio required to achieve successful reduction of GO.

The thermal stability of GO and RGO samples were evaluated by TGA in air atmosphere. The TGA curves of GO, RGO-1, RGO-2 and RGO-5 were shown in Figure 4.5. A three-stage weight loss was observed from the TGA curve of GO. The first weight loss was occurred at temperature below 100 ℃ due to the vaporization of moisture from the GO sample. The second weight loss of almost 22 wt% was observed to occur in the temperature range between 150 ℃ to 230 ℃. The significant weight loss in this temperature range was associated to the decomposition of the oxygen functional group in GO (Li et al., 2012a; Wang et al., 2011c). In addition, GO also underwent another weight loss in the temperature range between 450 ℃ to 565 ℃, primarily due to the burning or sublimation of the graphitic regions (Jeong et al., 2009; Young and Kinloch, 2013). Meanwhile, three-stage weight loss was also observed from the TGA curve of RGO-1 (weight ratio of GTP/GO=0.5). The first weight loss took place at the temperature below 100 ℃ due to the moisture vaporization. The second weight loss of 6.91 wt% was occurred in the temperature range between 150 ℃ to 230 ℃ due to the decomposition of the oxygen functionalities (Li et al., 2012a; Wang et al., 2011c). Although the weight loss of RGO-1 at temperature range of 150 ℃-230 ℃ was lower than the GO, the

almost 7 wt% weight loss of RGO-1 is still considered as slightly high which indicates that the amount of GTP used may not enough to remove the oxygen functionalities completely from the GO, in agreement with the observation of the UV-Vis (Figure 4.3) and FTIR spectra (Figure 4.4). The third weight loss of RGO-1 was occurred in the temperature range of 450 ºC-540 ºC due to the burning of the graphitic regions (Jeong et al., 2009; Young and Kinloch, 2013). In contrast to RGO-1, RGO-2 (weight ratio of GTP/GO=1) exhibits only a minor weight loss of 2.08 wt% at the temperature range of 150 ºC-230 ºC. This observation indicates that most of the oxygen functionalities were successfully removed during the reduction reaction using weight ratio of GTP/GO=1. Similarly, RGO-5 (weight ratio of GTP/GO=5) also shows a minor weight loss of 2.07 wt% at the temperature range of 150 ºC-230 ºC. This demonstrates that the use of weight ratio of GTP/GO=1 was enough to remove most of the oxygen functional group from GO without the needs to utilize excessive amount of GTP.
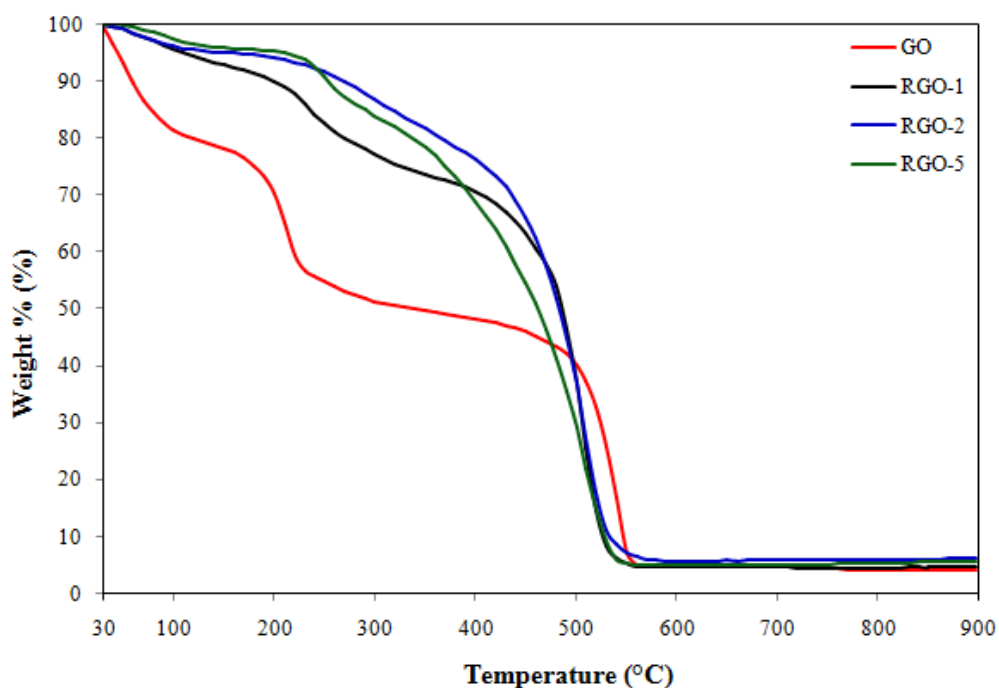
Figure 4.5: TGA curves of GO, RGO-1, RGO-2 and RGO-5. All RGO samples were reduced at 80 ºC for 8 hours.

4.2.3 Effect of Reaction Temperature on the Reduction of Graphene Oxide (GO)

The effect of reaction temperature on the reduction of GO was examined by conducting the reduction reaction of GO at temperature ranging from 60-97 ℃ using constant weight ratio of GTP/GO=1. Figure 4.6 depicts the UV-Vis absorption spectra of RGO suspension prepared at different reaction temperature ranging from 60 ℃ to 97 ℃ (RGO-6 to RGO-11). As been shown in Figure 4.6, the absorption intensities of the RGO peaks at 271 nm were observed to increase when the reaction temperature was raised from 60 ℃ to 90 ℃. This was due to the increase of the RGO concentration as been discussed earlier. On the contrary, when the reaction temperature was further increased to 95 ℃, the absorption intensity of the RGO peak at 271 nm was observed to be lower than the intensity of the RGO peak prepared at 60 ℃, while almost no absorption peak was observed at 271 nm when the GO was reduced at 97 ℃. These abnormal trends were observed possibly due to high aggregation of RGO sheets. At higher reduction temperatures (95 ℃ and 97 ℃), most of the oxygen functional groups may have been removed at a faster rate from GO. Ultimately, this led to the agglomeration and the instability of RGO suspensions as evidenced by the lower absolute zeta potential and electrophoretic mobility values as shown in Table 4.1 (this will be discussed in detail in Section 4.3). As a result, the abnormal trends of the UV-Vis spectra of RGO samples prepared at 95 ℃ and 97 ℃ were observed due to the unstable nature of the samples when performing the UV-Vis spectroscopy testing.
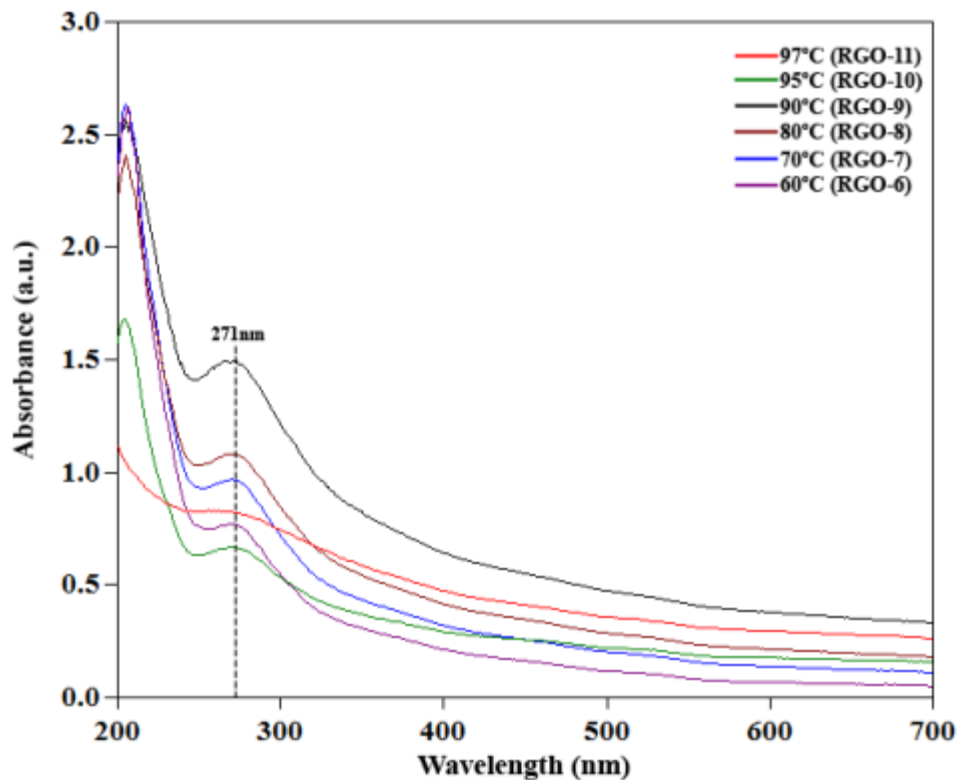
Figure 4.6: UV-Vis absorption spectra of RGO suspension prepared at different temperature ranging from 60-97 ℃. All samples were reduced using weight ratio of GTP/GO=1 for 8 hours.

As been demonstrated from Figure 4.6, the highest absorption intensity of the RGO peak at 271 nm was observed when the GO was reduced at 90 ℃ (RGO-9), which indicates that the RGO suspension with the highest concentration has been produced at this reaction temperature. Thus, RGO-9 was chosen for further analysis using FTIR and TGA to determine the efficiency of the eradication of oxygen functionalities at the reduction temperature of 90 ℃. The efficiency of the removal of oxygen functional groups was also examined when low reduction temperature of 60 ℃ (RGO-6) and elevated reduction temperature of 97 ℃ (RGO-11) were used for the GO reduction. The temperatures of 60 ℃ and 97 ℃ are the lowest and the highest reduction temperature that were investigated in this study. Ultimately, the removal efficiency of oxygen functionalities in RGO-9 was compared to those in

RGO-6 and RGO-11. Figure 4.7(a-d) illustrates the FTIR spectra of GO, RGO-6, RGO-9 and RGO-11, respectively.
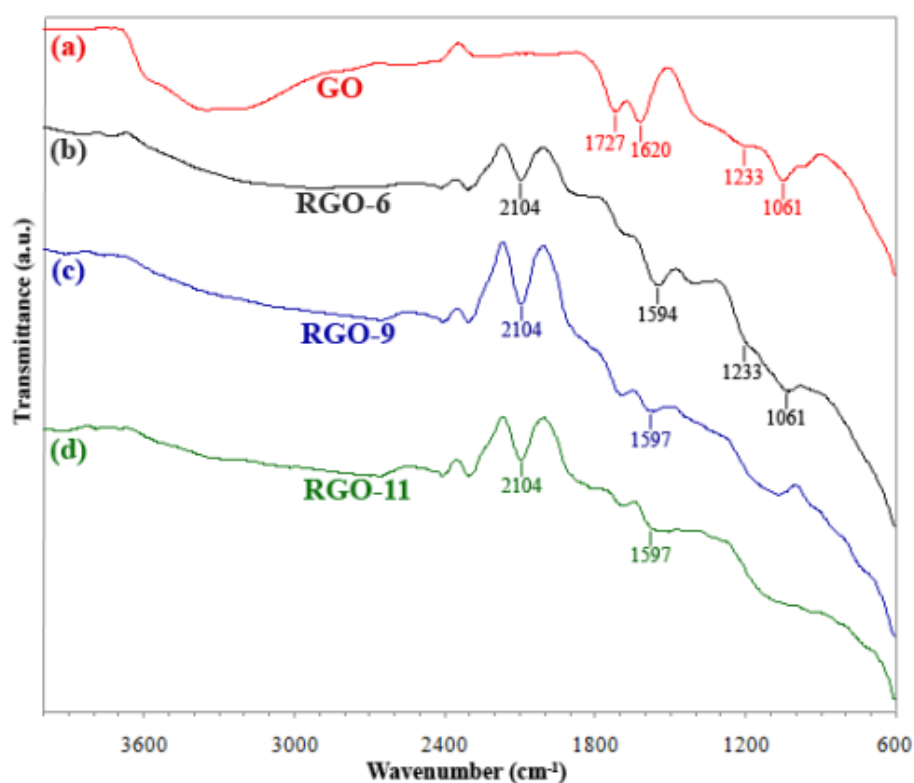
Figure 4.7: FTIR spectra of (a) GO, (b) RGO-6, (c) RGO-9 and (d) RGO-11. All RGO samples were reduced using weight ratio of GTP/GO=1 for 8 hours.

Multiple peaks between 1000 cm^{-1} to 1800 cm^{-1} were observed from FTIR spectrum of GO; these peaks were assigned to various oxygen functionalities of GO as been discussed earlier (Choi et al., 2010a; Li et al., 2012a; Wang et al., 2011c). When the reduction of GO was carried out at 60 ºC, the peaks that belong to hydroxyl (1061 cm^{-1}) and epoxy (1233 cm^{-1}) (Wang et al., 2011c) groups were only slightly reduced which indicates the inefficient removal of oxygen functionalities from GO at this reaction temperature. In contrast, when the GO was reduced at 90 ºC, the peaks that belong to hydroxyl, epoxy and carboxyl groups as well as the peak of the vibration of unoxidized graphitic domains were disappeared. Whilst, new

peaks were emerged at 1597 cm^{-1} and 2104 cm^{-1} in which these peaks were assigned to the cumulative double bond of the oxidized GTP (Chen et al., 2010b; Liao et al., 2011b). This observation indicates that a successful reduction of GO could be attained at this reaction temperature. Similarly, the peaks that were assigned to the hydroxyl, epoxy and carboxyl groups as well as the peak of the vibration of unoxidized graphitic domains were disappeared when the GO was reduced at 97 °C (RGO-11). This indicates that most of the oxygen functionalities may have been removed from the GO. This led to the agglomeration and the instability of RGO suspension, resulting in abnormal trend of UV-Vis spectrum of RGO-11 as can be observed in Figure 4.6. However, this abnormal trend was not observed in FTIR spectrum since the sample of RGO-11 for FTIR analysis was dried and analyzed in powder form.

Meanwhile, Figure 4.8 shows the TGA curves of GO, RGO-6, RGO-9 and RGO-11. GO exhibits three-stage weight loss in which almost 22 wt% weight loss was observed to occur in the temperature range of 150 °C-230 °C. The weight loss at this temperature range was associated to the decomposition of oxygen functionalities in GO (Li et al., 2012a; Wang et al., 2011c) as been discussed previously in section 4.2.2. The other weight losses of GO were took place at the temperature below 100 °C due to the moisture vaporization and at the temperature range of 450 °C-565 °C due to the burning of the graphitic regions (Jeong et al., 2009; Young and Kinloch, 2013). In the meantime, RGO-6 (reduction temperature of 60 °C) exhibits slightly high weight loss of almost 5 wt% in the temperature range between 150 °C to 230 °C suggesting the low efficiency of the removal of oxygen functionalities from GO at reduction temperature of 60 °C, in agreement with the observation of the UV-Vis (Figure 4.6) and FTIR spectra (Figure 4.7).
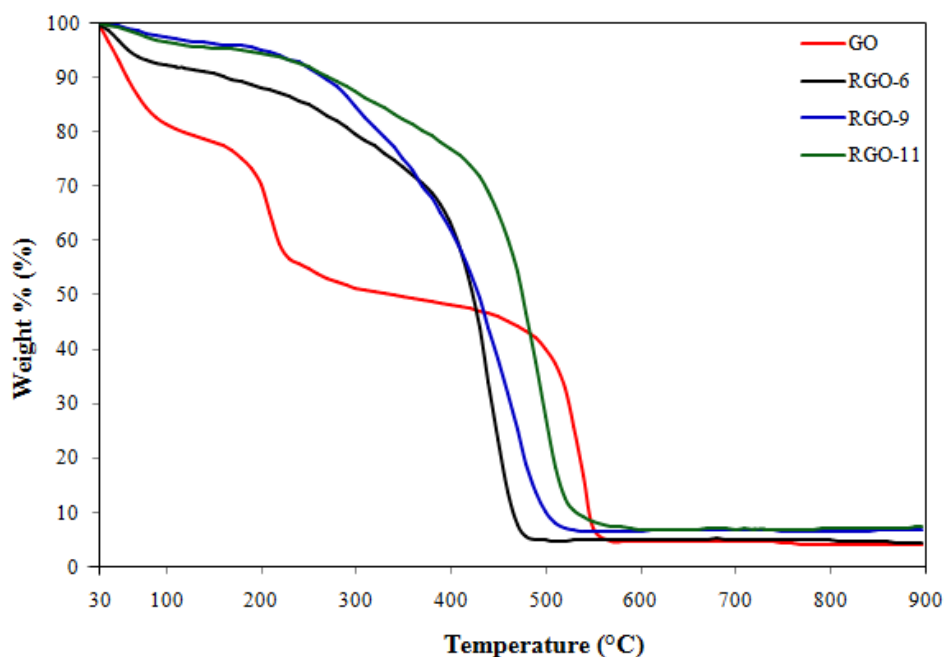
Figure 4.8: TGA curves of GO, RGO-6, RGO-9 and RGO-11. All RGO samples
were reduced using weight ratio of GTP/GO=1 for 8 hours.

On the contrary, the RGO sample prepared at 90 ℃ exhibits only minor weight loss of 2.35 wt% at the temperature range of 150 ℃-230 ℃, as observed from the TGA curve of RGO-9. This observation indicates that most of the oxygen functionalities were successfully removed during the reduction reaction at 90 ℃. Meanwhile, RGO-11 (reduction temperature of 97 ℃) shows slightly lower weight loss of 2.27 wt% at the temperature range of 150 ℃-230 ℃ as compared to RGO-9. It has been shown that nearly all of the oxygen-containing functional groups were already been eradicated through reduction reaction at 90 ℃. Thus, performing the GO reduction at elevated temperature of 97 ℃ may only resulted in a very little increase of the number of oxygen functionalities that been removed from GO as compared to the reduction at 90 ℃ which possibly elucidate the slightly different weight loss of RGO-11 in comparison with RGO-9. In other words, a nearly complete reduction of GO could be attained by performing the reduction reaction at 90 ℃ without further needs to increase the reaction temperature. Hence, in this

study, the reduction temperature of 90 ℃ was concluded to be the best temperature for the GO reduction using GTP.

4.2.4 Efficiency of Graphene Oxide (GO) Reduction by Green Tea Polyphenol (GTP)

As can be observed from the results of the UV-Vis spectroscopy, FTIR and TGA analyses in section 4.2.2 and section 4.2.3, the reduction temperature of 90 ℃ and weight ratio of GTP/GO=1 were concluded to be the best conditions for the GO reduction using GTP (RGO-9). Hence, in order to compare the reduction efficiency of GTP with the efficiency of N_2H_4 solution as a standard reducer, the GO was also reduced using N_2H_4 solution at similar reduction conditions (i.e., reduction temperature of 90 ℃ and weight ratio=1). N_2H_4 solution is known to be the most widely used and effective reducing agent for the chemical reduction of GO (Akhavan et al., 2012; Wang et al., 2011c). For the GO reduction using N_2H_4 solution, the weight ratio was referred to the weight ratio of N_2H_4 solution to GO while the product of the reduction reaction was denoted as N_2H_4-RGO. Figure 4.9 illustrates the UV-Vis absorption spectra of GO, RGO-9 and N_2H_4-RGO. Fernández-Merino et al. (2010) have suggested that the final position of the UV-Vis absorption peak can be used as an indicator to estimate the reduction efficiency of the reducing agent. Prior to the reduction reaction, GO exhibits an absorption peak at 228 nm in which this peak could be assigned to the π-π* transitions of aromatic C=C bonds and C=O bonds (Liao et al., 2011b), as been discussed earlier in section 4.2.1. Post reduction reaction for 8 hours, the final position of the absorption peaks of RGO-9 and N_2H_4-RGO were observed at 271 nm and 267 nm, respectively. RGO-9 exhibits final position of absorption peak that almost similar to the N_2H_4 solution suggesting the effective reduction property of GTP as compared to the N_2H_4

solution as a standard reducing agent. RGO-9 also shows strong absorption peak at 206 nm in which this peak was associated to the structure of benzene ring in EGCG, the most dominant catechin in GTP (Liao et al., 2011b; Zhao et al., 2012). This peak at 206 nm was occurred due to the incorporation of GTP (Liao et al., 2011b) in the RGO-9 suspension.
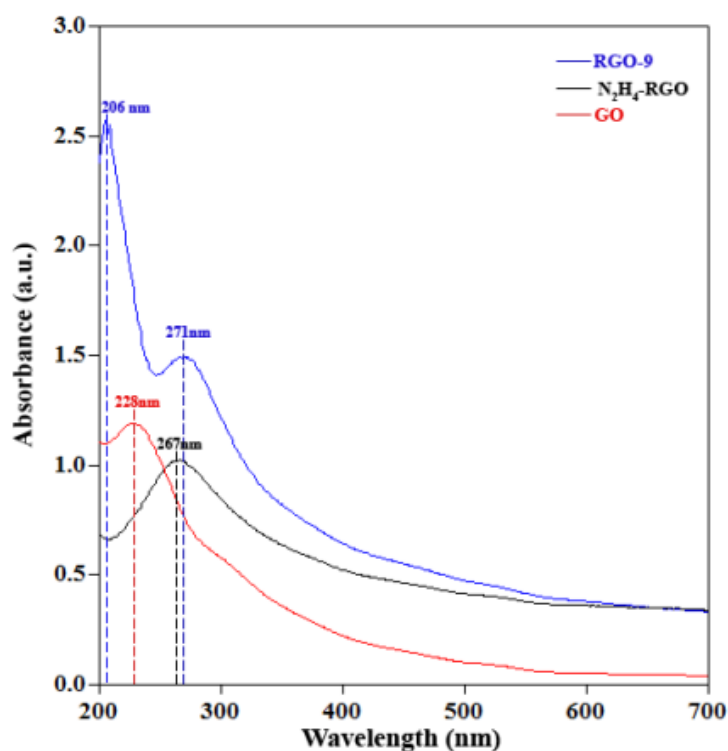
Figure 4.9: UV-Vis absorption spectra of GO, RGO-9 and N_2H_4-RGO. The reduction reaction of RGO-9 and N_2H_4-RGO was performed for 8 hours.

The variation of chemical states of GO, RGO-9 and N_2H_4-RGO were examined by using XPS analysis. Prior to the XPS analysis, the GO, RGO-9 and N_2H_4-RGO suspensions were dried in a vacuum oven to yield bulk powders of GO, RGO-9 and N_2H_4-RGO. Then, these solid powders were directly used for the XPS analysis. Figure 4.10(a-c) portrays the survey scans XPS spectra of GO, RGO-9 and N_2H_4-RGO, respectively. The intensity of C1s of GO was significantly lower than the C1s intensity of RGO-9 as can be observed from Figure 4.10(a) and Figure

4.10(b), respectively. This indicates that the sp^2 bonding network has been restored and the GO has been reduced successfully (Li et al., 2012a; Stankovich et al., 2007). Noted that the intensity of O1s of RGO-9 was higher than the intensity of O1s of GO, in which the adsorbed GTP may contribute to the addition of the oxygen group in RGO-9. From Figure 4.10(c), the intensity of O1s of N_2H_4-RGO was decreased significantly as compared to the GO suggesting the successful removal of oxygen functional groups. In addition, small intensity of N1s was also observed in survey scans XPS spectrum of N_2H_4-RGO indicating the presence of nitrogen in this sample (Stankovich et al., 2007).
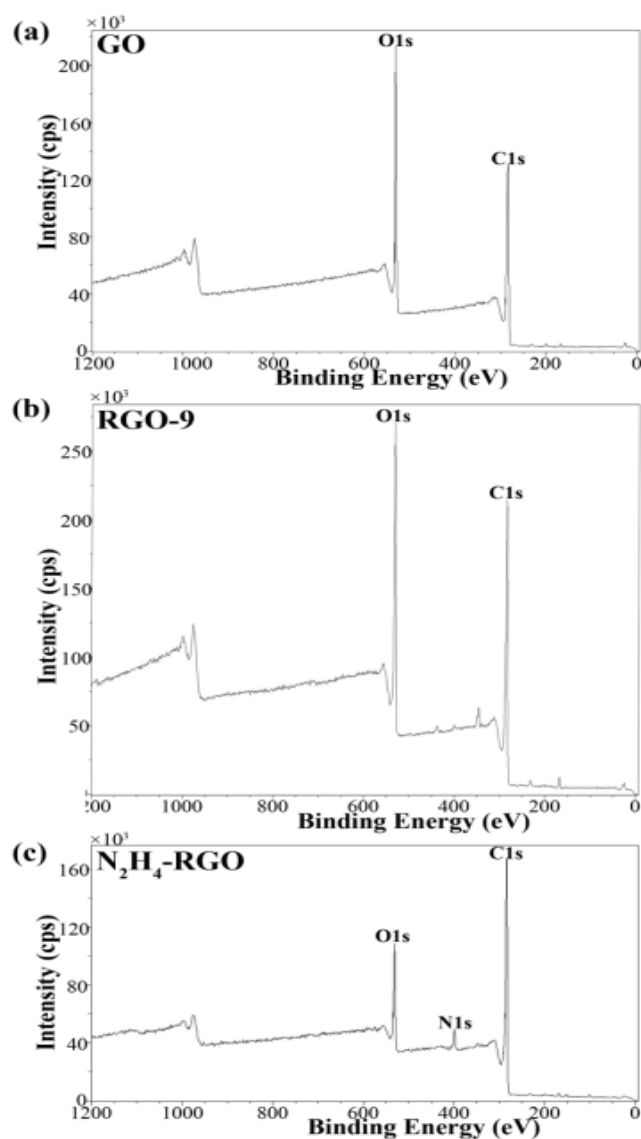
Figure 4.10: Survey scans XPS spectra of (a) GO, (b) RGO-9 and (c) N_2H_4-RGO.

The survey scans of XPS spectra were further processed at the C1s region in order to determine the constitutional changes before and after the reduction reaction. Figure 4.11(a-c) illustrates the XPS spectra at C1s region of GO, RGO-9 and N_2H_4-RGO, respectively. From Figure 4.11(a), four different types of carbon components were observed in GO namely, the sp^2 carbon (C-C, 284.8 eV), carbon in C-O bond (287.0 eV), the carbon in carbonyl (C=O, 289.3 eV) and the carboxylate carbon (O-C=O, 291.6 eV) (Stankovich et al., 2007; Wang et al., 2011c). Although the C1s XPS spectrum of RGO-9 also exhibits the same oxygen functionalities (C-O, C=O and O-C=O), their intensities are much smaller than those in GO as illustrated in Figure 4.11(b).

In addition, the intensity of sp^2 carbon in RGO-9 was increased significantly as compared to the GO indicating the establishment of sp^2 bonding network and the successful reduction of GO (Li et al., 2012a; Stankovich et al., 2007). Similarly, the intensities of oxygen functionalities in N_2H_4-RGO were reduced significantly as compared to those of GO as portrayed in Figure 4.11(c). This indicates the successful removal of oxygen functionalities from GO post reduction reaction with N_2H_4-solution (Stankovich et al., 2007). N_2H_4-RGO also exhibits the intensity of sp^2 carbon that almost similar to the intensity of sp^2 carbon of RGO-9 suggesting the effective reduction property of GTP as compared to the N_2H_4 solution as a standard reducer (Akhavan et al., 2012; Stankovich et al., 2007; Wang et al., 2011c).
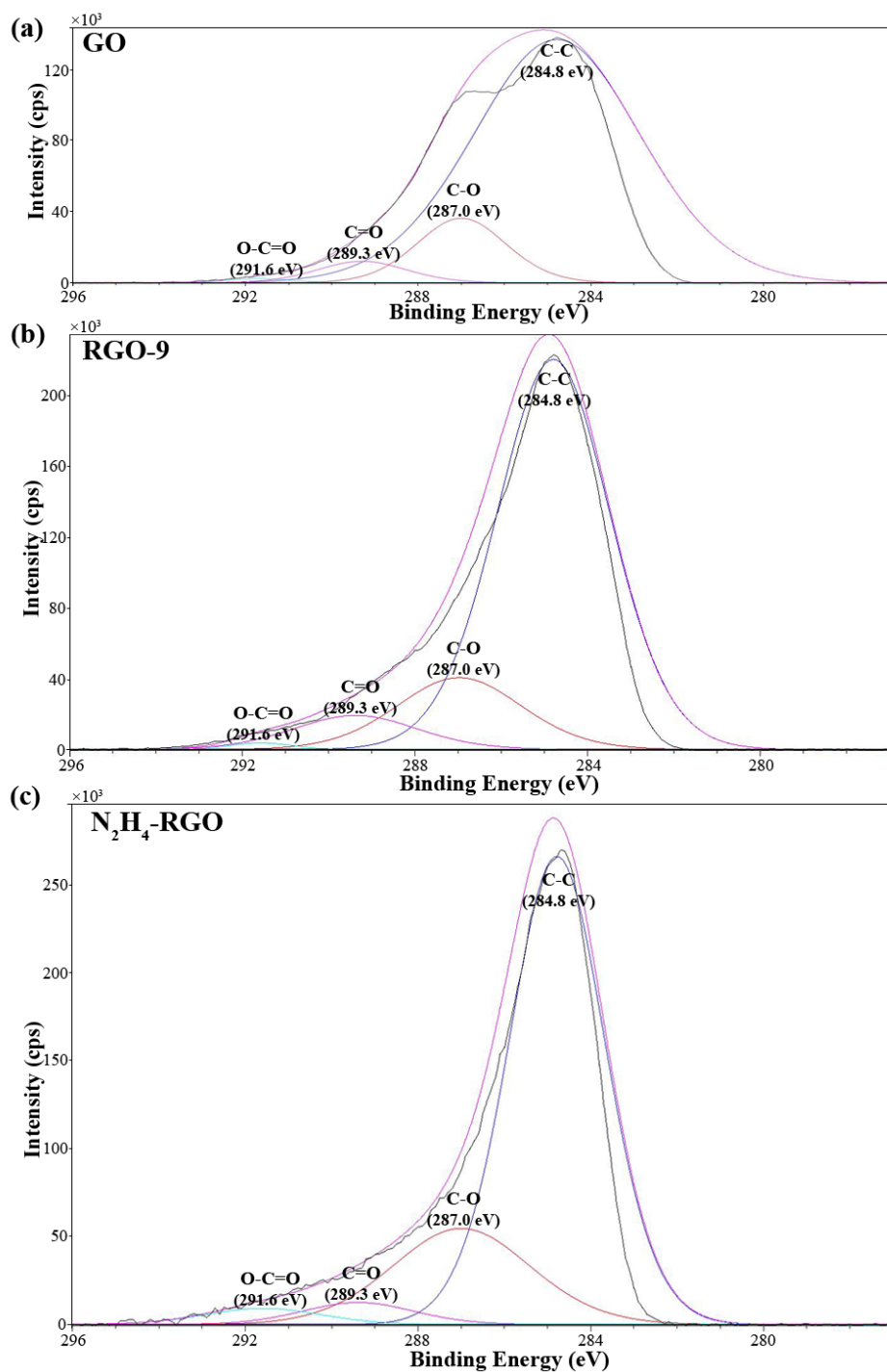
Figure 4.11: C1s XPS spectra of (a) GO, (b) RGO-9 and (c) N$_2$H$_4$-RGO.

4.3 Stability of Graphene Oxide (GO) and Reduced Graphene Oxide (RGO) Suspensions

In general, it is desirable to obtain stable RGO suspension for the easiness of further processing and the ability to be applied in a wide range of applications (Li et

al., 2008; Park and Ruoff, 2009). In this work, a stable and well-dispersed RGO suspension is highly desired in order to obtain successful deposition of RGO particles on SS substrate using EPD to yield GFs. Thus, the stability of the GO and RGO suspensions were examined by employing zeta potential and electrophoretic mobility measurements. All the GO and RGO samples subjected to these stability tests were prepared according to the experimental procedures of section 3.2.1 and 3.2.2. All the zeta potential and electrophoretic mobility measurements were carried out at pH=7. Table 4.1 and Table 4.2 show the zeta potential and electrophoretic mobility values of GO and RGO suspensions prepared using different weight ratio of GTP/GO and at different reduction temperature, respectively. Initially, the stability of GO and RGO suspensions were first investigated in terms of zeta potential as this parameter provides imperative information regarding the particles aggregation and the kinetic stability of the suspensions. High absolute zeta potential value is very much desired as it demonstrates that a well-dispersed and stable suspension has been produced (Konkena and Vasudevan, 2012; Luo et al., 2010). From Table 4.1, it can be concluded that a well-dispersed and stable aqueous suspension of GO has been prepared as high absolute zeta potential value of -57.43 mV was recorded. The GO was negatively charged due to the presence of oxygen functionalities including hydroxyl and carboxyl groups decorated at its basal planes and at the edges (Lerf et al., 1998; Szabó et al., 2006). In fact, the presence of these oxygen functionalities also resulted in the alteration of the van der Waals interactions between GO layers which make it hydrophilic in aqueous media (Stankovich et al., 2006a).

Table 4.1: Zeta potential and electrophoretic mobility values of GO, c-GO, N_2H_4-RGO and RGO suspensions prepared at different weight ratio of GTP/GO. All samples were measured at pH=7.

| Sample | Operating parameters | | Zeta potential (mV) | Electrophoretic mobility (μmcm/Vs) |
	Temperature (ºC)	Weight ratio of GTP/GO (g/g)		
GO (25 ºC)	-	-	-57.43 ± 0.72	-4.50 ± 0.06
c-GO	80	0.0	-47.70 ± 0.15	-3.74 ± 0.01
RGO-1	80	0.5	-28.37 ± 1.73	-2.22 ± 0.14
RGO-2	80	1.0	-38.47 ± 2.85	-3.02 ± 0.22
RGO-3	80	2.0	-26.63 ± 0.68	-2.09 ± 0.05
RGO-4	80	3.0	-25.87 ± 0.52	-2.03 ± 0.04
RGO-5	80	5.0	-25.10 ± 1.65	-1.97 ± 0.13
N_2H_4-RGO	90	1.0*	-15.50 ± 0.30	-1.21 ± 0.02

*The weight ratio of N_2H_4/GO used for the reduction of GO in control experiment.

The measurement for each sample was performed in triplicate (n = 3).

Table 4.2: Zeta potential and electrophoretic mobility values of RGO suspensions prepared at different reaction temperature. All samples were measured at pH=7.

| Sample | Operating parameters | | Zeta potential (mV) | Electrophoretic mobility (μmcm/Vs) |
	Temperature (ºC)	Weight ratio of GTP/GO (g/g)		
RGO-6	60	1.0	-30.47 ± 1.26	-2.39 ± 0.10
RGO-7	70	1.0	-33.93 ± 1.63	-2.66 ± 0.13
RGO-8	80	1.0	-38.47 ± 2.85	-3.02 ± 0.22
RGO-9	90	1.0	-39.43 ± 2.16	-3.09 ± 0.17
RGO-10	95	1.0	-24.87 ± 2.31	-1.95 ± 0.18
RGO-11	97	1.0	-16.67 ± 0.37	-1.31 ± 0.03

The measurement for each sample was performed in triplicate (n = 3).

As mentioned earlier, obtaining a stable GO suspension is crucial as it provides an ideal and appropriate medium to produce a stable and well-dispersed suspension of RGO. However, the stability of RGO suspension was also strongly dependent on the types of reductant used in the reduction reaction. When the GO was reduced by N_2H_4 solution, high agglomeration of N_2H_4-RGO sheets was

observed as the instability of RGO produced was clearly shown by the low absolute zeta potential value of N_2H_4-RGO (-15.50 mV). Although the N_2H_4-RGO sheets were tend to agglomerate due to the increase of the interlayer van der Waals interactions (Akhavan et al., 2012; Stankovich et al., 2007), the stability of N_2H_4-RGO suspension could be improved by adding stabilizers/surfactants (Hasan et al., 2011; Liang et al., 2009; Lomeda et al., 2008; Stankovich et al., 2006a; Stankovich et al., 2006b) or by including surface functionalization step (Veerapandian et al., 2012; Xu et al., 2009) in the reduction process. Nevertheless, the utilization of N_2H_4 in GO reduction has been deterred due to its corrosive and toxic nature (Powell and Gannett, 2002).

Meanwhile, the use of GTP in the GO reduction has resulted in higher stability of the as-produced RGO suspension as compared to the N_2H_4-RGO dispersion. The effect of weight ratio of GTP/GO to the stability of RGO suspension was examined by measuring the zeta potential of RGO suspension produced using different weight ratios of GTP/GO. Drawing from the result obtained as in Table 4.1, the stability of RGO suspensions arranged in an increasing order in term of their absolute zeta potential values were RGO-5 < RGO-4 < RGO-3 < RGO-1 < RGO-2, where these samples were prepared using weight ratio of GTP/GO equal to 5.0, 3.0, 2.0, 0.5 and 1.0, respectively.

The highest absolute zeta potential value of GTP-RGO suspension recorded was -38.47 mV, when the weight ratio of GTP/GO=1 was used. Everett (1988) has suggested that the absolute zeta potential values more than 30 mV represent an adequate mutual repulsion which ensures the stability of a suspension. This result shows that GTP possesses the capability to reduce GO as well as stabilizing the as-produced RGO sheets. The increase stability of the RGO suspension was suggested

to be primarily due to the π-π interactions between GTP and RGO layers (Liao et al., 2011b; Wang et al., 2011c), in addition to the steric effect caused by the incorporation of GTP (Lei et al., 2011).

When the weight ratio of GTP/GO was increased from 1 to 5, the absolute zeta potential values were decreased from -38.47 mV to -25.10 mV. It has been shown earlier from Figure 4.3 that the absorption intensities of the as-produced RGO suspensions were increased when the weight ratio of GTP/GO was increased from 1 to 5. This indicates that more oxygen functionalities have been removed from GO, which subsequently resulted in the increase of the aggregation of RGO sheets due to the stronger van der Waals attractive forces between RGO sheets. At the same time, increasing the weight ratio of GTP/GO also resulted in the increase of the steric effect and the π-π interactions between GTP and RGO. The increase of the weight ratio of GTP/GO has resulted in the incorporation of higher amount of GTP in the RGO suspension. As a result, more hydroxyl groups from gallic acid units in GTP can form strong hydrogen bonding interaction with epoxy and hydroxyl groups in RGO. Therefore, the π-π interactions between GTP and RGO were further enhanced. In addition, the steric effect was also improved due to the incorporation of higher amount of GTP. However, the van der Waals attractive forces between RGO sheets may be stronger than the steric effect and the π-π interactions between GTP and RGO when higher weight ratio of GTP/GO was used, which resulted in the decrease of the absolute zeta potential values due to the decrease stability of RGO suspension. Nonetheless, all of the RGO suspensions prepared using GTP were having higher stability than the N_2H_4-RGO dispersion which shows that the effective reduction of GO to yield a stable RGO suspension could be achieved by using GTP. Meanwhile, c-GO (weight ratio of GTP/GO=0) possesses high absolute

zeta potential value of -47.70 mV, which almost close to the absolute zeta potential value of GO. The high stability of c-GO was observed since the reduction of GO was not occurred without the presence of GTP.

At constant temperature of 80 ℃, the highest absolute zeta potential value of RGO suspension was obtained when weight ratio of GTP/GO=1 was used. Thus, the effect of reaction temperature to the stability of RGO suspension was investigated by recording the zeta potential values of RGO suspensions prepared at different reaction temperature using constant weight ratio of GTP/GO=1. In addition, it has been shown from Figure 4.3 and Figure 4.4 that the use of weight ratio of GTP/GO=1 was enough to eradicate most of the oxygen functionalities in GO without the needs to use excessive amount of GTP. From Table 4.2, the stability of RGO suspensions arranged in an increasing order according to their absolute zeta potential values were RGO-11 < RGO-10 < RGO-6 < RGO-7 < RGO-8 < RGO-9, where these samples were produced at 97 ℃, 95 ℃, 60 ℃, 70 ℃, 80 ℃ and 90 ℃, respectively.

The suspension prepared at 90 ℃ was determined to be the most stable RGO suspension as it possesses the highest absolute zeta potential value of -39.43 mV. This high stability was achieved due to the proposed steric effect and π-π interactions between GTP and RGO sheets. However, the absolute zeta potential value of RGO suspensions were reduced to -24.87 mV and -16.67 mV when the reaction temperature was further increased to 95 ℃ and 97 ℃, respectively. As been described earlier, the oxygen functionalities were possibly been eradicated at a faster rate from GO at higher temperatures (95 ℃ and 97 ℃) which subsequently, leading to the aggregation of RGO sheets. At this stage, the van der Waals attractive forces

between RGO sheets may be stronger than the steric effect and π-π interactions between GTP and RGO sheets, which resulting in the instability of RGO suspension.

Apart from the zeta potential measurement, the stability of GO and RGO suspensions were also examined by recording their respective electrophoretic mobility values. Hanaor et al. (2011) have defined the electrophoretic mobility as the velocity of a particle that moves under the influence of an electric field. Eq. (3.3) has shown that the electrophoretic mobility is directly proportional to the zeta potential value. As can be observed from Table 4.1 and Table 4.2, the resultant values of the zeta potential and electrophoretic mobility were reasonably matched with the Eq. (3.3) as a similar trend was obtained for both of these parameters. GO possesses the highest absolute electrophoretic mobility value at -4.50 μmcm/Vs, similar to the result of the zeta potential measurement. In investigating the effect of weight ratio of GTP/GO to the stability of RGO suspensions, the highest absolute electrophoretic mobility value of -3.02 μmcm/Vs was recorded when the GO was reduced using weight ratio of GTP/GO=1 at constant temperature of 80 ℃. Whereas, the RGO suspension prepared at 90 ℃ (using constant weight ratio of GTP/GO=1) possesses the highest absolute electrophoretic mobility value of -3.09 μmcm/Vs when examining the effect of different reaction temperature to the stability of RGO suspensions. Meanwhile, low absolute electrophoretic mobility value of N_2H_4-RGO was recorded (-1.21 μmcm/Vs) which reflecting the instability and high agglomeration of N_2H_4-RGO suspension, in agreement with the result from zeta potential measurement. As evidenced from the zeta potential and electrophoretic mobility measurements, a stable RGO suspension could be prepared by reducing GO at 90 ℃ using a weight ratio of GTP/GO=1.

4.4 Cytotoxicity Evaluation of Graphene Oxide (GO) and Reduced Graphene Oxide (RGO)

Graphene has attracted enormous attentions to be used in a wide variety of applications especially for biomedical applications due to its unique structural characteristics and intriguing physicochemical properties which are relevant to biological effects (Sanchez et al., 2012; Zhang et al., 2010b). The remarkable properties of graphene have drawn significant interests from researchers to investigate its interactions with microorganisms and biological cells in order to fulfill its exciting potential in biomedical applications (Hu et al., 2010). Despite the aforementioned promising potential of graphene in biomedical applications, its potential toxicity, biocompatibility and interactions with living cells in biological systems are yet to be fully understood (Chen et al., 2008b; Sanchez et al., 2012; Wojtoniszak et al., 2012). A number of factors particularly the concentration of GO and graphene have been suggested to significantly affect the toxicity behavior of GO and graphene toward bacteria, mammalian cells and other living cells in biological system (Wang et al., 2011a).

Herein, the cytotoxicity of GO and RGO suspensions were evaluated against CCD-18Co cells lines by inoculating and exposing the cells to different concentrations of GO and RGO samples ranging from 6.25 to 200 µg/mL. Drawing from the results of the UV-Vis spectroscopy, FTIR, TGA and zeta potential measurement, the reduction temperature of 90 ºC and weight ratio of GTP/GO=1 were concluded to be the best conditions for the GO reduction in which most of the oxygen functionalities were eradicated from GO and highly stable RGO suspension was prepared at these reduction conditions. Hence, the RGO suspension prepared at 90 ºC using weight ratio of GTP/GO=1 (RGO-9) was selected for cytotoxicity

evaluation towards CCD-18Co cells lines. Meanwhile, the RGO suspension prepared using weight ratio of GTP/GO=5 (RGO-5) was also subjected to cytotoxicity testing in order to investigate the effect of the incorporation of higher amount of GTP on the toxicological behavior of RGO suspension.

The effect of different concentrations of GO, RGO and GTP samples on the metabolic activity of CCD-18Co cells line was shown in Figure 4.12. For GO, RGO-9 and RGO-5 samples, the MTT assays reveal that the percentage inhibition of cell proliferation was increased with the increasing concentration of the test samples. As been depicted in Figure 4.12, the GO sample inhibits almost 50 % of the CCD-18Co cells proliferation even at the lowest concentration (6.25 µg/mL). This indicates that the GO is toxic towards CCD-18Co cells (Kim et al., 1998; Liao et al., 2011a; Wang et al., 2011a). However, at the concentration of 6.25 µg/mL, the percentage inhibition of cell proliferation of RGO-9 was reduced significantly as compared to the GO. The decrease of the toxicological effect of RGO-9 may be due to the incorporation of GTP in the RGO suspension. The MTT assay shows that the percentage inhibition of cell proliferation of RGO-5 was lower than RGO-9 at similar concentration of 6.25 µg/mL. This shows that the incorporation of higher amount of GTP resulted in further decrease of the toxicity of RGO samples. This was further supported by the zero percentage inhibition of cell proliferation of GTP sample at concentration of 6.25 µg/mL, which suggesting the non-toxicological effect of GTP and its ability to reduce the toxicity effects of RGO samples. Despite the promising results of RGO-9 and RGO-5 at low concentration (6.25 µg/mL), the percentage inhibition of cell proliferation (45-60 %) of these RGO samples at higher concentrations (100 and 200 µg/mL) indicate slightly toxic effects. Nevertheless, the toxicological effects of RGO at higher concentration could be reduced by adding

113

biocompatible materials including PEG, PTCA, chitosan and PEI in the RGO suspension (Feng et al., 2011a; Feng et al., 2011b; Yang et al., 2010a; Yang et al., 2010b).
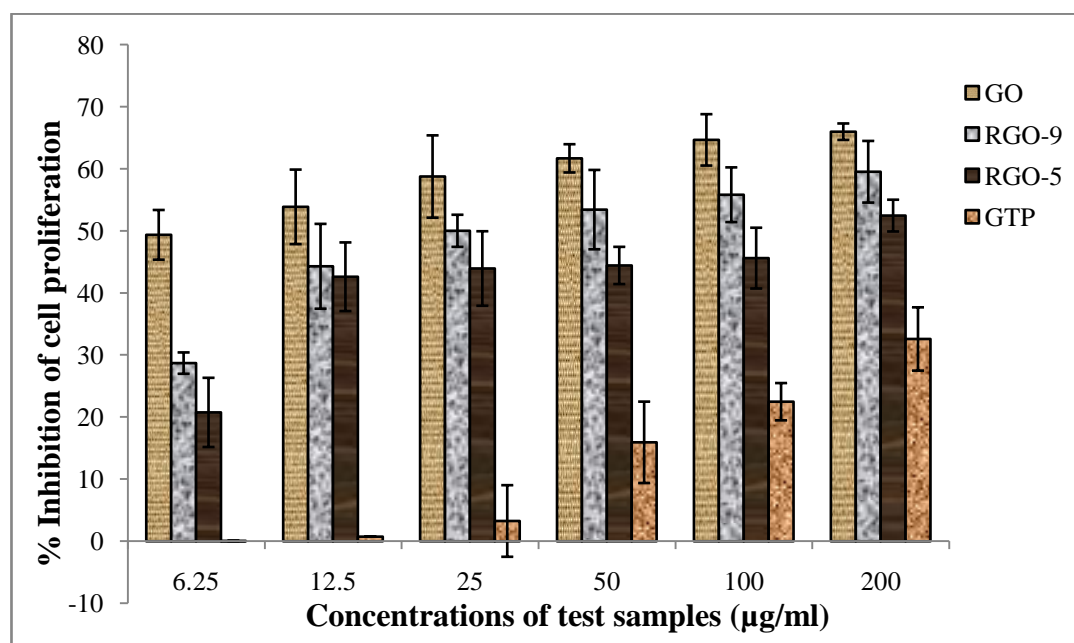
Figure 4.12: Effect of different concentrations (6.25-200 µg/mL) of GO, RGO-9, RGO-5 and GTP samples on the metabolic activity of CCD-18Co cells line as measured using MTT assay. The data were presented as means ± standard deviations with probability value, p <0.05 (each sample was examined in triplicate (n = 3)).

Figure 4.13(a-e) portrays the micrograph images of the untreated CCD-18Co cells and the cells line after 48 hours treatment with GO, RGO-9, RGO-5 and GTP samples at the concentration of 6.25 µg/mL, respectively. As been shown in Figure 4.13(a), the untreated cells from the control group show the normal features of healthy CCD-18Co cells line (Kim et al., 1998). Meanwhile, the morphology of the CCD-18Co cells line was distorted post treatment with GO at concentration of 6.25 µg/mL as illustrated in Figure 4.13(b). This reveals the significant inhibition in cell proliferation after treatment with GO even at low concentration (6.25 µg/mL). From Figure 4.13(c), the morphology of the cells was slightly distorted as compared to the

untreated cells. This indicates that the RGO-9 possesses slightly toxic effect towards CCD-18Co cells line at low concentration (6.25 µg/mL).
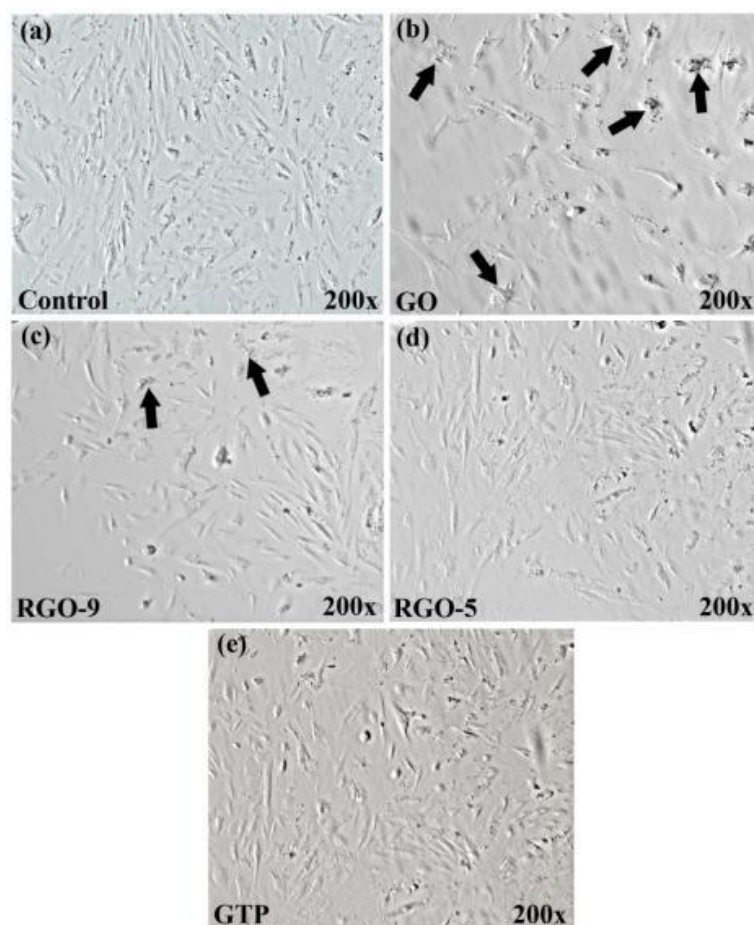
Figure 4.13: Micrograph images of CCD-18Co cells line after 48 hours treatment with the samples; (a) control cells, (b) GO, (c) RGO-9, (d) RGO-5 and (e) GTP. All images were taken under an inverted phase-contrast microscope at 200x magnification. The arrows show the location of the distorted cells line.

In the meantime, the cellular morphologies and populations of the cells treated with RGO-5 and GTP samples were almost similar to that of the control group as shown in Figure 4.13(d) and Figure 4.13(e), respectively. These indicate that the RGO-5 and GTP samples exhibit non-toxic effects towards CCD-18Co cells line at low concentration. The MTT assay and the micrograph images have revealed that the GO possesses toxic effect towards CCD-18Co cells line even at low

concentration (6.25 μg/mL). However, the toxicological effects of RGO-9 and RGO-5 were significantly reduced at low concentration (6.25 μg/mL) possibly due to the incorporation of GTP in the RGO suspension. The result from the cytotoxicity testing have shown that the GTP possesses the ability to reduce the toxicological effect of RGO in addition to its efficient reductive property in GO reduction, making GTP as the most effective reducing agent in GO reduction to produce the non-toxic RGO with views for future applications in biomedical field. Although the results from the cytotoxicity testing of RGO samples are promising at low concentration (6.25 μg/mL), the toxicological effect of RGO at higher concentrations (100-200 μg/mL) remains an issue. More intensive in vitro and in vivo studies were needed to be carried out in order to fully understand the interactions between the RGO and the living cells in biological system before any clinical applications could be realized.

4.5 Mechanism of Graphene Oxide (GO) Reduction by Green Tea Polyphenol (GTP)

The successful reduction of GO has been achieved through the employment of GTP as the reducing agent in the reduction reaction, as evidenced from the results of UV-Vis spectroscopy, FTIR and TGA analyses (section 4.2.1, 4.2.2 and 4.2.3). In addition, the results from the UV-Vis spectroscopy and XPS analysis (section 4.2.4) have shown that the reduction efficiency of GTP is comparable to the efficiency of N_2H_4 solution, which is widely regarded as the most effective reducing agent for the reduction of GO (Akhavan et al., 2012; Wang et al., 2011c). However, in order to further improve the efficiency of the reduction process, it is highly important to fully understand the reduction mechanism of GO. Therefore, the possible mechanism of the GO reduction by GTP was investigated using Gaussian 09 and GaussView 5

programs. All of the input and output structures were modeled using GaussView 5

program while all calculations involving the structures and energies were computed

using Gaussian 09 program. The structures of all the reactants (i.e., GO with epoxide

group and GTP (EGCG)) and products (i.e., RGO, galloyl-derived orthoquinone and

water (H$_2$O)) that involved in the GO reduction reaction were illustrated

schematically in Figure 4.14. In addition, all the structures of the reactants and the

products were modeled using GaussView 5 program (Figure 4.15) and these

structural models were used for geometry optimization and frequency calculation in

Gaussian 09 program.
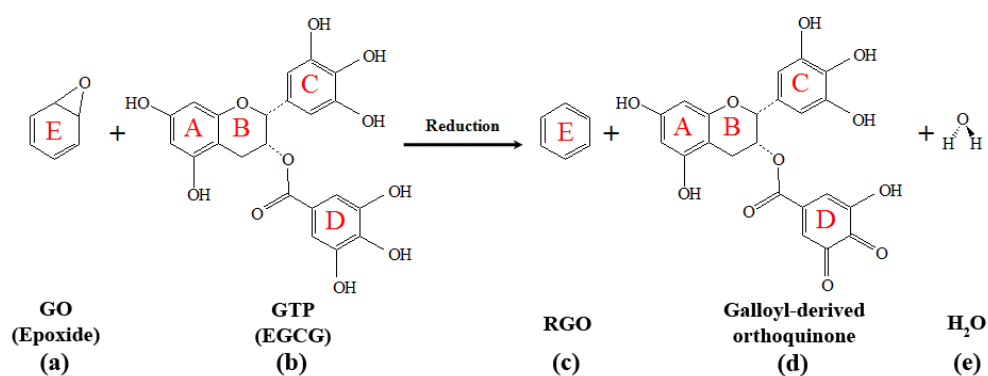
Figure 4.14: Schematic illustration of the structures of the reactants; (a) GO with epoxide group, (b) EGCG and the products; (c) RGO, (d) galloyl-derived orthoquinone, (e) H$_2$O that involved in the GO reduction reaction.
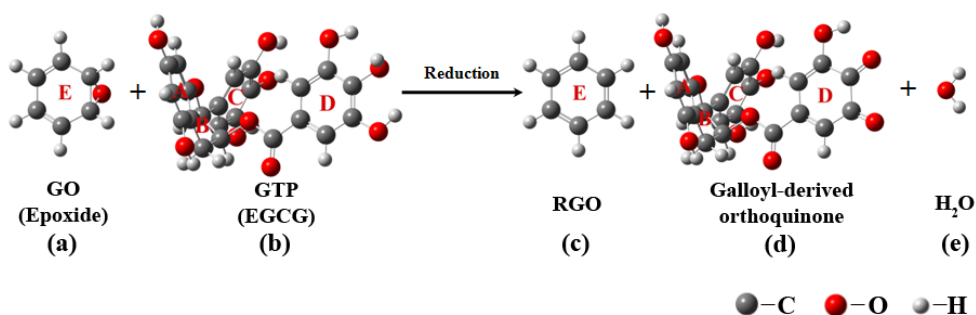
Figure 4.15: Structural models of the reactants; (a) GO with epoxide group, (b) EGCG and the products; (c) RGO, (d) galloyl-derived orthoquinone, (e) H$_2$O constructed using GaussView 5 program.

117

Most of the oxygen functionalities in GO were occurred in form of epoxy and hydroxyl groups as been shown from the solid state ^{13}C NMR and Raman spectra in previous studies (Cai et al., 2008; Kudin et al., 2008; Lerf et al., 1998). Additionally, numerous theoretical studies (Jelea et al., 2004; Kim et al., 2009b; Li et al., 2006) also have shown that most of the oxygen atoms were adsorbed above the C-C bond across the basal plane of graphite to form epoxy groups during the oxidation of graphite. Hence, the GO was modeled as a fragment of graphene sheets decorated with epoxy group as portrayed in Figure 4.14(a) and Figure 4.15(a). Meanwhile, EGCG was reported to be the most potent catechin in GTP (Chen et al., 2008a). Thus, the structure of EGCG was used to represent GTP in this computational study. The structure of EGCG is very complex and generally, composes of two major units namely flavonoid unit (ring A and ring B) and gallic acid unit (ring C and ring D) (Chen et al., 2008a; Mukhtar and Ahmad, 2000) as illustrated in Figure 4.14(b) and Figure 4.15(b). Liao et al. (2011b) have suggested that the gallic acid unit particularly ring D possesses the capability to donate electrons or hydrogen atoms easily. Since the EGCG was donating the hydrogen atoms, it is said to be oxidized (Valcic et al., 2000). The oxidation of EGCG was reported to generally yield galloyl-derived orthoquinone, in which its structure was shown as in Figure 4.14(d) and Figure 4.15(d) (Liao et al., 2011b; Valcic et al., 2000; Zhu et al., 2000). In this computational study, the reduction of GO was represented by the removal of epoxy group from the GO structure through the transfer of hydrogen atoms from the gallic acid unit (ring D) in EGCG. As the hydrogen atoms were transferred from ring D, the other structures in EGCG (ring A, ring B and ring C) were denoted as R for simplification in illustration purpose (Figure 4.16).
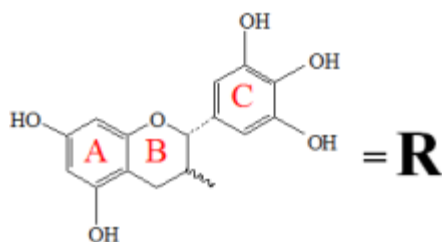
Figure 4.16: The flavonoid (ring A and ring B) and gallic acid (ring C) structures in EGCG were denoted as R for simplification.

In this work, all the calculations including optimization, locating transition structures and frequency analysis were computed using hybrid DFT method (B3LYP) which was incorporated within the Gaussian 09 program. Zhang and Xia (2011) have reported that the B3LYP hybrid functional is accurate in calculating the energy of the oxygen reduction reaction (ORR) on nitrogen-doped graphene. In addition, the B3LYP hybrid functional has attracted increasing attention from researchers to be used in computational study due to its significantly greater accuracy as compared to the other methods including semi-empirical method and HF method (Becke, 1993; Foresman and Frisch, 1996; Lee et al., 1988). The B3LYP hybrid functional possesses higher accuracy because the effects of electron correlation were included in this model (Becke, 1993; Lee et al., 1988). Therefore, the B3LYP hybrid functional was selected to be used as the computational method in this work. Meanwhile, the B3LYP method was used in combination with the 3-21G basis set. A basis set is the mathematical description of the orbitals within a system and it is used to perform the theoretical calculation (Foresman and Frisch, 1996). In general, the employment of larger basis set resulted in more accurate approximation to the solution. However, more accurate calculations will take significantly longer calculation time and require high-performance computational setup. Hence, the 3-21G basis set was employed in this work due to its reasonably

accurate representation of orbitals and practically feasible calculation time (Binkley et al., 1980; Li and Zhang, 2008).

Figure 4.17 shows the atomic structures for stationary points involved in the reduction of GO by using GTP (EGCG). A stationary point is referred to a point on the PES where the forces of the molecular system are zero (Foresman and Frisch, 1996). A stationary point could be either a local minima or a saddle point. Local minimum is the lowest point in some limited region of the PES in which this local minimum was occurred at equilibrium structures of a molecular system. On the other hand, the saddle point is a point which is a maximum in one direction and a minimum in the other direction (Foresman and Frisch, 1996). The saddle point corresponds to a TS structure which connects two equilibrium structures (Foresman and Frisch, 1996). The stationary point structure of a molecular system was predicted using geometry optimization tool which was incorporated within Gaussian 09 program. All the optimization calculations were computed at B3LYP/3-21G level of theory. As been shown in Figure 4.17, one intermediate structure and two TS structures were involved in the reduction mechanism of GO. All the reactant, product and intermediate are local minima while the TS is the saddle point that connects two equilibrium structures (local minima). The equilibrium structures of the reactant (GO with epoxide group and EGCG) were shown as in Figure 4.17(a). The EGCG (ring D) attacks the sp^2 carbon located at the meta position of epoxide in GO (ring E). One hydrogen atom was transferred from ring D to the oxygen atom of the epoxide group. In the meantime, the GO rotates in a rotatory mode and causes the epoxide group to revolve from the upper side to the lower side (as indicated by red arrow). The transfer of the hydrogen atom initiates the ring opening of epoxide group and led to the formation of hydroxyl group as shown in Figure 4.17(b). The

C-O-C bond between ring D and ring E is formed, yielding the intermediate structure as portrayed in Figure 4.17(c). As illustrated in Figure 4.17(d), another hydrogen atom is transferred from ring D to the hydroxyl group while the C-O-C bond between ring D and ring E is broken. This led to the formation of the product (RGO, galloyl-derived orthoquinone and a H_2O molecule) as shown in Figure 4.17(e).
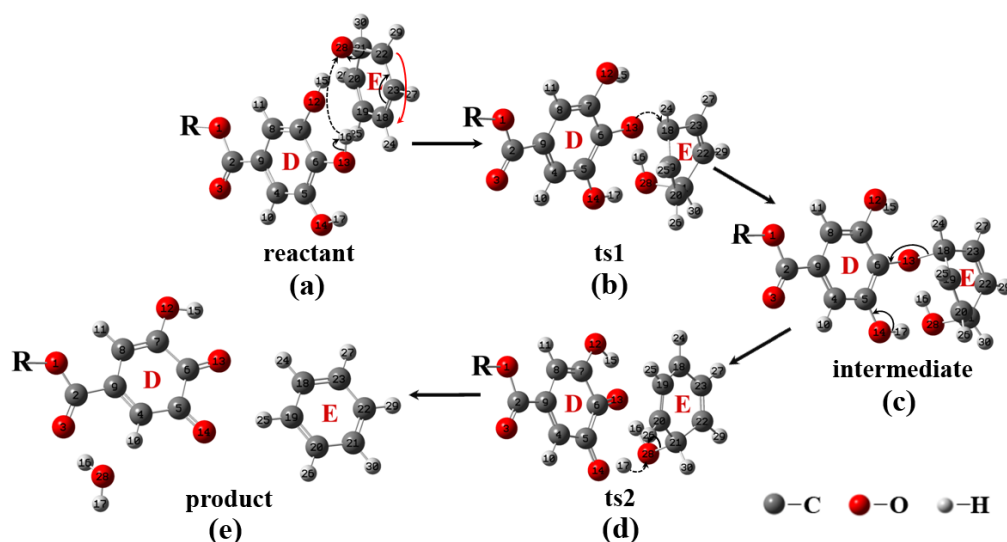
Figure 4.17: The atomic structures for stationary points involved in the reduction of GO by using GTP.

Meanwhile, Figure 4.18 shows the atomic structures for stationary points involved in the reduction of GO by using N_2H_4 solution. The equilibrium structures of the reactant (GO with epoxide group and N_2H_4 solution) were shown as in Figure 4.18(a). N_2H_4 attacks the sp^2 carbon nearest to the epoxide group from backside and transfers one hydrogen atom to the epoxide group, resulted in the initiation of ring opening of epoxide group and the formation of hydroxyl group as illustrated in Figure 4.18(b). The hydrazino group (-HNNH_2) was attached to the ring E and formed intermediate structure as illustrated in Figure 4.18(c). Another hydrogen atom was transferred from the hydrazino group to the hydroxyl group as shown in

121

Figure 4.18(d). The transfer of the hydrogen atom from the hydrazino group to the hydroxyl group yields N_2H_4-RGO, cis-diazene (N_2H_2) and a H_2O molecule as the product as portrayed in Figure 4.18(e). The reduction mechanism of GO by using N_2H_4 solution predicted in this work was found to be similar to the reaction mechanism of N_2H_4 de-epoxidation as reported by Gao et al. (2010b).
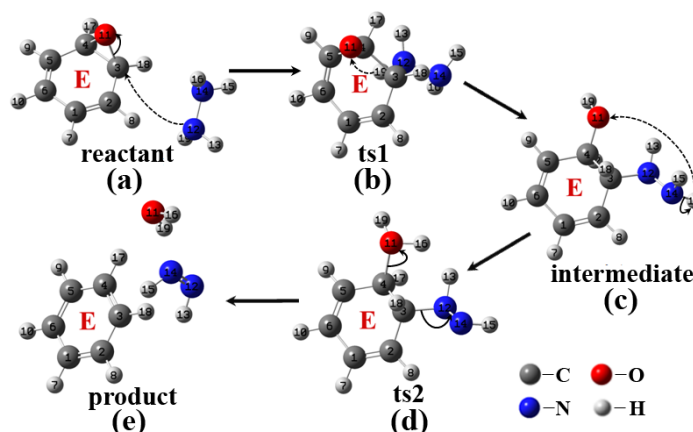
Figure 4.18: The atomic structures for stationary points involved in the reduction of GO by using N_2H_4 solution.

On the other hand, the thermodynamic quantities (i.e., ΔH, ΔG and ΔS) of the stationary points were calculated using frequency analysis tool which incorporated within Gaussian 09 program. As evidenced from the results of UV-Vis spectroscopy, FTIR and TGA analyses, the weight ratio of GTP/GO=1 and the reduction temperature of 90 ℃ were concluded as the best conditions for the GO reduction using GTP (section 4.2.1, 4.2.2 and 4.2.3). In order to compare the reduction efficiency of GO using GTP with that of N_2H_4 solution, the GO was also reduced using N_2H_4 solution at similar conditions (i.e., weight ratio of N_2H_4/GO=1 and reduction temperature of 90 ℃). Since both of the GO reduction using GTP and N_2H_4 solution were performed at 90 ℃, the frequency analyses for both of these systems were carried out at 90 ℃ and 1 atm of pressure, as well as using the principal isotope for each element type. The frequency calculations are valid only at

stationary points on the PES due to the nature of the computations involved (Foresman and Frisch, 1996). Hence, the frequency calculations must be performed on the optimized structures. Since all the optimizations calculations were computed at B3LYP/3-21G level of theory, thus, all the frequency calculations were also performed at the same level of theory. Table 4.3 shows the ΔH, ΔG and ΔS for all the stationary points involved in the reduction of GO by using GTP and N_2H_4 solution at 90 ºC. From Table 4.3, the ΔH for the GO reduction using GTP and N_2H_4 solution are -14.053 kcal/mol and -16.021 kcal/mol, respectively. The nature of a reaction could be determined from the sign of ΔH. Both of the GO reduction reactions using GTP and N_2H_4 solution are exothermic since both the ΔH of these reactions have negative sign. In other words, heat or energy is released from the GO reduction reaction using GTP and N_2H_4 solution.

Table 4.3: Reaction enthalpies, ΔH (kcal/mol), Gibbs free energies, ΔG (kcal/mol), and entropies, ΔS (kcal/mol·K) for stationary points involved in the reduction of GO by using GTP and N_2H_4 solution at 90 ºC. All of the thermodynamic quantities were calculated at the theory level of B3LYP/3-21G.

	GO + GTP			GO + N_2H_4 solution		
	ΔH	ΔG	ΔS	ΔH	ΔG	ΔS
reactant	0.000	0.000	0.000	0.000	0.000	0.000
ts1	9.204	36.096	-0.074	26.174	41.354	-0.042
intermediate	-35.020	-16.773	-0.050	-30.916	-16.193	-0.041
ts2	9.228	36.107	-0.074	68.122	83.499	-0.042
product	-14.053	-28.132	0.039	-16.021	-28.860	0.035

In the GO reduction reaction, energy must be supplied to the system to break the chemical bonds (e.g., ring opening of epoxide group and break of bond to transfer hydrogen atom from GTP or N_2H_4 solution to the epoxide group), in which this energy was supplied from the heat treatment (performing the reduction reaction

at 90 ℃). In addition, energy was also released due to the bond formation. In the GO reduction reaction using GTP and N_2H_4 solution, the energy released by bond formation is higher than the energy required to break the chemical bonds, which elucidates the exothermic nature of these reactions. For comparison, the GO reduction using N_2H_4 solution (-16.021 kcal/mol) releases higher amount of energy as compared to the reduction using GTP (-14.053 kcal/mol). As the H is a state function, its property depends only to the initial (reactant) and final states (product). Hence, due to this reason, only the ΔH of reactant and product were discussed in this section. All the values of thermodynamic quantities for reactant were zero since all the values of thermodynamic quantities for other stationary points were defined based on the values of the reactant.

Meanwhile, the ΔS for the GO reduction using GTP and N_2H_4 solution are 0.039 kcal/mol·K and 0.035 kcal/mol·K, respectively. S is also a state function in which it depends only on the initial and final state of the system, regardless of the path by which the changes take place (Keszei, 2012). A spontaneous process has a tendency for the S to increase. The GO reduction reaction using GTP has higher ΔS (0.039 kcal/mol·K) than the reduction reaction using N_2H_4 solution (0.035 kcal/mol·K) in which this indicates that the GO reduction using GTP is more spontaneous and more favorable to occur as compared to the GO reduction using N_2H_4 solution. On the other hand, the reaction energy profiles for the reduction of GO using GTP and N_2H_4 solution were shown in Figure 4.19. From Table 4.3 and Figure 4.19, the step change from the intermediate to ts2 is the rate-determining step for both the GO reduction reactions using GTP and N_2H_4 solution (Gao et al., 2010b). This step has G barrier of 52.880 kcal/mol and 99.692 kcal/mol for the GO reduction using GTP and N_2H_4 solution, respectively. The rate-determining step is

the mechanism step with the greater energy barrier (i.e., the slowest step) and thus, this step has the greatest influence on the reaction rate (Gao et al., 2010b; Müller and Müller, 2009). Since the G barrier of GO reduction using GTP is lower than that of N_2H_4 solution, hence, the GO reduction reaction using GTP is more efficient and it is relatively takes place faster than the GO reduction using N_2H_4 solution. The predicted results of the thermodynamic quantities from the frequency analyses suggest that the GTP is a more efficient reducing agent than the N_2H_4 solution for the reduction of GO.
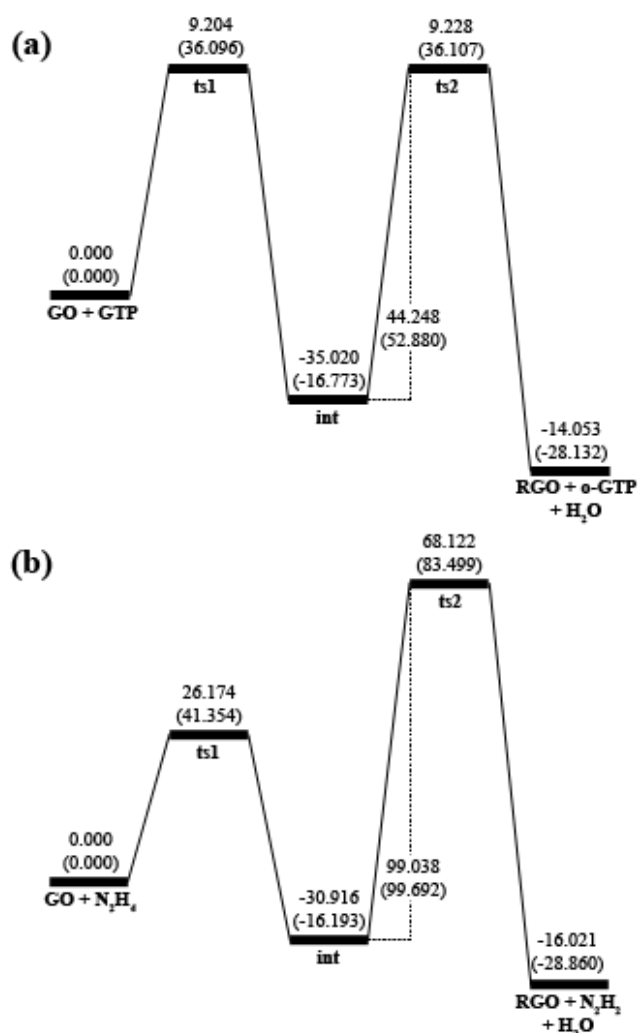
Figure 4.19: Reaction energy profiles for the reduction of GO using (a) GTP and (b) N_2H_4 solution calculated at the theory level of B3LYP/3-21G. The values of ΔH (kcal/mol) and ΔG (kcal/mol) at 90 °C were shown in normal typefaces without and with parentheses, respectively.

4.6 Fabrication of Graphene Films (GFs) using Electrophoretic Deposition (EPD)

4.6.1 Deposition of Reduced Graphene Oxide (RGO) Particles on Stainless Steel (SS) Substrate

Most of the exciting applications of graphene particularly in biomedical field require a uniform growth of graphene layers on a substrate in large scale (Choi et al., 2010b; Park and Ruoff, 2009). Herein, the EPD process was proposed as the most promising technique to develop the graphene layers on the type 316L SS substrate from the RGO suspension. The as-developed graphene layers on the SS substrate were referred as the GFs. In this research project, the type 316L SS was chosen as the substrate primarily due to its cost effective as well as its reasonable biocompatibility, tensile strength, corrosion resistance and suitable density for load-bearing purposes. The aforementioned characteristics make the type 316L SS as one of the desired materials for biomedical applications especially as temporary metal implant (Balamurugan et al., 2008; Kamachi Mudali et al., 2003). It is imperative to prepare a well-dispersed and stable RGO suspension prior EPD process in order to yield uniform and homogeneous RGO deposits. Drawing from the result of the zeta potential measurement, the RGO suspension prepared at 90 ℃ using weight ratio of GTP/GO=1 (RGO-9) possesses the highest absolute zeta potential value of -39.43 mV which indicates the high stability of the suspension. Therefore, the suspension of RGO-9 was selected to be used for all EPD experiments.

After EPD process, the deposition of RGO particles was observed to occur on the anode. The migration of the negatively charged particles of RGO towards the positive electrode was illustrated schematically as in Figure 4.20. The movement of

126

the negatively charged particles of RGO to the electrode of opposite charge was taken place only after the direct current (DC) voltage was applied. This is the first step of EPD process (electrophoresis). In the second step, the migrated RGO particles coagulate and deposit on the anode to form GFs (deposition). The deposition of RGO particles may be induced by the electrochemical coagulation process as suggested by De and Nicholson (1999). In RGO suspension, the electrochemical reactions took place at both the anode and cathode during the EPD process due to the presence of water. As a result, the ionic strength is getting higher at the electrode surface which in turn reduces the repulsive forces between RGO particles near the electrode (anode) surface. This led to the decrease of the zeta potential of RGO particles that close to the anode and ultimately, resulted in the precipitation of RGO particles onto the anode surface.
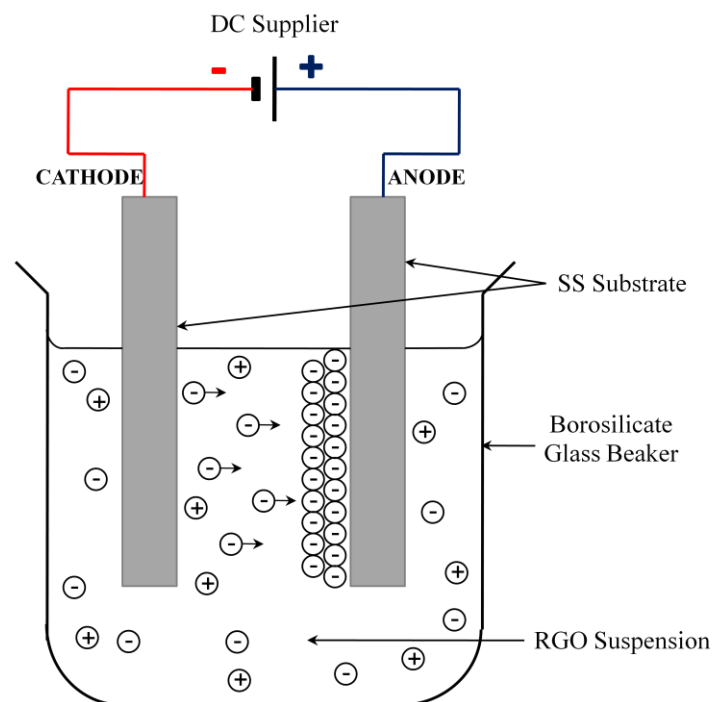
Figure 4.20: Schematic diagram of EPD cell demonstrating the movement of negatively charged particles of RGO towards the positive electrode.

4.6.2 Effect of Electrophoretic Deposition (EPD) Parameters on the Deposition Weight, Uniformity and Thickness of Graphene Films (GFs)

The variation of the deposition weight and the thickness of GFs were depended on a number of factors including the applied voltage, deposition time and the concentration of RGO suspension. However, only the effects of the applied voltage and deposition time were investigated since the concentration of RGO suspension was fixed at 0.3 mg/mL for all EPD experiments. In the section of GO reduction (Section 4.2), GO suspension with constant concentration at 0.3 mg/mL was prepared prior to the reduction reaction while the concentration of the as-produced RGO suspension was also maintained at 0.3 mg/mL. Hence, RGO suspension with constant concentration at 0.3 mg/mL was used for all EPD experiments. Figure 4.21(a) and Figure 4.21(b) show the variation of deposition weight of GFs on anode as a function of applied voltage and deposition time, respectively. Initially, the effect of applied voltage was first examined by applying voltage ranging from 10-50 V at fixed deposition time of 500 s and the result was shown as in Figure 4.21(a). The variation of applied voltage has a substantial effect on the efficiency of EPD and the uniformity of the deposits. In this work, the applied voltage ranging from 10-50 V was selected in order to investigate the effects of different amount of electric field and the possible generation of gas bubbles on the deposition weight and the uniformity of GFs. Drawing from the result obtained as in Figure 4.21(a), the GFs samples arranged in an increasing order according to their deposition weights were GFs-10V/500s < GFs-50V/500s < GFs-40V/500s < GFs-20V/500s < GFs-30V/500s.
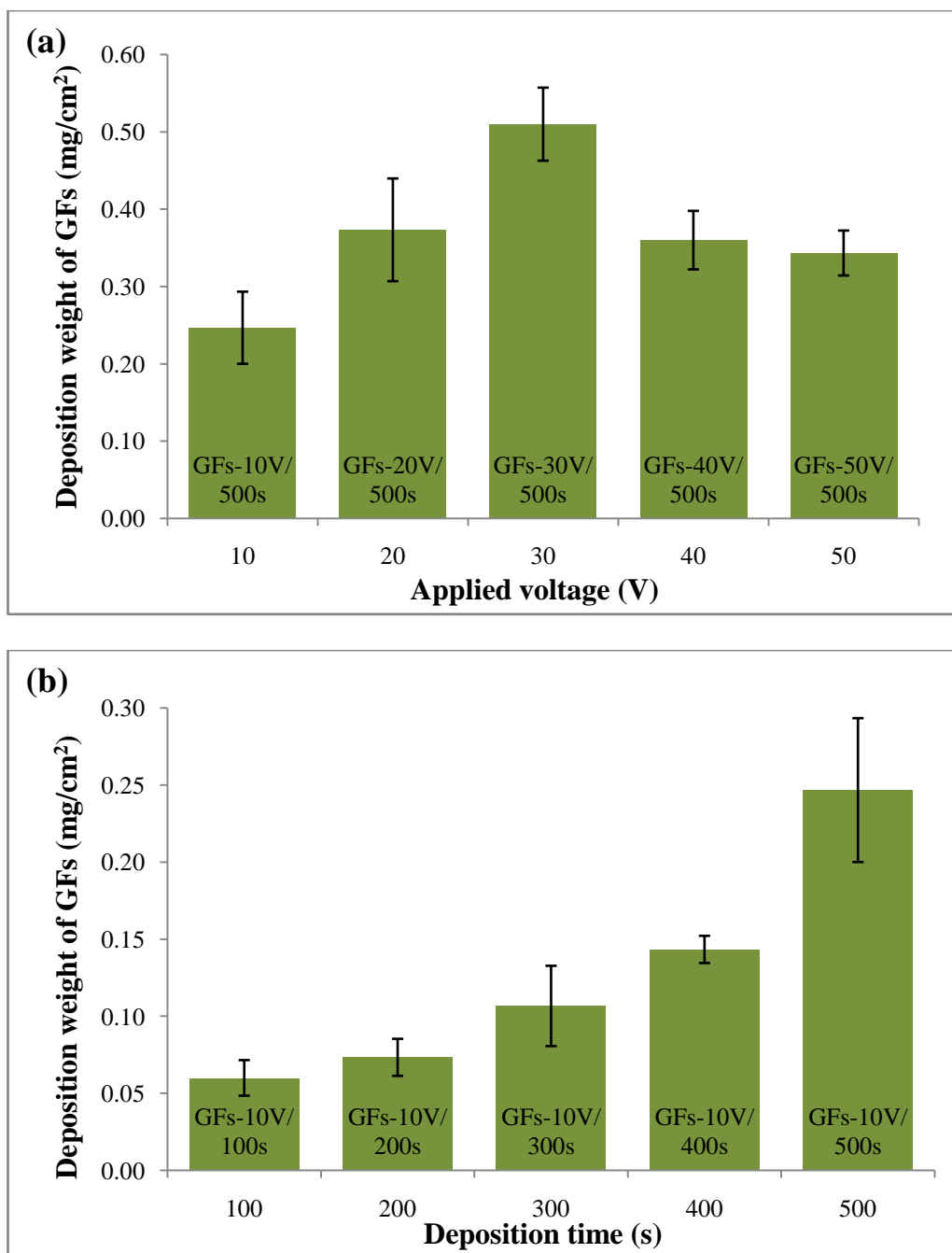
Figure 4.21: Variation of deposition weight of GFs on anode as a function of (a) applied voltage and (b) deposition time in EPD process. For every different applied voltage and deposition time, the EPD process was performed in triplicate (n = 3) at pH=7.

As can be observed from Figure 4.21(a), the deposition weight of GFs was increased with the increasing applied voltage from 10-30 V. This observation was in agreement with the Hamaker equation (Eq. (3.1)) which was widely used to analyze the EPD process in planar geometries (Hamaker, 1940). Since all the RGO

suspension properties (i.e., solid loading and electrophoretic mobility) and the deposition time were held constant, the deposition weight of GFs was increasing proportionally with the electric field (applied voltage). This elucidates the observation from Figure 4.21(a) for the applied voltage of 10-30 V.

However, the deposition weight of GFs was decreased when higher voltages of 40 V and 50 V were applied. The decrease of the deposition weight of GFs at higher voltages (40 V and 50 V) may due to peel-off during the removal of the samples after EPD process. At higher voltages, the deposited GFs may consist of two layers. The outer layer of the GFs may have weaker deposition bonding as compared to the inner layer. As a result, the outer layer of the GFs was peeled-off during the removal of the sample from the borosilicate beaker. Ultimately, this resulted in the decrease of the deposition weight of GFs fabricated at applied voltage of 40 V and 50 V. Apart from reducing the deposition weight of GFs, the outer layer that was peeled-off also resulted in the formation of voids and pores on the surface of the GFs. In addition, the use of higher voltage may also generate the emission of gas bubbles at the anode. The emission of gas bubbles also contribute to the formation of pores and voids on the surface of the GFs as can be observed from the optical and SEM images. The pores also can be observed on the surface of GFs prepared using applied voltage of 30 V which indicates the formation of gas bubbles at this voltage. However, the amount of the gas bubbles generated may be less than those formed at 40 V and 50 V, which may resulted in insignificant effect to the electrophoresis of the RGO particles as evidenced by the high deposition weight of GFs prepared at the applied voltage of 30 V.

Although the highest deposition weight of GFs was obtained when the applied voltage of 30 V was used, the GFs prepared at this applied voltage (GFs-

30V/500s) possess non-uniform morphology with large voids and pores as can be seen from the optical and SEM images in Figure 4.22(c) and Figure 4.23, respectively (this will be discussed in the next paragraph). Among the five different applied voltages that been investigated, the uniform GFs with no voids or pores could be obtained when the applied voltage of 10 V was used since the generation of gas bubbles was minimum at this applied voltage. Therefore, the applied voltage of 10 V was held constant when the effect of the deposition time on the thickness and the deposition weight of the GFs were investigated. From Figure 4.21(b), the GFs samples arranged in a decreasing order according to their deposition weights were GFs-10V/500s > GFs-10V/400s > GFs-10V/300s > GFs-10V/200s > GFs-10V/100s. This observation was consistent with the Hamaker equation (Eq. (3.1)) which has been described in section 3.2.3. As the suspension properties (i.e., solid loading and electrophoretic mobility) were held constant and the applied voltage was fixed (10 V), the deposition weight of GFs was decreased with the decreasing deposition time. Initially, the deposition of the RGO particles on the SS substrate was conducted for 500 s. This resulted in the production of GFs with thickness of ~430 nm (this will be discussed further in the next paragraph). Hence, the deposition time was reduced from 500 s to 100 s in order to demonstrate that very thin GFs (less than 400 nm) could be developed by varying the deposition time.

The optical images of GFs prepared at constant deposition time of 500 s using different applied voltage of 10 V, 20 V, 30 V, 40 V and 50 V were portrayed in Figure 4.22(a-e), respectively. As illustrated in Figure 4.22(a), the GFs prepared using applied voltage of 10 V (GFs-10V/500s) possess uniform morphology without any voids or pores. This was due to the minimum generation of gas bubbles at applied voltage of 10 V. In contrast, all the GFs prepared using applied voltage of 20

V, 30 V, 40 V and 50 V were not uniform and contain voids and pores as illustrated in Figure 4.22(b) to Figure 4.22(e), respectively. At higher voltages (40 V and 50 V), the non-uniform GFs and the formation of voids and pores might be due to peel-off during the removal of the sample, as been discussed earlier. In addition, the formation of voids and pores also might be contributed by the higher generation of gas bubbles at the applied voltage of 20 V, 30 V, 40 V and 50 V. As been discussed in the previous paragraph, the GFs produced using applied voltage of 30 V (GFs-30V/500s) were not uniform and contain large voids and pores despite possessing the highest deposition weight. Thus, the GFs-30V/500s sample was further inspected using SEM analysis in order to observe the surface morphology of the sample at higher magnification. The SEM images of the surface at low (5000x) and high magnification (30,000x) as well as the cross section view of the GFs-30V/500s sample were illustrated in Figure 4.23(a-c), respectively. From Figure 4.23(a) and Figure 4.23(b), the non-uniform surface morphology of the GFs-30V/500s sample was observed in which there are some parts of the SS substrate that were not covered by the RGO particles due to the formation of gas bubbles. The GFs-30V/500s sample also possesses non-uniform thickness as observed from the cross-section view in Figure 4.23(c).
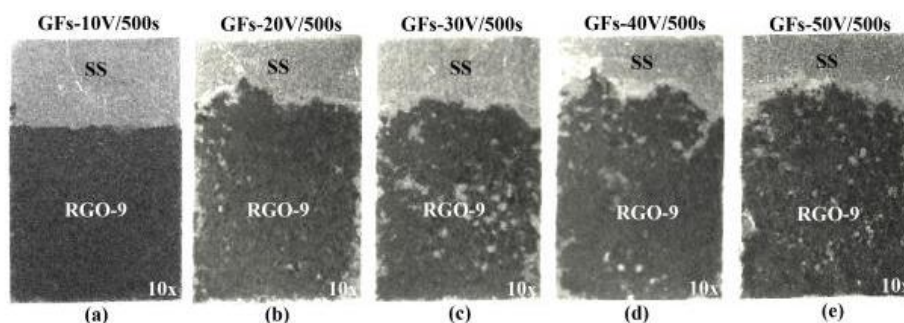
Figure 4.22: Top view optical images of GFs on anode prepared at constant deposition time of 500 s using different applied voltage of (a) 10 V, (b) 20 V, (c) 30 V, (d) 40 V and (e) 50 V. All images were taken at 10x magnification.

132
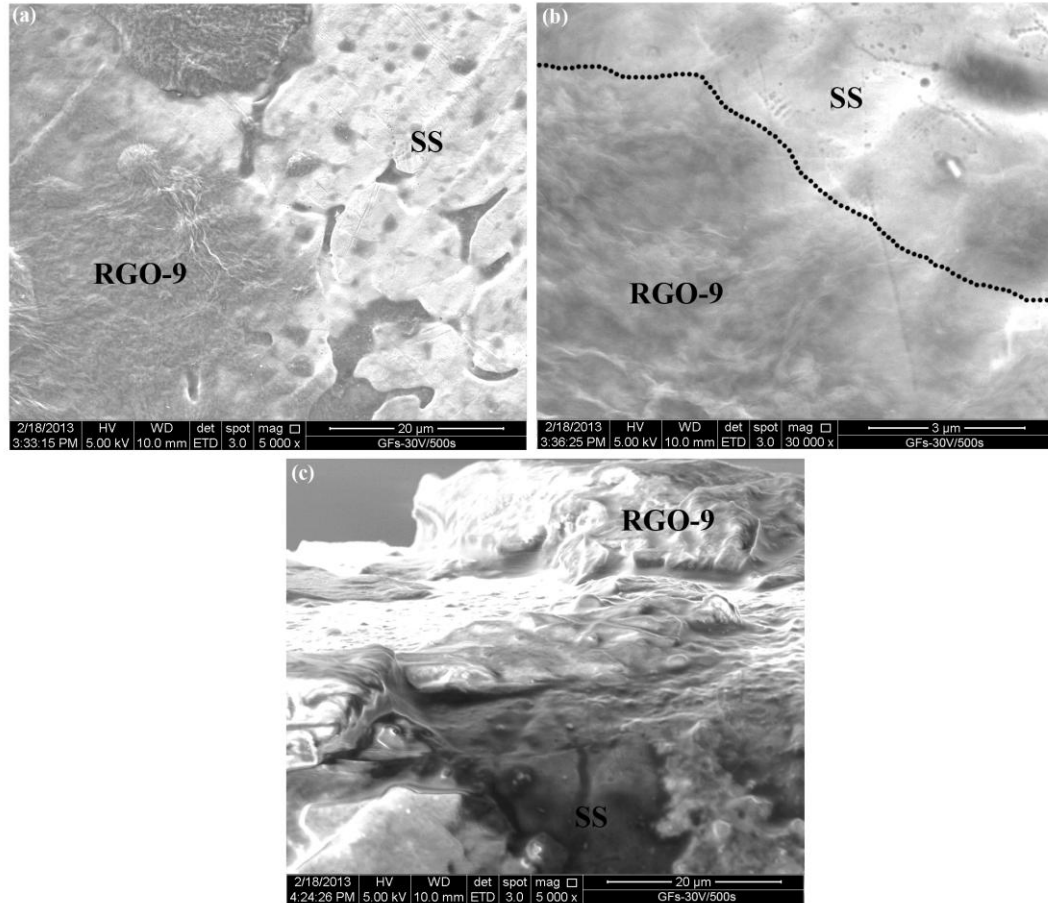
Figure 4.23: SEM images of the surface at (a) low (5000x) and (b) high magnification (30,000x) as well as (c) the cross-section view of the GFs-30V/500s sample on anode.

The optical images of GFs produced using constant voltage of 10 V at deposition time of 100 s, 200 s, 300 s, 400 s and 500 s were shown in Figure 4.24(a-e), respectively. Non-uniform surface morphology of GFs was observed with some parts of the SS substrate were not covered by the RGO particles when the GFs were prepared at deposition time of 100 s (GFs-10V/100s) and 200 s (GFs-10V/200s) as illustrated in Figure 4.24(a) and Figure 4.24(b), respectively. At very short deposition time (100 s and 200 s), there are less amount of RGO particles that could migrated and deposited on the SS substrate, resulted in the non-uniform surface morphology of the GFs-10V/100s and GFs-10V/200s samples. On the contrary, the

GFs prepared at deposition time of 300 s, 400 s and 500 s possess uniform morphology without any voids or pores as can be observed in Figure 4.24(c-e), respectively, in agreement with the observation of Wu et al. (2009a).
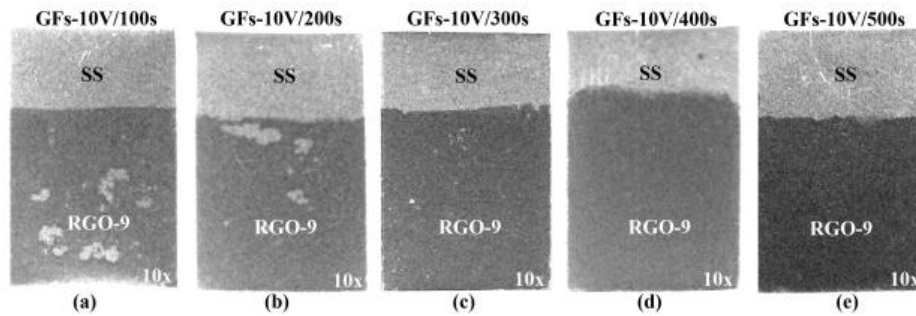
Figure 4.24: Top view optical images of GFs on anode produced using constant applied voltage of 10 V at deposition time of (a) 100 s, (b) 200 s, (c) 300 s, (d) 400 s and (e) 500 s. All images were taken at 10x magnification.

The GFs prepared at 100 s, 300 s and 500 s were further examined using SEM analysis in order to observe the surface morphology at higher magnification and to determine the thickness of the GFs produced at low (100 s), medium (300 s) and high deposition time (500 s). Figure 4.25(a-c) shows the SEM images of the surface at low (5000x) and high magnification (30,000x) as well as the cross-section view of the GFs-10V/100s sample on anode, respectively. Since the cross-section view was taken by tilting the SEM stage at 45°, the actual value of the thickness of the GFs was calculated by implementing Eq. (3.2). From Figure 4.25(a) and Figure 4.25(b), non-uniform surface morphology of GFs-10V/100s sample was observed with some area of the SS substrate was not covered by the RGO particles, in agreement with the observation of the optical image in Figure 4.24(a). However, very thin layer with thickness of around 185 nm could be developed at deposition time of 100 s as illustrated in Figure 4.25(c). Meanwhile, the SEM images of the surface at low (5000x) and high magnification (30,000x) as well as the cross-section

view of the GFs-10V/300s and GFs-10V/500s samples were depicted in Figure 4.26(a-c) and Figure 4.27(a-c), respectively. The uniform surface morphology was observed for the GFs prepared at deposition time of 300 s and 500 s as shown in Figure 4.26(a-b) and Figure 4.27(a-b), respectively. The thickness of the GFs was observed to increase with the increasing deposition time. As illustrated in Figure 4.26(c) and Figure 4.27(c), the thickness of the GFs-10V/300s and GFs-10V/500s samples was determined to be around 220 nm and 430 nm, respectively. This observation indicates that very thin GFs (less than 400 nm) could be developed by varying the deposition time. Although very thin GFs was developed at deposition time of 100 s, the non-uniform surface morphology of the GFs produced at this deposition time remains a problem. This problem may be overcome by further modification of the EPD parameter (e.g., performing EPD under magnetic field (Dusoulier et al., 2006)). It is a great advantage to be able to control the thickness of the GFs as a specific application especially in biomedical field may require a specific thickness of the film. On the other hand, the EDS spectra of the GFs and the SS substrate were shown in Figure 4.27(d) and Figure 4.27(e), respectively. As illustrated in Figure 4.27(d), an intense peak of carbon (C) and a small peak of oxygen (O) that reflect to the composition of the RGO particles were observed from the EDS spectrum of the GFs. This confirms that the GFs was successfully developed through the deposition of the RGO particles on the SS substrate. Meanwhile, the area of the substrate that was not covered by the RGO particles was confirmed to be composed of the SS material as reflected by the intense peaks of ferum (Fe) and chromium (Cr) as portrayed in Figure 4.27(e). As been discussed in section 4.4, the RGO possesses very low toxicity effects at low concentration. Hence, the GFs prepared by the deposition of RGO particles on SS substrate were

expected to possess similar low toxicity effects, making GFs as the promising material to be applied in biomedical applications particularly as biosensors (Huang et al., 2010; Nguyen et al., 2013) or scaffold in tissue engineering (Fan et al., 2010; Ryu and Kim, 2013).
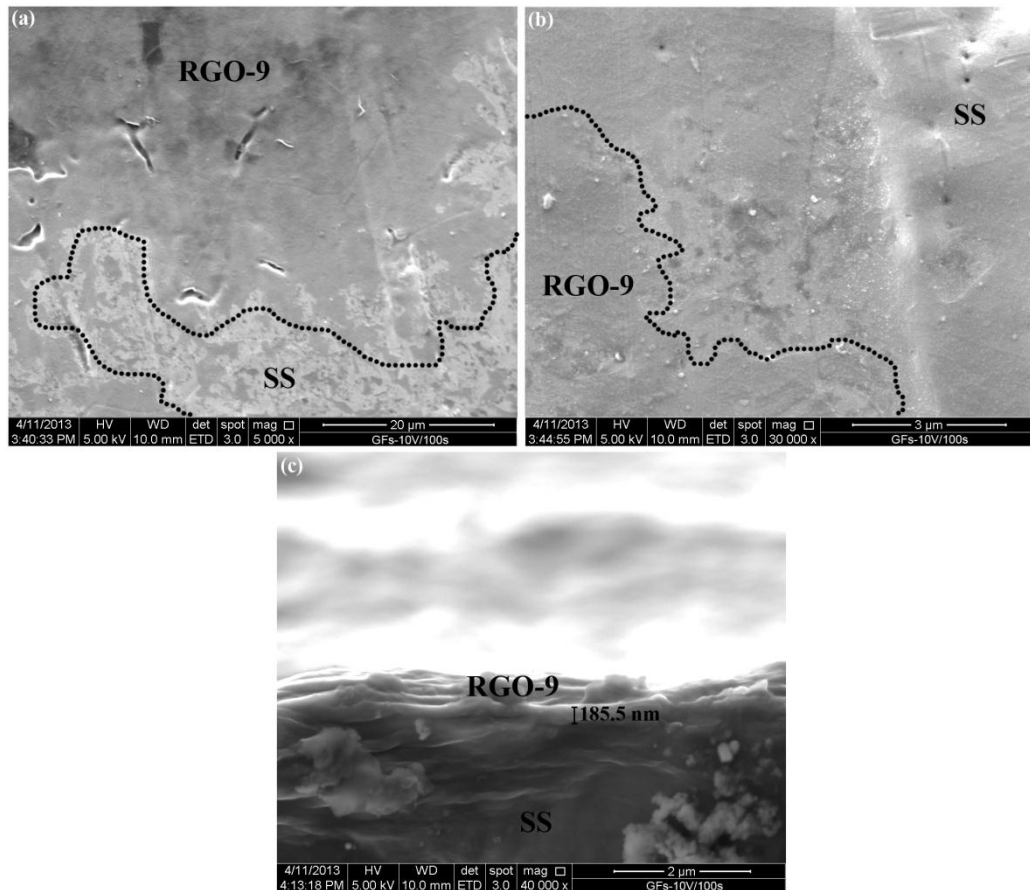
Figure 4.25: SEM images of the surface at (a) low (5000x) and (b) high magnification (30,000x) as well as (c) the cross-section view of the GFs-10V/100s sample on anode.
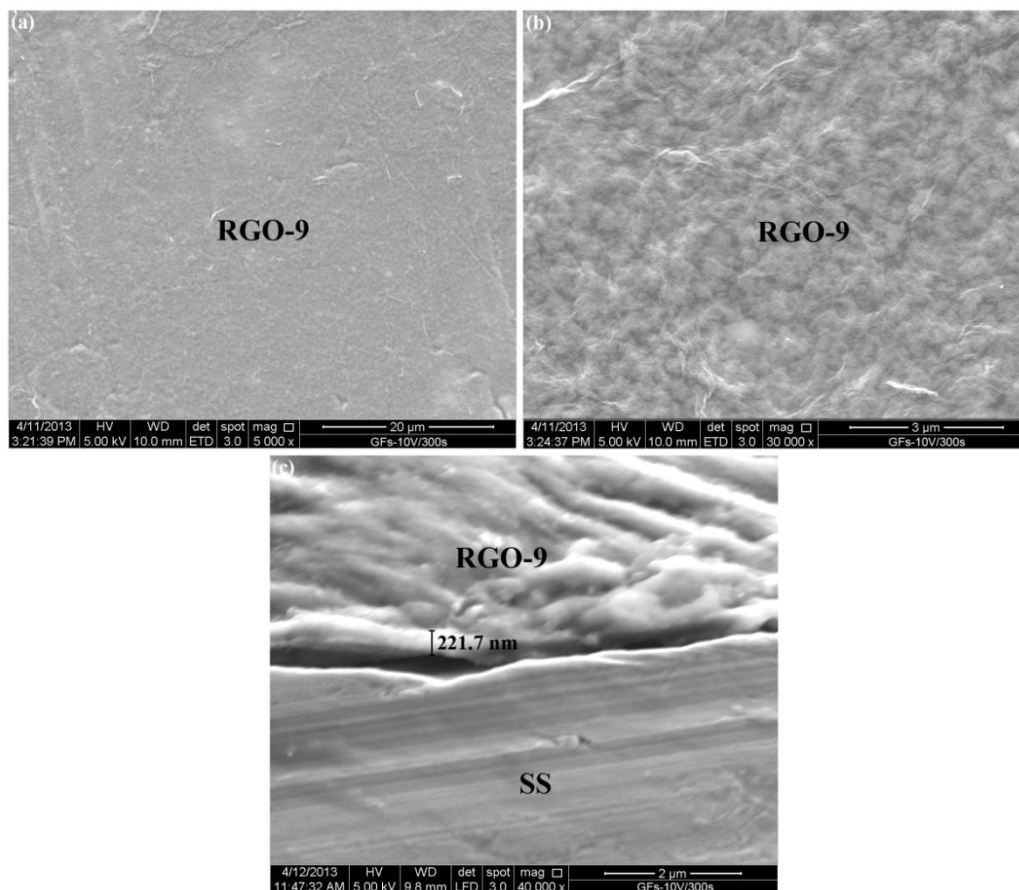
Figure 4.26: SEM images of the surface at (a) low (5000x) and (b) high magnification (30,000x) as well as (c) the cross-section view of the GFs-10V/300s sample on anode.
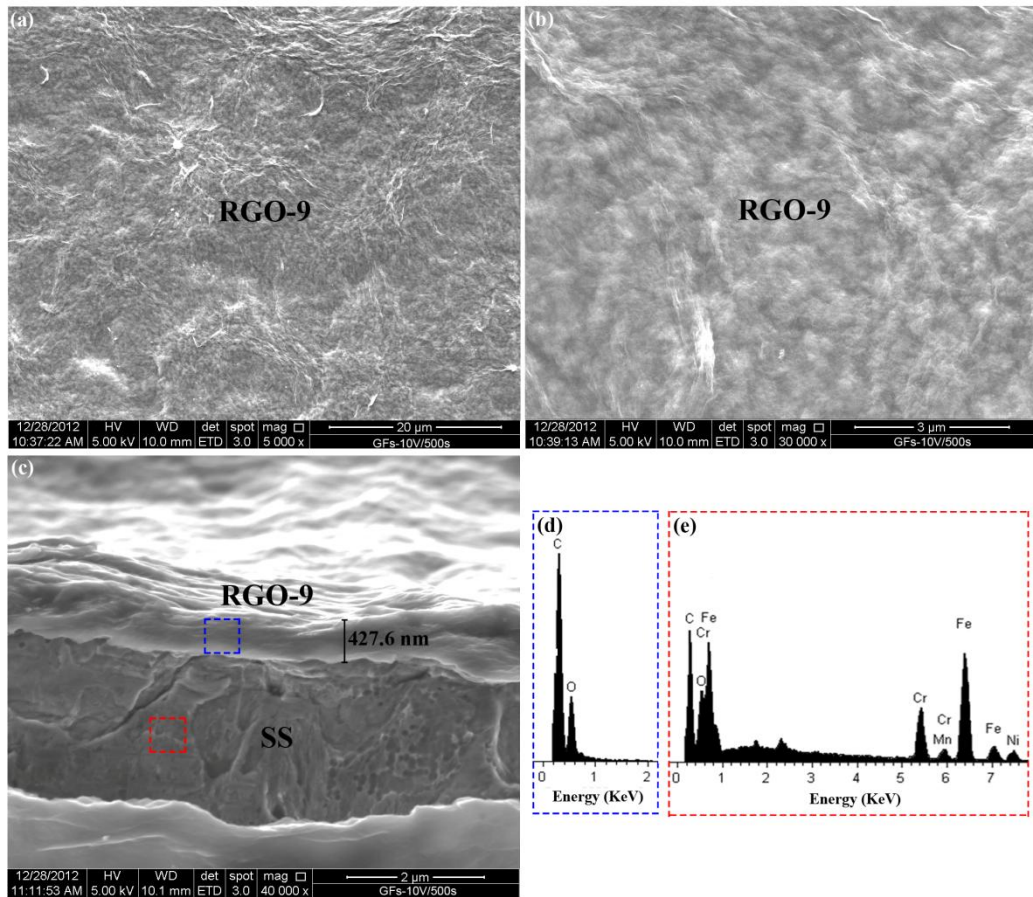
Figure 4.27: SEM images of the surface at (a) low (5000x) and (b) high magnification (30,000x) as well as (c) the cross-section view of the GFs-10V/500s sample on anode. EDS spectra of the GFs and the SS substrate were shown in (d) blue and (e) red dash line-box, respectively.

CHAPTER 5

CONCLUSION AND RECOMMENDATIONS

5.1   Conclusion

The reduction of GO is the most promising and efficient route to produce graphene in large scale owing to its cost effective, versatility for chemical functionalization and requiring only simple equipment setup as well as non-complex reaction procedures. In this study, the employment of GTP as the reducing agent has resulted in the successful reduction of GO and the preparation of a stable and well-dispersed RGO suspension in aqueous media. The successful reduction of GO has been confirmed through physical inspection of the GO suspension and the observation of the UV-Vis absorption spectra of the GO and RGO samples. Post reduction reaction with GTP, the colour of the GO suspension was changed from yellow-brownish to black colour and the UV-Vis absorption peak of GO was shifted from 228 nm to 271 nm indicating the establishment of the sp^2 bonding network of GO and the successful reduction of GO.

The effects of the weight ratio of GTP/GO and reaction temperature on the reduction of GO were examined in details by using UV-Vis spectroscopy, FTIR and TGA analyses. The results from the UV-Vis spectroscopy, FTIR and TGA analyses have shown that the use of weight ratio of GTP/GO=1 was enough to eradicate most of the oxygen functionalities from GO without the needs to utilize excessive amount of GTP. Thus, it was concluded that the weight ratio of GTP/GO=1 is the minimum weight ratio required to achieve successful reduction of GO. The aforementioned

analyses have also revealed that a nearly complete reduction of GO could be attained by performing the reduction reaction at 90 ºC without further needs to increase the reaction temperature. Therefore, in this study, the weight ratio of GTP/GO=1 and the reaction temperature of 90 ºC were concluded to be the best conditions for the GO reduction. The reduction efficiency of GTP also has been compared to the reduction efficiency of N_2H_4 solution as a standard reducing agent. The UV-Vis spectroscopy and XPS analysis have revealed that the RGO produced using GTP exhibits final position of absorption peak and intensity of sp^2 carbon that almost similar to the RGO prepared using N_2H_4 solution suggesting the effective reduction property of GTP as compared to the N_2H_4 solution as a standard reducer.

In this work, a stable and well-dispersed RGO suspension was highly desired in order to obtain successful deposition of RGO particles on SS substrate using EPD to yield GFs. Hence, the effects of the weight ratio of GTP/GO and reaction temperature on the stability of the as-produced RGO suspension were investigated by employing zeta potential and electrophoretic mobility measurements. The highest absolute zeta potential and electrophoretic mobility values of the RGO suspension were recorded when the weight ratio of GTP/GO=1 was used and the reduction reaction was performed at 90 ºC. Thus, it was concluded that the most stable RGO suspension was prepared at 90 ºC using weight ratio of GTP/GO=1. Meanwhile, although RGO has attracted substantial attentions to be used in biomedical applications, its potential toxicity, biocompatibility and interactions with living cells in biological systems are yet to be fully understood. Thus, in this regard, the cytotoxicity of GO and RGO were evaluated against CCD-18Co cells lines. The MTT assays have revealed that for GO and RGO samples, the percentage inhibition of cell proliferation was increased with the increasing concentration. The results

from the MTT assay and the micrograph images have shown that the GO is toxic towards CCD-18Co cells lines even at low concentration (6.25 μg/mL). In contrast, the RGO possesses low toxicological effects against CCD-18Co cells lines at low concentration (6.25 μg/mL) although the RGO sample shows slightly toxic effects at higher concentration (100 μg/mL and 200 μg/mL). It is revealed that the incorporation of GTP has resulted in the decrease of the toxicological effect of the RGO sample.

On the other hand, the possible mechanism of the GO reduction by GTP was investigated using Gaussian 09 and GaussView 5 programs in order to further improve the efficiency of the reduction process. It has been shown that the reduction of GO (i.e., the removal of the epoxy group) was occurred due to the transfer of two hydrogen atoms from GTP to the epoxy group in GO. The transfer of these hydrogen atoms initiates the ring opening of epoxy group and led to the formation of the products namely, RGO, galloyl-derived orthoquinone and a H_2O molecule. Similar reduction mechanism was observed when the GO was reduced using N_2H_4 solution. In addition, frequency analysis was performed for the GO reduction using GTP and N_2H_4 solution in order to determine the thermodynamic quantities (i.e., ΔH, ΔG and ΔS) for both of these systems. The results from the frequency analyses have shown that the GO reduction using GTP took place faster than the GO reduction using N_2H_4 solution which indicates that the GTP is a more efficient reducing agent than the N_2H_4 solution for the reduction of GO.

Most of the applications of graphene especially in biomedical field require uniform growth of graphene layers on a substrate. Thus, in this regard, the RGO particles were deposited on the SS substrate using EPD process to yield the GFs. The deposition weight, uniformity and the thickness of the GFs were shown to be

significantly affected by the applied voltage and the deposition time. The highest deposition weight of GFs was obtained when the applied voltage of 30 V and the deposition time of 500 s were applied. At constant deposition time, the uniform GFs was obtained when the applied voltage of 10 V was used. Whereas all the GFs prepared using higher applied voltage (i.e., 20 V, 30 V, 40 V and 50 V) were not uniform and contain voids and pores due to the generation of gas bubbles at the higher applied voltage. Meanwhile, it is revealed that the thickness of the GFs depends on the deposition time. The thickness of the GFs was shown to be decreased with the decreasing deposition time in which very thin GFs with thickness of around 185 nm could be developed at deposition time of 100 s.

In conclusion, the overall results of the present work suggests that the successful and efficient reduction of GO could be attained by employing GTP as the reducing agent. Apart from offering the non-detrimental route for the production of graphene, the employment of GTP as the reducing agent in the GO reduction has resulted in the reduction of the cytotoxicity of the RGO suspension. Hence, it is anticipated that the GFs prepared by the deposition of RGO particles on SS substrate could be applied in biomedical applications especially as scaffold in tissue engineering or biosensors.

5.2   Recommendations

Despite the successful reduction of GO and the promising cytotoxicity result of RGO sample, the present study is still at a nascent stage. There are still many extensive works that need to be carried out in order to improvise the current researches before they can be considered for the clinical applications. Thus, in this

regard, the following recommendations were proposed for future perspective of this research work:

i. Structural modification of the RGO sheets by the functionalization step to induce the solubility of RGO in other solvents such as NMP, DMF, DMSO, acetone and isopropanol.

ii. Biocompatible materials including PEG, PTCA, chitosan, hydroxyapatite (HA) and PEI could be added in the RGO suspension in order to reduce the toxicological effect of RGO at high concentration (higher than 100 µg/mL).

iii. Performing in vivo biological investigations of the RGO sample in order to ensure the long term clinical applications in biomedical field.

iv. Performing EPD under magnetic field in order to develop uniform and well-deposited nanosize-GFs (thickness less than 100 nm) on various types of substrates materials including ceramics (e.g., alumina (Al_2O_3), glass and zirconia (ZrO_2)) and polymers (e.g., polyethylene (PE) and polypropylene (PP)).

REFERENCES

Akhavan, O. 2010. The effect of heat treatment on formation of graphene thin films from graphene oxide nanosheets. *Carbon,* 48**,** 509-519.

Akhavan, O. & Ghaderi, E. 2010. Toxicity of graphene and graphene oxide nanowalls against bacteria. *ACS Nano,* 4**,** 5731-5736.

Akhavan, O., Kalaee, M., Alavi, Z. S., Ghiasi, S. M. A. & Esfandiar, A. 2012. Increasing the antioxidant activity of green tea polyphenols in the presence of iron for the reduction of graphene oxide. *Carbon,* 50**,** 3015-3025.

Albanese, A., Tang, P. S. & Chan, W. C. W. 2012. The effect of nanoparticle size, shape, and surface chemistry on biological systems. *Annual Review of Biomedical Engineering.*

Ammam, M. 2012. Electrophoretic deposition under modulated electric fields: A review. *RSC Advances,* 2**,** 7633-7646.

An, S. J., Zhu, Y., Lee, S. H., Stoller, M. D., Emilsson, T., Park, S., Velamakanni, A., An, J. & Ruoff, R. S. 2010. Thin film fabrication and simultaneous anodic reduction of deposited graphene oxide platelets by electrophoretic deposition. *Journal of Physical Chemistry Letters,* 1**,** 1259-1263.

Ang, P. K., Chen, W., Wee, A. T. S. & Kian, P. L. 2008. Solution-gated epitaxial graphene as pH sensor. *Journal of the American Chemical Society,* 130**,** 14392-14393.

Babu, P. V. A. & Liu, D. 2008. Green tea catechins and cardiovascular health: An update. *Current Medicinal Chemistry,* 15**,** 1840-1850.

Bae, S., Kim, H., Lee, Y., Xu, X., Park, J. S., Zheng, Y., Balakrishnan, J., Lei, T., Ri Kim, H., Song, Y. I., Kim, Y. J., Kim, K. S., Özyilmaz, B., Ahn, J. H., Hong, B. H. & Iijima, S. 2010. Roll-to-roll production of 30-inch graphene films for transparent electrodes. *Nature nanotechnology,* 5**,** 574-578.

Bagri, A., Mattevi, C., Acik, M., Chabal, Y. J., Chhowalla, M. & Shenoy, V. B. 2010. Structural evolution during the reduction of chemically derived graphene oxide. *Nature Chemistry,* 2**,** 581-587.

Balamurugan, A., Rajeswari, S., Balossier, G., Rebelo, A. H. S. & Ferreira, J. M. F. 2008. Corrosion aspects of metallic implants - An overview. *Materials and Corrosion,* 59**,** 855-869.

Balandin, A. A., Ghosh, S., Bao, W., Calizo, I., Teweldebrhan, D., Miao, F. & Lau, C. N. 2008. Superior thermal conductivity of single-layer graphene. *Nano Letters,* 8**,** 902-907.

Barone, V., Hod, O., Peralta, J. E. & Scuseria, G. E. 2011. Accurate prediction of the electronic properties of low-dimensional graphene derivatives using a screened hybrid density functional. *Accounts of Chemical Research,* 44**,** 269-279.

Becerril, H. A., Mao, J., Liu, Z., Stoltenberg, R. M., Bao, Z. & Chen, Y. 2008. Evaluation of solution-processed reduced graphene oxide films as transparent conductors. *ACS Nano,* 2**,** 463-470.

Becke, A. D. 1993. Density-functional thermochemistry. III. The role of exact exchange. *Journal of Chemical Physics,* 98**,** 5648-5652.

Bergin, S. D., Sun, Z., Rickard, D., Streich, P. V., Hamilton, J. P. & Coleman, J. N. 2009. Multicomponent solubility parameters for single-walled carbon nanotube-solvent mixtures. *ACS Nano,* 3**,** 2340-2350.

Besra, L. & Liu, M. 2007. A review on fundamentals and applications of electrophoretic deposition (EPD). *Progress in Materials Science,* 52**,** 1-61.

Binkley, J. S., Pople, J. A. & Hehre, W. J. 1980. Self-Consistent Molecular Orbital Methods. 21. Small Split-Valence Basis Sets for First-Row Elements. *Journal of the American Chemical Society,* 102**,** 939-947.

Blake, P., Brimicombe, P. D., Nair, R. R., Booth, T. J., Jiang, D., Schedin, F., Ponomarenko, L. A., Morozov, S. V., Gleeson, H. F., Hill, E. W., Geim, A. K. & Novoselov, K. S. 2008. Graphene-based liquid crystal device. *Nano Letters,* 8**,** 1704-1708.

Boccaccini, A. R., Cho, J., Roether, J. A., Thomas, B. J. C., Jane Minay, E. & Shaffer, M. S. P. 2006. Electrophoretic deposition of carbon nanotubes. *Carbon,* 44**,** 3149-3160.

Boccaccini, A. R., Keim, S., Ma, R., Li, Y. & Zhitomirsky, I. 2010. Electrophoretic deposition of biomaterials. *Journal of The Royal Society Interface,* 7**,** S581-S613.

Boccaccini, A. R. & Zhitomirsky, I. 2002. Application of electrophoretic and electrolytic deposition techniques in ceramics processing. *Current Opinion in Solid State and Materials Science,* 6**,** 251-260.

Bolotin, K. I., Sikes, K. J., Jiang, Z., Klima, M., Fudenberg, G., Hone, J., Kim, P. & Stormer, H. L. 2008. Ultrahigh electron mobility in suspended graphene. *Solid State Communications,* 146**,** 351-355.

Borm, P. J. A., Robbins, D., Haubold, S., Kuhlbusch, T., Fissan, H., Donaldson, K., Schins, R., Stone, V., Kreyling, W., Lademann, J., Krutmann, J., Warheit, D. B. & Oberdorster, E. 2006. The potential risks of nanomaterials: A review carried out for ECETOC. *Particle and Fibre Toxicology,* 3.

Boukhvalov, D. W., Dreyer, D. R., Bielawski, C. W. & Son, Y. W. 2012. A Computational Investigation of the Catalytic Properties of Graphene Oxide: Exploring Mechanisms by using DFT Methods. *ChemCatChem,* 4**,** 1844-1849.

Bourlinos, A. B., Gournis, D., Petridis, D., Szabó, T., Szeri, A. & Dékány, I. 2003. Graphite oxide: Chemical reduction to graphite and surface modification with primary aliphatic amines and amino acids. *Langmuir,* 19**,** 6050-6055.

Brodie, B. C. 1859. On the Atomic Weight of Graphite. *Philosophical Transactions of the Royal Society of London,* 149**,** 249-259.

Brodie, B. C. 1860. XXIII. - Researches on the atomic weight of graphite. *Quarterly Journal of the Chemical Society of London,* 12**,** 261-268.

Cai, W. & Hong, H. 2012. In a "nutshell": Intrinsically radio-labeled quantum dots. *American Journal of Nuclear Medicine and Molecular Imaging,* 2**,** 136-140.

Cai, W., Piner, R. D., Stadermann, F. J., Park, S., Shaibat, M. A., Ishii, Y., Yang, D., Velamakanni, A., An, S. J., Stoller, M., An, J., Chen, D. & Ruoff, R. S. 2008. Synthesis and Solid-State NMR Structural Characterization of 13C-Labeled Graphite Oxide. *Science,* 321**,** 1815-1817.

Cai, W., Zhu, Y., Li, X., Piner, R. D. & Ruoff, R. S. 2009. Large area few-layer graphene/graphite films as transparent thin conducting electrodes. *Applied Physics Letters,* 95.

Calais, J.-L. 1990. Computational quantum chemistry. A. Hinchliffe, John Wiley & Sons, Chichester, 1988. *International Journal of Quantum Chemistry,* 37**,** 821-821.

Cao, H., Yu, Q., Colby, R., Pandey, D., Park, C. S., Lian, J., Zemlyanov, D., Childres, I., Drachev, V., Stach, E. A., Hussain, M., Li, H., Pei, S. S. & Chen, Y. P. 2010. Large-scale graphitic thin films synthesized on Ni and transferred to insulators: Structural and electronic properties. *Journal of Applied Physics,* 107.

Casey, A., Herzog, E., Davoren, M., Lyng, F. M., Byrne, H. J. & Chambers, G. 2007. Spectroscopic analysis confirms the interactions between single walled carbon nanotubes and various dyes commonly used to assess cytotoxicity. *Carbon,* 45**,** 1425-1432.

Chang, H., Tang, L., Wang, Y., Jiang, J. & Li, J. 2010. Graphene fluorescence resonance energy transfer aptasensor for the thrombin detection. *Analytical Chemistry,* 82**,** 2341-2346.

Chang, Y., Yang, S. T., Liu, J. H., Dong, E., Wang, Y., Cao, A., Liu, Y. & Wang, H. 2011. In vitro toxicity evaluation of graphene oxide on A549 cells. *Toxicology Letters,* 200**,** 201-210.

Chartarrayawadee, W., Moulton, S. E., Li, D., Too, C. O. & Wallace, G. G. 2012. Novel composite graphene/platinum electro-catalytic electrodes prepared by electrophoretic deposition from colloidal solutions. *Electrochimica Acta,* 60**,** 213-223.

Chavez-Valdez, A., Shaffer, M. S. P. & Boccaccini, A. R. 2013. Applications of graphene electrophoretic deposition. A review. *Journal of Physical Chemistry B,* 117**,** 1502-1515.

Che, J., Shen, L. & Xiao, Y. 2010. A new approach to fabricate graphene nanosheets in organic medium: Combination of reduction and dispersion. *Journal of Materials Chemistry,* 20**,** 1722-1727.

Chen, B., Liu, M., Zhang, L., Huang, J., Yao, J. & Zhang, Z. 2011. Polyethylenimine-functionalized graphene oxide as an efficient gene delivery vector. *Journal of Materials Chemistry,* 21**,** 7736-7741.

Chen, D., Milacic, V., Chen, M. S., Wan, S. B., Lam, W. H., Huo, C., Landis-Piwowar, K. R., Cui, Q. C., Wali, A., Chan, T. H. & Ping Dou, Q. 2008a. Tea polyphenols, their biological effects and potential molecular targets. *Histology and Histopathology,* 23**,** 487-496.

Chen, H., Müller, M. B., Gilmore, K. J., Wallace, G. G. & Li, D. 2008b. Mechanically strong, electrically conductive, and biocompatible graphene paper. *Advanced Materials,* 20**,** 3557-3561.

Chen, W., Yan, L. & Bangal, P. R. 2010a. Chemical reduction of graphene oxide to graphene by sulfur-containing compounds. *Journal of Physical Chemistry C,* 114**,** 19885-19890.

Chen, Y., Lee, Y. D., Vedala, H., Allen, B. L. & Star, A. 2010b. Exploring the chemical sensitivity of a carbon nanotube/green tea composite. *ACS Nano,* 4**,** 6854-6862.

Chen, Y., Zhang, X., Yu, P. & Ma, Y. 2010c. Electrophoretic deposition of graphene nanosheets on nickel foams for electrochemical capacitors. *Journal of Power Sources,* 195**,** 3031-3035.

Choi, E.-Y., Han, T. H., Hong, J., Kim, J. E., Lee, S. H., Kim, H. W. & Kim, S. O. 2010a. Noncovalent functionalization of graphene with end-functional polymers. *Journal of Materials Chemistry,* 20**,** 1907-1912.

Choi, W., Lahiri, I., Seelaboyina, R. & Kang, Y. S. 2010b. Synthesis of graphene and its applications: A review. *Critical Reviews in Solid State and Materials Sciences,* 35**,** 52-71.

Choi, W. M., Shin, K. S., Lee, H. S., Choi, D., Kim, K., Shin, H. J., Yoon, S. M., Choi, J. Y. & Kim, S. W. 2011. Selective growth of ZnO nanorods on SiO$_2$/Si substrates using a graphene buffer layer. *Nano Research,* 4**,** 440-447.

Compton, O. C. & Nguyen, S. T. 2010. Graphene Oxide, Highly Reduced Graphene Oxide, and Graphene: Versatile Building Blocks for Carbon-Based Materials. *Small*, 6**,** 711-723.

Corni, I., Ryan, M. P. & Boccaccini, A. R. 2008. Electrophoretic deposition: From traditional ceramics to nanotechnology. *Journal of the European Ceramic Society,* 28**,** 1353-1367.

Cote, L. J., Cruz-Silva, R. & Huang, J. 2009. Flash reduction and patterning of graphite oxide and its polymer composite. *Journal of the American Chemical Society,* 131**,** 11027-11032.

De, D. & Nicholson, P. S. 1999. Role of Ionic Depletion in Deposition during Electrophoretic Deposition. *Journal of the American Ceramic Society,* 82**,** 3031-3036.

Demazeau, G. 1999. Solvothermal processes: A route to the stabilization of new material. *Journal of Materials Chemistry,* 9**,** 15-18.

Denis, P. A. & Iribarne, F. 2012. A first-principles study on the interaction between alkyl radicals and graphene. *Chemistry - A European Journal,* 18**,** 7568-7574.

Dennington, R., Keith, T. & Millam, J. 2009. GaussView 5. 5 ed. Shawnee Mission KS, Semichem Inc.

Dreyer, D. R., Park, S., Bielawski, C. W. & Ruoff, R. S. 2010. The chemistry of graphene oxide. *Chemical Society Reviews,* 39**,** 228-240.

Dua, V., Surwade, S. P., Ammu, S., Agnihotra, S. R., Jain, S., Roberts, K. E., Park, S., Ruoff, R. S. & Manohar, S. K. 2010. All-organic vapor sensor using inkjet-printed reduced graphene oxide. *Angewandte Chemie - International Edition,* 49**,** 2154-2157.

Dusoulier, L., Denis, S., Nutal, N., Henrist, C., Vanderheyden, B., Vanderbemden, P., Rulmont, A., Dirickx, M., Ausloos, M., Cloots, R. & Vertruyen, B. 2006. Texturation of YBa$_2$Cu$_3$O$_{7-\delta}$ thick films by electrophoretic deposition under magnetic field. *Key Engineering Materials.*

Eda, G., Lin, Y. Y., Mattevi, C., Yamaguchi, H., Chen, H. A., Chen, I. S., Chen, C. W. & Chhowalla, M. 2010. Blue photoluminescence from chemically derived graphene oxide. *Advanced Materials,* 22**,** 505-509.

Emerich, D. F. & Thanos, C. G. 2003. Nanotechnology and medicine. *Expert Opinion on Biological Therapy,* 3**,** 655-663.

Esfandiar, A., Akhavan, O. & Irajizad, A. 2011. Melatonin as a powerful bio-antioxidant for reduction of graphene oxide. *Journal of Materials Chemistry,* 21**,** 10907-10914.

Everett, D. H. 1988. *Basic Principles of Colloid Science,* London, Royal Society of Chemistry.

Fan, H., Wang, L., Zhao, K., Li, N., Shi, Z., Ge, Z. & Jin, Z. 2010. Fabrication, mechanical properties, and biocompatibility of graphene-reinforced chitosan composites. *Biomacromolecules,* 11**,** 2345-2351.

Fan, X., Peng, W., Li, Y., Li, X., Wang, S., Zhang, G. & Zhang, F. 2008. Deoxygenation of Exfoliated Graphite Oxide under Alkaline Conditions: A Green Route to Graphene Preparation. *Advanced Materials,* 20**,** 4490-4493.

Fang, M., Wang, K., Lu, H., Yang, Y. & Nutt, S. 2010. Single-layer graphene nanosheets with controlled grafting of polymer chains. *Journal of Materials Chemistry,* 20**,** 1982-1992.

Feng, L., Chen, Y., Ren, J. & Qu, X. 2011a. A graphene functionalized electrochemical aptasensor for selective label-free detection of cancer cells. *Biomaterials,* 32**,** 2930-2937.

Feng, L., Zhang, S. & Liu, Z. 2011b. Graphene based gene transfection. *Nanoscale,* 3**,** 1252-1257.

Fernández-Merino, M. J., Guardia, L., Paredes, J. I., Villar-Rodil, S., Solís-Fernández, P., Martínez-Alonso, A. & Tascón, J. M. D. 2010. Vitamin C is an ideal substitute for hydrazine in the reduction of graphene oxide suspensions. *Journal of Physical Chemistry C,* 114**,** 6426-6432.

Ferrari, B. & Moreno, R. 2010. EPD kinetics: A review. *Journal of the European Ceramic Society,* 30**,** 1069-1078.

Ferrari, M. 2005. Cancer nanotechnology: Opportunities and challenges. *Nature Reviews Cancer,* 5**,** 161-171.

Fisher, C., Rider, A. E., Jun Han, Z., Kumar, S., Levchenko, I. & Ostrikov, K. 2012. Applications and nanotoxicity of carbon nanotubes and graphene in biomedicine. *Journal of Nanomaterials,* 2012.

Foresman, J. B. & Frisch, A. 1996. *Exploring chemistry with electronic structure methods,* Pittsburgh, PA, Gaussian, Inc.

Frisch, M. J., Head-Gordon, M. & Pople, J. A. 1990. Semi-direct algorithms for the MP2 energy and gradient. *Chemical Physics Letters,* 166**,** 281-289.

Frisch, M. J., Trucks, G. W., Schlegel, H. B., Scuseria, G. E., Robb, M. A., Cheeseman, J. R., Scalmani, G., Barone, V., Mennucci, B., Petersson, G. A., Nakatsuji, H., Caricato, M., Li, X., Hratchian, H. P., Izmaylov, A. F., Bloino, J., Zheng, G., Sonnenberg, J. L., Hada, M., Ehara, M., Toyota, K., Fukuda, R., Hasegawa, J., Ishida, M., Nakajima, T., Honda, Y., Kitao, O., Nakai, H., Vreven, T., Montgomery, J., J. A., Peralta, J. E., Ogliaro, F., Bearpark, M., Heyd, J. J., Brothers, E., Kudin, K. N., Staroverov, V. N., Kobayashi, R.,

Normand, J., Raghavachari, K., Rendell, A., Burant, J. C., Iyengar, S. S., Tomasi, J., Cossi, M., Rega, N., Millam, J. M., Klene, M., Knox, J. E., Cross, J. B., Bakken, V., Adamo, C., Jaramillo, J., Gomperts, R., Stratmann, R. E., Yazyev, O., Austin, A. J., Cammi, R., Pomelli, C., Ochterski, J. W., Martin, R. L., Morokuma, K., Zakrzewski, V. G., Voth, G. A., Salvador, P., Dannenberg, J. J., Dapprich, S., Daniels, A. D., Farkas, Ö., Foresman, J. B., Ortiz, J. V., Cioslowski, J. & Fox, D. J. 2009. Gaussian 09. Wallingford CT, Gaussian, Inc.

Fu, W., Shenoy, D., Li, J., Crasto, C., Jones, G., Dimarzio, C., Sridhar, S. & Amiji, M. 2005. Biomedical applications of gold nanoparticles functionalized using hetero-bifunctional poly(ethylene glycol) spacer. *Materials Research Society Symposium Proceedings.*

Fukada, Y., Nagarajan, N., Mekky, W., Bao, Y., Kim, H. S. & Nicholson, P. S. 2004. Electrophoretic deposition—mechanisms, myths and materials. *Journal of Materials Science,* 39**,** 787-801.

Gani, M. S. J. 1994. Electrophoretic deposition - a review. *Industrial Ceramics,* 14**,** 163-174.

Gao, J., Liu, F., Liu, Y., Ma, N., Wang, Z. & Zhang, X. 2010a. Environment-friendly method to produce graphene that employs vitamin C and amino acid. *Chemistry of Materials,* 22**,** 2213-2218.

Gao, W., Alemany, L. B., Ci, L. & Ajayan, P. M. 2009. New insights into the structure and reduction of graphite oxide. *Nat Chem,* 1**,** 403-408.

Gao, X., Jang, J. & Nagase, S. 2010b. Hydrazine and thermal reduction of graphene oxide: Reaction mechanisms, product structures, and reaction design. *Journal of Physical Chemistry C,* 114**,** 832-842.

Geim, A. K. 2009. Graphene: Status and prospects. *Science,* 324**,** 1530-1534.

Geim, A. K. & Novoselov, K. S. 2007. The rise of graphene. *Nature Materials,* 6**,** 183-191.

Georgakilas, V., Bourlinos, A. B., Zboril, R., Steriotis, T. A., Dallas, P., Stubos, A. K. & Trapalis, C. 2010. Organic functionalisation of graphenes. *Chemical Communications,* 46**,** 1766-1768.

Georgakilas, V., Otyepka, M., Bourlinos, A. B., Chandra, V., Kim, N., Kemp, K. C., Hobza, P., Zboril, R. & Kim, K. S. 2012. Functionalization of graphene: Covalent and non-covalent approaches, derivatives and applications. *Chemical Reviews,* 112**,** 6156-6214.

Gholami, F., Zein, S. H. S., Gerhardt, L.-C., Low, K. L., Tan, S. H., McPhail, D. S., Grover, L. M. & Boccaccini, A. R. 2013. Cytocompatibility, bioactivity and mechanical strength of calcium phosphate cement reinforced with multi-

walled carbon nanotubes and bovine serum albumin. *Ceramics International,* 39**,** 4975-4983.

Gómez-Navarro, C., Weitz, R. T., Bittner, A. M., Scolari, M., Mews, A., Burghard, M. & Kern, K. 2007. Electronic transport properties of individual chemically reduced graphene oxide sheets. *Nano Letters,* 7**,** 3499-3503.

Gordon, M. S., Binkley, J. S., Pople, J. A., Pietro, W. J. & Hehre, W. J. 1982. Self-Consistent Molecular Orbital Methods. 22. Small Split-Valence Basis Sets for Second-Row Elements. *Journal of the American Chemical Society,* 104 2797-2803.

Grande, L., Chundi, V. T., Wei, D., Bower, C., Andrew, P. & Ryhänen, T. 2012. Graphene for energy harvesting/storage devices and printed electronics. *Particuology,* 10**,** 1-8.

Green, A. A. & Hersam, M. C. 2009. Solution phase production of graphene with controlled thickness via density differentiation. *Nano Letters,* 9**,** 4031-4036.

Guo, H. L., Wang, X. F., Qian, Q. Y., Wang, F. B. & Xia, X. H. 2009. A green approach to the synthesis of graphene nanosheets. *ACS Nano,* 3**,** 2653-2659.

Guo, L., Von Dem Bussche, A., Buechner, M., Yan, A., Kane, A. B. & Hurt, R. H. 2008. Adsorption of essential micronutrients by carbon nanotubes and the implications for nanotoxicity testing. *Small,* 4**,** 721-727.

Guo, Y., Sun, X., Liu, Y., Wang, W., Qiu, H. & Gao, J. 2012. One pot preparation of reduced graphene oxide (RGO) or Au (Ag) nanoparticle-RGO hybrids using chitosan as a reducing and stabilizing agent and their use in methanol electrooxidation. *Carbon,* 50**,** 2513-2523.

Hamaker, H. C. 1940. Formation of a deposit by electrophoresis. *Transactions of the Faraday Society,* 35**,** 279-287.

Hanaor, D., Michelazzi, M., Veronesi, P., Leonelli, C., Romagnoli, M. & Sorrell, C. 2011. Anodic aqueous electrophoretic deposition of titanium dioxide using carboxylic acids as dispersing agents. *Journal of the European Ceramic Society,* 31**,** 1041-1047.

Hasan, K. u., Sandberg, M., Nur, O. & Willander, M. 2011. Polycation stabilization of graphene suspensions. *Nanoscale Research Letters,* 6**,** 493.

Hasan, S. A., Rigueur, J. L., Harl, R. R., Krejci, A. J., Gonzalo-Juan, I., Rogers, B. R. & Dickerson, J. H. 2010. Transferable Graphene Oxide Films with Tunable Microstructures. *ACS Nano,* 4**,** 7367-7372.

Hass, J., De Heer, W. A. & Conrad, E. H. 2008. The growth and morphology of epitaxial multilayer graphene. *Journal of Physics Condensed Matter,* 20.

He, H., Klinowski, J., Forster, M. & Lerf, A. 1998. A new structural model for graphite oxide. *Chemical Physics Letters,* 287**,** 53-56.

Hernandez, Y., Nicolosi, V., Lotya, M., Blighe, F. M., Sun, Z., De, S., McGovern, I. T., Holland, B., Byrne, M., Gun'ko, Y. K., Boland, J. J., Niraj, P., Duesberg, G., Krishnamurthy, S., Goodhue, R., Hutchison, J., Scardaci, V., Ferrari, A. C. & Coleman, J. N. 2008. High-yield production of graphene by liquid-phase exfoliation of graphite. *Nature nanotechnology,* 3**,** 563-568.

Hill, E. W., Vijayaragahvan, A. & Novoselov, K. 2011. Graphene sensors. *IEEE Sensors Journal,* 11**,** 3161-3170.

Hirata, M., Gotou, T., Horiuchi, S., Fujiwara, M. & Ohba, M. 2004. Thin-film particles of graphite oxide 1: High-yield synthesis and flexibility of the particles. *Carbon,* 42**,** 2929-2937.

Hirsch, L. R., Gobin, A. M., Lowery, A. R., Tam, F., Drezek, R. A., Halas, N. J. & West, J. L. 2006. Metal nanoshells. *Annals of Biomedical Engineering,* 34**,** 15-22.

Hofmann, U. & Holst, R. 1939. Über die Säurenatur und die Methylierung von Graphitoxyd. *Berichte der deutschen chemischen Gesellschaft (A and B Series),* 72**,** 754-771.

Hu, W., Peng, C., Luo, W., Lv, M., Li, X., Li, D., Huang, Q. & Fan, C. 2010. Graphene-based antibacterial paper. *ACS Nano,* 4**,** 4317-4323.

Huang, L. C. L. & Chang, H. C. 2004. Adsorption and immobilization of cytochrome c on nanodiamonds. *Langmuir,* 20**,** 5879-5884.

Huang, Y., Dong, X., Shi, Y., Li, C. M., Li, L. J. & Chen, P. 2010. Nanoelectronic biosensors based on CVD grown graphene. *Nanoscale,* 2**,** 1485-1488.

Hummers, W. S. & Offeman, R. E. 1958. Preparation of Graphitic Oxide. *Journal of the American Chemical Society,* 80**,** 1339-1339.

Iijima, S., Yudasaka, M. & Yamada, R. 1999. Nano-aggregates of single-walled graphitic carbon nanohorns. *Chemical Physic Letter,* 309**,** 165-170.

Ishikawa, R., Ko, P. J., Kurokawa, Y., Konagai, M. & Sandhu, A. 2012. Electrophoretic deposition of high quality transparent conductive graphene films on insulating glass substrates *Journal of Physics: Conference Series,* 352**,** 012003.

Jayakumar, R., Prabaharan, M., Nair, S. V. & Tamura, H. 2010. Novel chitin and chitosan nanofibers in biomedical applications. *Biotechnology Advances,* 28**,** 142-150.

Jelea, A., Marinelli, F., Ferro, Y., Allouche, A. & Brosset, C. 2004. Quantum study of hydrogen–oxygen–graphite interactions. *Carbon,* 42**,** 3189-3198.

Jeong, H. K., Lee, Y. P., Jin, M. H., Kim, E. S., Bae, J. J. & Lee, Y. H. 2009. Thermal stability of graphite oxide. *Chemical Physics Letters,* 470**,** 255-258.

Juang, Z. Y., Wu, C. Y., Lo, C. W., Chen, W. Y., Huang, C. F., Hwang, J. C., Chen, F. R., Leou, K. C. & Tsai, C. H. 2009. Synthesis of graphene on silicon carbide substrates at low temperature. *Carbon,* 47**,** 2026-2031.

Jun, L., Jiangtao, C., Baomin, L., Xingbin, Y. & Qunji, X. 2012. The improvement of the field emission properties from graphene films: Ti transition layer and annealing process. *AIP Advances,* 2**,** 022101.

Kajiya, K., Kumazawa, S. & Nakayama, T. 2001. Steric effects on interaction of tea catechins with lipid bilayers. *Bioscience, Biotechnology and Biochemistry,* 65**,** 2638-2643.

Kalbacova, M., Broz, A., Kong, J. & Kalbac, M. 2010. Graphene substrates promote adherence of human osteoblasts and mesenchymal stromal cells. *Carbon,* 48**,** 4323-4329.

Kamachi Mudali, U., Sridhar, T. M. & Baldev, R. A. J. 2003. Corrosion of bio implants. *Sadhana - Academy Proceedings in Engineering Sciences,* 28**,** 601-637.

Kanwar, J., Taskeen, M., Mohammad, I., Huo, C., Chan, T. H. & Dou, Q. P. 2012. Recent advances on tea polyphenols. *Frontiers in Bioscience,* E4**,** 111-131.

Keszei, E. 2012. *Chemical Thermodynamics: An Introduction*, Springer.

Kim, B. Y. S., Rutka, J. T. & Chan, W. C. W. 2010. Current concepts: Nanomedicine. *New England Journal of Medicine,* 363**,** 2434-2443.

Kim, E. C., Zhu, Y., Andersen, V., Sciaky, D., Cao, H. J., Meekins, H., Smith, T. J. & Lance, P. 1998. Cytokine-mediated PGE2 expression in human colonic fibroblasts. *American Journal of Physiology - Cell Physiology,* 275**,** C988-C994.

Kim, K. S., Zhao, Y., Jang, H., Lee, S. Y., Kim, J. M., Ahn, J. H., Kim, P., Choi, J. Y. & Hong, B. H. 2009a. Large-scale pattern growth of graphene films for stretchable transparent electrodes. *Nature,* 457**,** 706-710.

Kim, M. C., Hwang, G. S. & Ruoff, R. S. 2009b. Epoxide reduction with hydrazine on graphene: A first principles study. *Journal of Chemical Physics,* 131.

Konkena, B. & Vasudevan, S. 2012. Understanding aqueous dispersibility of graphene oxide and reduced graphene oxide through p K a measurements. *Journal of Physical Chemistry Letters,* 3**,** 867-872.

Kovtyukhova, N. I. 1999. Layer-by-layer assembly of ultrathin composite films from micron-sized graphite oxide sheets and polycations. *Chemistry of Materials,* 11**,** 771-778.

Krishnamoorthy, K., Veerapandian, M., Zhang, L. H., Yun, K. & Kim, S. J. 2012. Antibacterial Efficiency of Graphene Nanosheets against Pathogenic Bacteria via Lipid Peroxidation. *The Journal of Physical Chemistry C,* 116**,** 17280–17287.

Kudin, K. N., Ozbas, B., Schniepp, H. C., Prud'homme, R. K., Aksay, I. A. & Car, R. 2008. Raman spectra of graphite oxide and functionalized graphene sheets. *Nano Letters,* 8**,** 36-41.

Kuila, T., Bose, S., Mishra, A. K., Khanra, P., Kim, N. H. & Lee, J. H. 2012. Chemical functionalization of graphene and its applications. *Progress in Materials Science,* 57**,** 1061-1105.

Lacerda, L., Bianco, A., Prato, M. & Kostarelos, K. 2006. Carbon nanotubes as nanomedicines: From toxicology to pharmacology. *Advanced Drug Delivery Reviews,* 58**,** 1460-1470.

Lam, K.-T. & Liang, G. 2012. Electronic Structure of Bilayer Graphene Nanoribbon and Its Device Application: A Computational Study. IN Raza, H. (Ed.) *Graphene Nanoelectronics: Metrology, Synthesis, Properties and Applications.* Springer.

Lang, B. 1975. A LEED study of the deposition of carbon on platinum crystal surfaces. *Surface Science,* 53**,** 317-329.

Lavik, E. & Von Recum, H. 2011. The role of nanomaterials in translational medicine. *ACS Nano,* 5**,** 3419-3424.

Lee, C., Wei, X., Kysar, J. W. & Hone, J. 2008. Measurement of the elastic properties and intrinsic strength of monolayer graphene. *Science,* 321**,** 385-388.

Lee, C., Yang, W. & Parr, R. G. 1988. Development of the Colle-Salvetti correlation-energy formula into a functional of the electron density. *Physical Review B,* 37**,** 785-789.

Lee, S.-B., Lee, W., Yi, J.-W., Jeong, B.-H. & Um, M.-K. 2011. Relationship between Dispersion and UV-Visible Transmittance in Nanocarbons Reinforced Composites. *18th International Conference on Composite Materials.* Jeju Island, South Korea.

Lee, S., Lee, K. & Zhong, Z. 2010. Wafer scale homogeneous bilayer graphene films by chemical vapor deposition. *Nano Letters,* 10**,** 4702-4707.

Lehn, J. M. 2002. Toward self-organization and complex matter. *Science,* 295**,** 2400-2403.

Lei, Y., Tang, Z., Liao, R. & Guo, B. 2011. Hydrolysable tannin as environmentally friendly reducer and stabilizer for graphene oxide. *Green Chemistry,* 13**,** 1655-1658.

Lerf, A., He, H., Forster, M. & Klinowski, J. 1998. Structure of graphite oxide revisited. *Journal of Physical Chemistry B,* 102**,** 4477-4482.

Leung, V. & Ko, F. 2011. Biomedical applications of nanofibers. *Polymers for Advanced Technologies,* 22**,** 350-365.

Li, C., Wang, X., Liu, Y., Wang, W., Wynn, J. & Gao, J. 2012a. Using glucosamine as a reductant to prepare reduced graphene oxide and its nanocomposites with metal nanoparticles. *Journal of Nanoparticle Research,* 14.

Li, D., Müller, M. B., Gilje, S., Kaner, R. B. & Wallace, G. G. 2008. Processable aqueous dispersions of graphene nanosheets. *Nature Nanotechnology,* 3**,** 101-105.

Li, J., Chen, J., Luo, B., Yan, X. & Xue, Q. 2012b. The improvement of the field emission properties from graphene films: Ti transition layer and annealing process. *AIP Advances,* 2.

Li, J. L., Kudin, K. N., McAllister, M. J., Prud'homme, R. K., Aksay, I. A. & Car, R. 2006. Oxygen-driven unzipping of graphitic materials. *Physical Review Letters,* 96.

Li, N., Zhang, X., Song, Q., Su, R., Zhang, Q., Kong, T., Liu, L., Jin, G., Tang, M. & Cheng, G. 2011. The promotion of neurite sprouting and outgrowth of mouse hippocampal cells in culture by graphene substrates. *Biomaterials,* 32**,** 9374-9382.

Li, Q. S. & Zhang, R. Q. 2008. Computation of large systems with an economic basis set: systems in excited states. *Theoretical Chemistry Accounts,* 119**,** 437–443.

Li, X., Cai, W., An, J., Kim, S., Nah, J., Yang, D., Piner, R., Velamakanni, A., Jung, I., Tutuc, E., Banerjee, S. K., Colombo, L. & Ruoff, R. S. 2009. Large-area synthesis of high-quality and uniform graphene films on copper foils. *Science,* 324**,** 1312-1314.

Li, Z., Barnes, J. C., Bosoy, A., Stoddart, J. F. & Zink, J. I. 2012c. Mesoporous silica nanoparticles in biomedical applications. *Chemical Society Reviews,* 41**,** 2590-2605.

Liang, Y., Wu, D., Feng, X. & Müllen, K. 2009. Dispersion of graphene sheets in organic solvent supported by ionic interactions. *Advanced Materials,* 21**,** 1679-1683.

Liao, K. H., Lin, Y. S., MacOsko, C. W. & Haynes, C. L. 2011a. Cytotoxicity of graphene oxide and graphene in human erythrocytes and skin fibroblasts. *ACS Applied Materials and Interfaces,* 3**,** 2607-2615.

Liao, R., Tang, Z., Lei, Y. & Guo, B. 2011b. Polyphenol-reduced graphene oxide: Mechanism and derivatization. *Journal of Physical Chemistry C,* 115**,** 20740-20746.

Liu, J., Fu, S., Yuan, B., Li, Y. & Deng, Z. 2010a. Toward a universal "adhesive nanosheet" for the assembly of multiple nanoparticles based on a protein-induced reduction/decoration of graphene oxide. *Journal of the American Chemical Society,* 132**,** 7279-7281.

Liu, M., Yan, Y., Zhang, L., Wang, X. & Wang, C. 2012. Hydrothermal preparation of carbon nanosheets and their supercapacitive behavior. *Journal of Materials Chemistry,* 22**,** 11458-11461.

Liu, S., Ou, J., Wang, J., Liu, X. & Yang, S. 2011. A simple two-step electrochemical synthesis of graphene sheets film on the ITO electrode as supercapacitors. *Journal of Applied Electrochemistry,* 41**,** 881-884.

Liu, S., Wang, J., Zeng, J., Ou, J., Li, Z., Liu, X. & Yang, S. 2010b. "Green" electrochemical synthesis of Pt/graphene sheet nanocomposite film and its electrocatalytic property. *Journal of Power Sources,* 195**,** 4628-4633.

Liu, Z., Robinson, J. T., Sun, X. & Dai, H. 2008. PEGylated nanographene oxide for delivery of water-insoluble cancer drugs. *Journal of the American Chemical Society,* 130**,** 10876-10877.

Lomeda, J. R., Doyle, C. D., Kosynkin, D. V., Hwang, W. F. & Tour, J. M. 2008. Diazonium functionalization of surfactant-wrapped chemically converted graphene sheets. *Journal of the American Chemical Society,* 130**,** 16201-16206.

Lotya, M., Hernandez, Y., King, P. J., Smith, R. J., Nicolosi, V., Karlsson, L. S., Blighe, F. M., De, S., Zhiming, W., McGovern, I. T., Duesberg, G. S. & Coleman, J. N. 2009. Liquid phase production of graphene by exfoliation of graphite in surfactant/water solutions. *Journal of the American Chemical Society,* 131**,** 3611-3620.

Lu, C.-H., Zhu, C.-L., Li, J., Liu, J.-J., Chen, X. & Yang, H.-H. 2010. Using graphene to protect DNA from cleavage during cellular delivery. *Chemical Communications,* 46**,** 3116-3118.

Lu, X., Yu, M., Huang, H. & Ruoff, R. S. 1999. Tailoring graphite with the goal of achieving single sheets. *Nanotechnology,* 10**,** 269-272.

Luo, J., Cote, L. J., Tung, V. C., Tan, A. T. L., Goins, P. E., Wu, J. & Huang, J. 2010. Graphene oxide nanocolloids. *Journal of the American Chemical Society,* 132**,** 17667-17669.

Maiti, U. N., Maiti, S., Das, N. S. & Chattopadhyay, K. K. 2011. Hierarchical graphene nanocones over 3D platform of carbon fabrics: A route towards fully foldable graphene based electron source. *Nanoscale,* 3**,** 4135-4141.

Malesevic, A., Vitchev, R., Schouteden, K., Volodin, A., Zhang, L., Tendeloo, G. V., Vanhulsel, A. & Haesendonck, C. V. 2008. Synthesis of few-layer graphene via microwave plasma-enhanced chemical vapour deposition. *Nanotechnology,* 19.

Mao, S., Pu, H. & Chen, J. 2012. Graphene oxide and its reduction: Modeling and experimental progress. *RSC Advances,* 2**,** 2643-2662.

Marcano, D. C., Kosynkin, D. V., Berlin, J. M., Sinitskii, A., Sun, Z., Slesarev, A., Alemany, L. B., Lu, W. & Tour, J. M. 2010. Improved synthesis of graphene oxide. *ACS Nano,* 4**,** 4806-4814.

Matranga, C., Chen, L., Smith, M., Bittner, E., Johnson, J. K. & Bockrath, B. 2003. Trapped CO_2 in Carbon Nanotube Bundles. *Journal of Physical Chemistry B,* 107**,** 12930-12941.

Mattevi, C., Eda, G., Agnoli, S., Miller, S., Mkhoyan, K. A., Celik, O., Mastrogiovanni, D., Cranozzi, C., Carfunkel, E. & Chhowalla, M. 2009. Evolution of electrical, chemical, and structural properties of transparent and conducting chemically derived craphene thin films. *Advanced Functional Materials,* 19**,** 2577-2583.

Matthews, C. M. 2010. Steep your genes in health: drink tea. *Proceedings (Baylor University Medical Center),* 23**,** 142-144.

McAllister, M. J., Li, J. L., Adamson, D. H., Schniepp, H. C., Abdala, A. A., Liu, J., Herrera-Alonso, M., Milius, D. L., Car, R., Prud'homme, R. K. & Aksay, I. A. 2007. Single sheet functionalized graphene by oxidation and thermal expansion of graphite. *Chemistry of Materials,* 19**,** 4396-4404.

McCarthy, T. D., Karellas, P., Henderson, S. A., Giannis, M., O'Keefe, D. F., Heery, G., Paull, J. R. A., Matthews, B. R. & Holan, G. 2005. Dendrimers as drugs: Discovery and preclinical and clinical development of dendrimer-based microbicides for HIV and STI prevention. *Molecular Pharmaceutics,* 2**,** 312-318.

McMurray, R., Dalby, M. J. & Gadegaard, N. 2011. Nanopatterned Surfaces for Biomedical Applications. IN Laskovski, A. N. (Ed.) *Biomedical Engineering: Trends in Materials Science.* InTech.

McWeeny, R. & Dierksen, G. 1968. Self-consistent perturbation theory. 2. Extension to open shells. *Journal of Chemical Physics,* 49**,** 4852.

Mehra, J. 2002. Richard Phillips Feynman. 11 May 1918 - 15 February 1988. *Biographical Memoirs of Fellows of the Royal Society,* 48**,** 97-128.

Meng, Z. X., Zheng, W., Ding, M. H., Zhou, H. M., Chen, X. Q., Chen, J. C., Liu, M. K. & Zheng, Y. F. 2011. Fabrication and characterization of elastomeric polyester/carbon nanotubes nanocomposites for biomedical application. *Journal of nanoscience and nanotechnology,* 11**,** 3126-3133.

Mermin, N. D. 1968. Crystalline order in two dimensions. *Physical Review,* 176**,** 250-254.

Mermoux, M., Chabre, Y. & Rousseau, A. 1991. FTIR and 13C NMR study of graphite oxide. *Carbon,* 29**,** 469-474.

Mishra, A. K. & Ramaprabhu, S. 2011. Functionalized Graphene-Based Nanocomposites for Supercapacitor Application. *The Journal of Physical Chemistry C,* 115**,** 14006-14013.

Moghimi, S. M., Hunter, A. C. & Murray, J. C. 2005. Nanomedicine: Current status and future prospects. *FASEB Journal,* 19**,** 311-330.

Mohanty, N. & Berry, V. 2008. Graphene-based single-bacterium resolution biodevice and DNA transistor: Interfacing graphene derivatives with nanoscale and microscale biocomponents. *Nano Letters,* 8**,** 4469-4476.

Moon, I. K., Lee, J., Ruoff, R. S. & Lee, H. 2010. Reduced graphene oxide by chemical graphitization. *Nature Communications,* 1.

Mosmann, T. 1983. Rapid colorimetric assay for cellular growth and survival: Application to proliferation and cytotoxicity assays. *Journal of Immunological Methods,* 65**,** 55-63.

Moulton, M. C., Braydich-Stolle, L. K., Nadagouda, M. N., Kunzelman, S., Hussain, S. M. & Varma, R. S. 2010. Synthesis, characterization and biocompatibility of "green" synthesized silver nanoparticles using tea polyphenols. *Nanoscale,* 2**,** 763-770.

Mukhtar, H. & Ahmad, N. 2000. Tea polyphenols: Prevention of cancer and optimizing health. *American Journal of Clinical Nutrition,* 71**,** 1698S-1704S.

Müller, I. & Müller, W. H. 2009. *Fundamentals of Thermodynamics and Applications*, Springer.

Muszynski, R., Seger, B. & Kamat, P. V. 2008. Decorating graphene sheets with gold nanoparticles. *Journal of Physical Chemistry C,* 112**,** 5263-5266.

Nadagouda, M. N. & Varma, R. S. 2008. Green synthesis of silver and palladium nanoparticles at room temperature using coffee and tea extract. *Green Chemistry,* 10**,** 859-862.

Nakajima, T. & Matsuo, Y. 1994. Formation process and structure of graphite oxide. *Carbon,* 32**,** 469-475.

Neirinck, B., Fransaer, J., Biest, O. V. d. & Vleugels, J. 2009. Aqueous electrophoretic deposition in asymmetric AC electric fields (AC-EPD). *Electrochemistry Communications,* 11**,** 57-60.

Nel, A. E., Mädler, L., Velegol, D., Xia, T., Hoek, E. M. V., Somasundaran, P., Klaessig, F., Castranova, V. & Thompson, M. 2009. Understanding biophysicochemical interactions at the nano-bio interface. *Nature Materials,* 8**,** 543-557.

Neto, A. C., Guinea, F. & Peres, N. M. 2006. Drawing conclusions from graphene. *Physics World,* 19**,** 33-37.

Nguyen, H. B., Nguyen, V. C., Nguyen, V. T., Le, H. D., Nguyen, V. Q., Ngo, T. T. T., Do, Q. P., Nguyen, X. N., Phan, N. M. & Tran, D. L. 2013. Development of the layer-by-layer biosensor using graphene films: application for cholesterol determination. *Advances in Natural Sciences: Nanoscience and Nanotechnology,* 4**,** 5013-5017.

Nguyen, P. & Berry, V. 2012. Graphene interfaced with biological cells: Opportunities and challenges. *Journal of Physical Chemistry Letters,* 3**,** 1024-1029.

Novoselov, K. S., Geim, A. K., Morozov, S. V., Jiang, D., Zhang, Y., Dubonos, S. V., Grigorieva, I. V. & Firsov, A. A. 2004. Electric field in atomically thin carbon films. *Science,* 306**,** 666-669.

Nune, S. K., Chanda, N., Shukla, R., Katti, K., Kulkarni, R. R., Thilakavathy, S., Mekapothula, S., Kannan, R. & Katti, K. V. 2009. Green nanotechnology from tea: Phytochemicals in tea as building blocks for production of biocompatible gold nanoparticles. *Journal of Materials Chemistry,* 19**,** 2912-2920.

Nuvoli, D., Valentini, L., Alzari, V., Scognamillo, S., Bon, S. B., Piccinini, M., Illescas, J. & Mariani, A. 2011. High concentration few-layer graphene sheets obtained by liquid phase exfoliation of graphite in ionic liquid. *Journal of Materials Chemistry,* 21**,** 3428-3431.

Obraztsov, A. N. 2009. Chemical vapour deposition: Making graphene on a large scale. *Nature nanotechnology,* 4**,** 212-213.

Obraztsov, A. N., Zolotukhin, A. A., Ustinov, A. O., Volkov, A. P., Svirko, Y. & Jefimovs, K. 2003. DC discharge plasma studies for nanostructured carbon CVD. *Diamond and Related Materials,* 12**,** 917-920.

Paredes, J. I., Villar-Rodil, S., Fernández-Merino, M. J., Guardia, L., Martínez-Alonso, A. & Tascón, J. M. D. 2011. Environmentally friendly approaches toward the mass production of processable graphene from graphite oxide. *Journal of Materials Chemistry,* 21**,** 298-306.

Park, S., An, J., Jung, I., Piner, R. D., An, S. J., Li, X., Velamakanni, A. & Ruoff, R. S. 2009. Colloidal suspensions of highly reduced graphene oxide in a wide variety of organic solvents. *Nano Letters,* 9**,** 1593-1597.

Park, S., Mohanty, N., Suk, J. W., Nagaraja, A., An, J., Piner, R. D., Cai, W., Dreyer, D. R., Berry, V. & Ruoff, R. S. 2010. Biocompatible, robust free-standing paper composed of a TWEEN/graphene composite. *Advanced Materials,* 22**,** 1736-1740.

Park, S. & Ruoff, R. S. 2009. Chemical methods for the production of graphenes. *Nature nanotechnology,* 4**,** 217-224.

Peer, D., Karp, J. M., Hong, S., Farokhzad, O. C., Margalit, R. & Langer, R. 2007. Nanocarriers as an emerging platform for cancer therapy. *Nature nanotechnology,* 2**,** 751-760.

Pei, S. & Cheng, H.-M. 2012. The reduction of graphene oxide. *Carbon,* 50**,** 3210-3228.

Pei, S., Zhao, J., Du, J., Ren, W. & Cheng, H. M. 2010. Direct reduction of graphene oxide films into highly conductive and flexible graphene films by hydrohalic acids. *Carbon,* 48**,** 4466-4474.

Peng, C. & Schlegel, H. B. 1993. Combining Synchronous Transit and Quasi-Newton Methods to Find Transition States. *Israel Journal of Chemistry,* 33**,** 449-454.

Penuelas, J., Ouerghi, A., Lucot, D., David, C., Gierak, J., Estrade-Szwarckopf, H. & Andreazza-Vignolle, C. 2009. Surface morphology and characterization of thin graphene films on SiC vicinal substrate. *Physical Review B - Condensed Matter and Materials Physics,* 79.

Pham, V. H., Pham, H. D., Dang, T. T., Hur, S. H., Kim, E. J., Kong, B. S., Kim, S. & Chung, J. S. 2012. Chemical reduction of an aqueous suspension of graphene oxide by nascent hydrogen. *Journal of Materials Chemistry,* 22**,** 10530-10536.

Pietro, W. J., Francl, M. M., Hehre, W. J., Defrees, D. J., Pople, J. A. & Binkley, J. S. 1982. Self-Consistent Molecular Orbital Methods. 24. Supplemented small split-valence basis-sets for 2nd-row elements. *Journal of the American Chemical Society,* 104 5039-5048.

Powell, J. H. & Gannett, P. M. 2002. Mechanisms of carcinogenicity of aryl hydrazines, aryl hydrazides, and arenediazonium ions. *Journal of Environmental Pathology, Toxicology and Oncology,* 21**,** 1-31.

Radich, J. G., McGinn, P. J. & Kamat, P. V. 2011. Graphene-based composites for electrochemical energy storage. *Electrochemical Society Interface,* 20**,** 63-66.

Raghavachari, K. & Pople, J. A. 1978. Approximate 4th-order perturbation-theory of electron correlation energy. *International Journal of Quantum Chemistry,* 14**,** 91-100.

Ramesha, G. K. & Sampath, N. S. 2009. Electrochemical reduction of oriented Graphene oxide films: An in situ Raman spectroelectrochemical study. *Journal of Physical Chemistry C,* 113**,** 7985-7989.

Rao, C. N. R. & Cheetham, A. K. 2001. Science and technology of nanomaterials: Current status and future prospects. *Journal of Materials Chemistry,* 11**,** 2887-2894.

Rao, C. N. R., Sood, A. K., Subrahmanyam, K. S. & Govindaraj, A. 2009. Graphene: The new two-dimensional nanomaterial. *Angewandte Chemie - International Edition,* 48**,** 7752-7777.

Reina, A., Jia, X., Ho, J., Nezich, D., Son, H., Bulovic, V., Dresselhaus, M. S. & Jing, K. 2009. Large area, few-layer graphene films on arbitrary substrates by chemical vapor deposition. *Nano Letters,* 9**,** 30-35.

Roco, M. C. 2003. Nanotechnology: Convergence with modern biology and medicine. *Current Opinion in Biotechnology,* 14**,** 337-346.

Rodríguez, A. M. & Jiménez, P. S. V. 1986. Some new aspects of graphite oxidation at 0°c in a liquid medium. A mechanism proposal for oxidation to graphite oxide. *Carbon,* 24**,** 163-167.

Roy, H. V., Kallinger, C., Marsen, B. & Sattler, K. 1998. Manipulation of graphitic sheets using a tunneling microscope. *Journal of Applied Physics,* 83**,** 4695-4699.

Ruess, G. 1947. Über das Graphitoxyhydroxyd (Graphitoxyd). *Monatshefte für Chemie,* 76**,** 381-417.

Ryu, S. & Kim, B.-S. 2013. Culture of neural cells and stem cells on graphene. *Tissue Engineering and Regenerative Medicine,* 10**,** 39-46.

Sahoo, S. K., Parveen, S. & Panda, J. J. 2007. The present and future of nanotechnology in human health care. *Nanomedicine: Nanotechnology, Biology, and Medicine,* 3**,** 20-31.

Sanchez, V. C., Jachak, A., Hurt, R. H. & Kane, A. B. 2012. Biological interactions of graphene-family nanomaterials: An interdisciplinary review. *Chemical Research in Toxicology,* 25**,** 15-34.

Santos, C. M., Mangadlao, J., Ahmed, F., Leon, A., Advincula, R. C. & Rodrigues, D. F. 2012. Graphene nanocomposite for biomedical applications: Fabrication, antimicrobial and cytotoxic investigations. *Nanotechnology,* 23.

Sarkar, P. & Nicholson, P. S. 1996. Electrophoretic deposition (EPD): mechanisms, kinetics, and application to ceramics. *Journal of the American Ceramic Society,* 79**,** 1987-2002.

Schafhaeutl, C. 1840. On the combinations of carbon with silicon and iron, and other metals, forming the different species of cast iron, steel, and malleable iron. *Philosophical Magazine Series 3,* 16**,** 426-434.

Schniepp, H. C., Li, J. L., McAllister, M. J., Sai, H., Herrera-Alonson, M., Adamson, D. H., Prud'homme, R. K., Car, R., Seville, D. A. & Aksay, I. A. 2006. Functionalized single graphene sheets derived from splitting graphite oxide. *Journal of Physical Chemistry B,* 110**,** 8535-8539.

Scholz, W. & Boehm, H. P. 1969. Untersuchungen am Graphitoxid. VI. Betrachtungen zur Struktur des Graphitoxids. *Zeitschrift für anorganische und allgemeine Chemie,* 369**,** 327-340.

Schrödinger, E. 1926. Quantisierung als Eigenwertproblem. *Annalen der Physik,* 384**,** 361-376.

Seger, B. & Kamat, P. V. 2009. Electrocatalytically Active Graphene-Platinum Nanocomposites. Role of 2-D Carbon Support in PEM Fuel Cells. *The Journal of Physical Chemistry C,* 113**,** 7990-7995.

Seo, S.-D., Hwang, I.-S., Lee, S.-H., Shim, H.-W. & Kim, D.-W. 2012. 1D/2D carbon nanotube/graphene nanosheet composite anodes fabricated using electrophoretic assembly. *Ceramics International,* 38**,** 3017-3021.

Shen, H., Zhang, L., Liu, M. & Zhang, Z. 2012. Biomedical Applications of Graphene. *Theranostics,* 2**,** 283-294.

Shenderova, O. A., Zhirnov, V. V. & Brenner, D. W. 2002. Carbon nanostructures. *Critical Reviews in Solid State and Materials Sciences,* 27**,** 227-356.

Shin, H. J., Kim, K. K., Benayad, A., Yoon, S. M., Park, H. K., Jung, I. S., Jin, M. H., Jeong, H. K., Kim, J. M., Choi, J. Y. & Lee, Y. H. 2009. Efficient reduction of graphite oxide by sodium borohydride and its effect on electrical conductance. *Advanced Functional Materials,* 19**,** 1987-1992.

Si, Y. & Samulski, E. T. 2008. Synthesis of water soluble graphene. *Nano Letters,* 8**,** 1679-1682.

Singh, M. K., Shokuhfar, T., De Almeida Gracio, J. J., De Sousa, A. C. M., Da Fonte Fereira, J. M., Garmestani, H. & Ahzi, S. 2008. Hydroxyapatite modified with carbon-nanotube-reinforced poly(methyl methacrylate): A nanocomposite material for biomedical applications. *Advanced Functional Materials,* 18**,** 694-700.

Singh, V., Joung, D., Zhai, L., Das, S., Khondaker, S. I. & Seal, S. 2011. Graphene based materials: Past, present and future. *Progress in Materials Science,* 56**,** 1178-1271.

Sinha, N. & Yeow, J. T. W. 2005. Carbon nanotubes for biomedical applications. *IEEE Transactions on Nanobioscience,* 4**,** 180-195.

Sinitskii, A., Dimiev, A., Corley, D. A., Fursina, A. A., Kosynkin, D. V. & Tour, J. M. 2010. Kinetics of diazonium functionalization of chemically converted graphene nanoribbons. *ACS Nano,* 4**,** 1949-1954.

Somani, P. R., Somani, S. P. & Umeno, M. 2006. Planer nano-graphenes from camphor by CVD. *Chemical Physics Letters,* 430**,** 4-4.

Sprinkle, M., Siegel, D., Hu, Y., Hicks, J., Tejeda, A., Taleb-Ibrahimi, A., Le Fèvre, P., Bertran, F., Vizzini, S., Enriquez, H., Chiang, S., Soukiassian, P., Berger, C., De Heer, W. A., Lanzara, A. & Conrad, E. H. 2009. First direct observation of a nearly ideal graphene band structure. *Physical Review Letters,* 103.

Sreeprasad, T. S. & Pradeep, T. 2012. Graphene for environmental and biological applications a review. *International Journal of Modern Physics B,* 26.

Srinivas, G., Zhu, Y., Piner, R., Skipper, N., Ellerby, M. & Ruoff, R. 2010. Synthesis of graphene-like nanosheets and their hydrogen adsorption capacity. *Carbon,* 48**,** 630-635.

Srivastava, S., Kumar, V., Ali, M. A., Solanki, P. R., Srivastava, A., Sumana, G., Saxena, P. S., Joshi, A. G. & Malhotra, B. D. 2013. Electrophoretically deposited reduced graphene oxide platform for food toxin detection. *Nanoscale,* 5**,** 3043-3051.

Stankovich, S., Dikin, D. A., Piner, R. D., Kohlhaas, K. A., Kleinhammes, A., Jia, Y., Wu, Y., Nguyen, S. T. & Ruoff, R. S. 2007. Synthesis of graphene-based nanosheets via chemical reduction of exfoliated graphite oxide. *Carbon,* 45**,** 1558-1565.

Stankovich, S., Piner, R. D., Chen, X., Wu, N., Nguyen, S. T. & Ruoff, R. S. 2006a. Stable aqueous dispersions of graphitic nanoplatelets via the reduction of exfoliated graphite oxide in the presence of poly(sodium 4-styrenesulfonate). *Journal of Materials Chemistry,* 16**,** 155-158.

Stankovich, S., Piner, R. D., Nguyen, S. T. & Ruoff, R. S. 2006b. Synthesis and exfoliation of isocyanate-treated graphene oxide nanoplatelets. *Carbon,* 44**,** 3342-3347.

Staudenmaier, L. 1898. Verfahren zur Darstellung der Graphitsäure. *Berichte der deutschen chemischen Gesellschaft,* 31**,** 1481-1487.

Stine, R., Mulvaney, S. P., Robinson, J. T., Tamanaha, C. R. & Sheehan, P. E. 2012. Fabrication, Optimization, and Use of Graphene Field Effect Sensors. *Analytical Chemistry,* 85**,** 509-521.

Sun, X., Liu, Z., Welsher, K., Robinson, J., Goodwin, A., Zaric, S. & Dai, H. 2008. Nano-graphene oxide for cellular imaging and drug delivery. *Nano Research,* 1**,** 203-212.

Sundararajan, G. & Rao, T. N. 2009. Commercial prospects for nanomaterials in India. *Journal of the Indian Institute of Science,* 89**,** 35-41.

Svenson, S. & Tomalia, D. A. 2005. Dendrimers in biomedical applications - Reflections on the field. *Advanced Drug Delivery Reviews,* 57**,** 2106-2129.

Szabo, A. & Ostlund, N. S. 1982. *Modern Quantum Chemistry,* New York, McGraw-Hill.

Szabó, T., Berkesi, O., Forgó, P., Josepovits, K., Sanakis, Y., Petridis, D. & Dekány, I. 2006. Evolution of surface functional groups in a series of progressively oxidized graphite oxides. *Chemistry of Materials,* 18**,** 2740-2749.

Tang, L., Feng, H., Cheng, J. & Li, J. 2010a. Uniform and rich-wrinkled electrophoretic deposited graphene film: a robust electrochemical platform for TNT sensing. *Chemical Communications,* 46**,** 5882-5884.

Tang, S. & Cao, Z. 2012. Adsorption and dissociation of ammonia on graphene oxides: A first-principles study. *Journal of Physical Chemistry C,* 116**,** 8778-8791.

Tang, Y.-B., Lee, C.-S., Xu, J., Liu, Z.-T., Chen, Z.-H., He, Z., Cao, Y.-L., Yuan, G., Song, H., Chen, L., Luo, L., Cheng, H.-M., Zhang, W.-J., Bello, I. & Lee, S.-T. 2010b. Incorporation of Graphenes in Nanostructured TiO2 Films via Molecular Grafting for Dye-Sensitized Solar Cell Application. *ACS Nano,* 4**,** 3482-3488.

Terao, T., Bando, Y., Mitome, M., Zhi, C., Tang, C. & Golberg, D. 2009. Thermal conductivity improvement of polymer films by catechin-modified boron nitride nanotubes. *Journal of Physical Chemistry C,* 113**,** 13605-13609.

Thompson, T. E., Falardeau, E. R. & Hanlon, L. R. 1977. The electrical conductivity and optical reflectance of graphite-SbF5 compounds. *Carbon,* 15**,** 39-43.

Thorek, D. L. J., Chen, A. K., Czupryna, J. & Tsourkas, A. 2006. Superparamagnetic iron oxide nanoparticle probes for molecular imaging. *Annals of Biomedical Engineering,* 34**,** 23-38.

Turchanin, A., Beyer, A., Nottbohm, C. T., Zhang, X., Stosch, R., Sologubenko, A., Mayer, J., Hinze, P., Weimann, T. & Gölzhäuser, A. 2009. One nanometer thin carbon nanosheets with tunable conductivity and stiffness. *Advanced Materials,* 21**,** 1233-1237.

Ubbelohde, A. R. & Lewis, L. A. 1960. Graphite and its crystal compounds. *Oxford University Press.* London.

Valcic, S., Burr, J. A., Timmermann, B. N. & Liebler, D. C. 2000. Antioxidant Chemistry of Green Tea Catechins. New Oxidation Products of (−)-Epigallocatechin Gallate and (−)-Epigallocatechin from Their Reactions with Peroxyl Radicals. *Chemical Research in Toxicology,* 13**,** 801-810.

Van der Biest, O. O. & Vandeperre, L. J. 1999. Electrophoretic deposition of materials. *Annual Review of Materials Science,* 29**,** 327-352.

Van Tassel, J. J. & Randall, C. A. 2006. Mechanisms of electrophoretic deposition. *Key Engineering Materials,* 314**,** 167-174.

Veerapandian, M., Seo, Y. T., Shin, H., Yun, K. & Lee, M. H. 2012. Functionalized graphene oxide for clinical glucose biosensing in urine and serum samples. *International Journal of Nanomedicine,* 7**,** 6123-6136.

Viculis, L. H., Mack, J. J. & Kaner, R. B. 2003. A chemical route to carbon nanoscrolls. *Science,* 299**,** 1361.

Vitchev, R., Malesevic, A., Petrov, R. H., Kemps, R., Mertens, M., Vanhulsel, A. & Van Haesendonck, C. 2010. Initial stages of few-layer graphene growth by microwave plasma-enhanced chemical vapour deposition. *Nanotechnology,* 21.

Wang, G., Wang, B., Park, J., Wang, Y., Sun, B. & Yao, J. 2009a. Highly efficient and large-scale synthesis of graphene by electrolytic exfoliation. *Carbon,* 47**,** 3242-3246.

Wang, G., Yang, J., Park, J., Gou, X., Wang, B., Liu, H. & Yao, J. 2008a. Facile synthesis and characterization of graphene nanosheets. *Journal of Physical Chemistry C,* 112**,** 8192-8195.

Wang, H., Robinson, J. T., Li, X. & Dai, H. 2009b. Solvothermal reduction of chemically exfoliated graphene sheets. *Journal of the American Chemical Society,* 131**,** 9910-9911.

Wang, J., Zhu, M., Outlaw, R. A., Zhao, X., Manos, D. M. & Holloway, B. C. 2004a. Synthesis of carbon nanosheets by inductively coupled radio-frequency plasma enhanced chemical vapor deposition. *Carbon,* 42**,** 2867-2872.

Wang, J. J., Zhu, M. Y., Outlaw, R. A., Zhao, X., Manos, D. M., Holloway, B. C. & Mammana, V. P. 2004b. Free-standing subnanometer qraphite sheets. *Applied Physics Letters,* 85**,** 1265-1267.

Wang, K., Ruan, J., Song, H., Zhang, J., Wo, Y., Guo, S. & Cui, D. 2011a. Biocompatibility of Graphene Oxide. *Nanoscale Research Letters,* 6**,** 1-8.

Wang, S. J., Geng, Y., Zheng, Q. & Kim, J. K. 2010. Fabrication of highly conducting and transparent graphene films. *Carbon,* 48**,** 1815-1823.

Wang, X., You, H., Liu, F., Li, M., Wan, L., Li, S., Li, Q., Xu, Y., Tian, R., Yu, Z., Xiang, D. & Cheng, J. 2009c. Large-scale synthesis of few-layered graphene using CVD. *Chemical Vapor Deposition,* 15**,** 53-56.

Wang, X., Zhi, L. & Müllen, K. 2008b. Transparent, conductive graphene electrodes for dye-sensitized solar cells. *Nano Letters,* 8**,** 323-327.

Wang, Y., Li, Z., Wang, J., Li, J. & Lin, Y. 2011b. Graphene and graphene oxide: Biofunctionalization and applications in biotechnology. *Trends in Biotechnology,* 29**,** 205-212.

Wang, Y., Shi, Z. & Yin, J. 2011c. Facile synthesis of soluble graphene via a green reduction of graphene oxide in tea solution and its biocomposites. *ACS Applied Materials & Interfaces,* 3**,** 1127-1133.

West, J. L. & Halas, N. J. 2003. Engineered nanomaterials for biophotonics applications: Improving sensing, imaging, and therapeutics. *Annual Review of Biomedical Engineering.*

Whitesides, G. M. 2003. The 'right' size in nanobiotechnology. *Nature Biotechnology,* 21**,** 1161-1165.

Wojtoniszak, M., Chen, X., Kalenczuk, R. J., Wajda, A., Łapczuk, J., Kurzewski, M., Drozdzik, M., Chu, P. K. & Borowiak-Palen, E. 2012. Synthesis, dispersion, and cytocompatibility of graphene oxide and reduced graphene oxide. *Colloids and Surfaces B: Biointerfaces,* 89**,** 79-85.

Worle-Knirsch, J. M., Pulskamp, K. & Krug, H. F. 2006. Oops they did it again! Carbon nanotubes hoax scientists in viability assays. *Nano Letters,* 6**,** 1261-1268.

Wu, L., Chu, H. S., Koh, W. S. & Li, E. P. 2010. Highly sensitive graphene biosensors based on surface plasmon resonance. *Optics Express,* 18**,** 14395-14400.

Wu, Z.-S., Pei, S., Ren, W., Tang, D., Gao, L., Liu, B., Li, F., Liu, C. & Cheng, H.-M. 2009a. Field Emission of Single-Layer Graphene Films Prepared by Electrophoretic Deposition. *Advanced Materials,* 21**,** 1756-1760.

Wu, Z. S., Ren, W., Gao, L., Liu, B., Jiang, C. & Cheng, H. M. 2009b. Synthesis of high-quality graphene with a pre-determined number of layers. *Carbon,* 47**,** 493-499.

Xia, X., Tu, J., Mai, Y., Chen, R., Wang, X., Gu, C. & Zhao, X. 2011. Graphene Sheet/Porous NiO Hybrid Film for Supercapacitor Applications. *Chemistry – A European Journal,* 17**,** 10898-10905.

Xu, Y., Bai, H., Lu, G., Li, C. & Shi, G. 2008. Flexible graphene films via the filtration of water-soluble noncovalent functionalized graphene sheets. *Journal of the American Chemical Society,* 130**,** 5856 - 5857.

Xu, Y., Liu, Z., Zhang, X., Wang, Y., Tian, J., Huang, Y., Ma, Y., Zhang, X. & Chen, Y. 2009. A Graphene Hybrid Material Covalently Functionalized with Porphyrin: Synthesis and Optical Limiting Property. *Advanced Materials,* 21**,** 1275-1279.

Yamashita, K., Nagai, M. & Umegaki, T. 1997. Fabrication of green films of single- and multi-component ceramic composites by electrophoretic deposition technique. *Journal of Materials Science,* 32**,** 6661-6664.

Yan, L., Zhao, F., Li, S., Hu, Z. & Zhao, Y. 2011. Low-toxic and safe nanomaterials by surface-chemical design, carbon nanotubes, fullerenes, metallofullerenes, and graphenes. *Nanoscale,* 3**,** 362-382.

Yang, K., Wan, J., Zhang, S., Zhang, Y., Lee, S. T. & Liu, Z. 2011. In vivo pharmacokinetics, long-term biodistribution, and toxicology of pegylated graphene in mice. *ACS Nano,* 5**,** 516-522.

Yang, K., Zhang, S., Zhang, G., Sun, X., Lee, S. T. & Liu, Z. 2010a. Graphene in mice: Ultrahigh in vivo tumor uptake and efficient photothermal therapy. *Nano Letters,* 10**,** 3318-3323.

Yang, W., Thordarson, P., Gooding, J. J., Ringer, S. P. & Braet, F. 2007. Carbon nanotubes for biological and biomedical applications. *Nanotechnology,* 18.

Yang, X., Tu, Y., Li, L., Shang, S. & Tao, X. M. 2010b. Well-dispersed chitosan/graphene oxide nanocomposites. *ACS Applied Materials and Interfaces,* 2**,** 1707-1713.

Yang, X., Zhang, X., Liu, Z., Ma, Y., Huang, Y. & Chen, Y. 2008. High-efficiency loading and controlled release of doxorubicin hydrochloride on graphene oxide. *Journal of Physical Chemistry C,* 112**,** 17554-17558.

Yi, M., Shen, Z., Zhang, X. & Ma, S. 2013. Achieving concentrated graphene dispersions in water/acetone mixtures by the strategy of tailoring Hansen solubility parameters. *Journal of Physics D: Applied Physics,* 46**,** 025301.

Young, R. J. & Kinloch, I. A. 2013. Graphene and graphene-based nanocomposites. IN O'Brien, P. (Ed.) *Nanoscience: Nanostructures Through Chemistry.* Royal Society of Chemistry.

Yu, L., Pan, X., Cao, X., Hu, P. & Bao, X. 2011. Oxygen reduction reaction mechanism on nitrogen-doped graphene: A density functional theory study. *Journal of Catalysis,* 282**,** 183-190.

Yu, Q., Lian, J., Siriponglert, S., Li, H., Chen, Y. P. & Pei, S. S. 2008. Graphene segregated on Ni surfaces and transferred to insulators. *Applied Physics Letters,* 93.

Yu, W. & Xie, H. 2012. A Review on Nanofluids: Preparation, Stability Mechanisms and Applications. *Journal of Nanomaterials***,** 1-48.

Yuan, J., Gao, H., Sui, J., Duan, H., Chen, W. N. & Ching, C. B. 2012. Cytotoxicity evaluation of oxidized single-walled carbon nanotubes and graphene oxide on human hepatoma HepG2 cells: An iTRAQ-coupled 2D LC-MS/MS proteome analysis. *Toxicological Sciences,* 126**,** 149-161.

Zhang, L., Niu, J., Dai, L. & Xia, Z. 2012a. Effect of microstructure of nitrogen-doped graphene on oxygen reduction activity in fuel cells. *Langmuir,* 28**,** 7542-7550.

Zhang, L. & Xia, Z. 2011. Mechanisms of oxygen reduction reaction on nitrogen-doped graphene for fuel cells. *Journal of Physical Chemistry C,* 115**,** 11170-11176.

Zhang, Q., Qiao, Y., Hao, F., Zhang, L., Wu, S., Li, Y., Li, J. & Song, X. M. 2010a. Fabrication of a biocompatible and conductive platform based on a singlestranded DNA/graphene nanocomposite for direct electrochemistry and electrocatalysis. *Chemistry - A European Journal,* 16**,** 8133-8139.

Zhang, Q., Wan, X., Xing, F., Huang, L., Long, G., Yi, N., Ni, W., Liu, Z., Tian, J. & Chen, Y. 2013. Solution-processable graphene mesh transparent electrodes for organic solar cells. *Nano Research,* 6**,** 478-484.

Zhang, Y., Ali, S. F., Dervishi, E., Xu, Y., Li, Z., Casciano, D. & Biris, A. S. 2010b. Cytotoxicity effects of graphene and single-wall carbon nanotubes in neural phaeochromocytoma-derived pc12 cells. *ACS Nano,* 4**,** 3181-3186.

Zhang, Y., Guo, L., Wei, S., He, Y., Xia, H., Chen, Q., Sun, H. B. & Xiao, F. S. 2010c. Direct imprinting of microcircuits on graphene oxides film by femtosecond laser reduction. *Nano Today,* 5**,** 15-20.

Zhang, Y., Nayak, T. R., Hong, H. & Cai, W. 2012b. Graphene: A versatile nanoplatform for biomedical applications. *Nanoscale,* 4**,** 3833-3842.

Zhao, B., Guo, Q. & Xin, W. 2001. Free Radical Scavenging by Green Tea Polyphenols. IN Packer, L. (Ed.) *Flavonoids and Other Polyphenols: Methods in Enzymology.* London, United Kingdom, Academic Press.

Zhao, H., Song, H., Li, Z., Yuan, G. & Jin, Y. 2005. Electrophoretic deposition and field emission properties of patterned carbon nanotubes. *Applied Surface Science,* 251**,** 4-242.

Zhao, J., Pei, S., Ren, W., Gao, L. & Cheng, H. M. 2010. Efficient preparation of large-area graphene oxide sheets for transparent conductive films. *ACS Nano,* 4**,** 5245-5252.

Zhao, Y., Chen, L., Yakubov, G., Aminiafshar, T., Han, L. & Lian, G. 2012. Experimental and Theoretical Studies on the Binding of Epigallocatechin Gallate to Purified Porcine Gastric Mucin. *The Journal of Physical Chemistry B,* 116**,** 13010-13016.

Zhitomirsky, I. 2000. Electrophoretic hydroxyapatite coatings and fibers. *Materials Letters,* 42**,** 262-271.

Zhitomirsky, I. 2002. Cathodic electrodeposition of ceramic and organoceramic materials. Fundamental aspects. *Advances in Colloid and Interface Science,* 97**,** 277-315.

Zhou, M., Wang, Y., Zhai, Y., Zhai, J., Ren, W., Wang, F. & Dong, S. 2009a. Controlled synthesis of large-area and patterned electrochemically reduced graphene oxide films. *Chemistry - A European Journal,* 15**,** 6116-6120.

Zhou, Y., Bao, Q., Tang, L. A. L., Zhong, Y. & Loh, K. P. 2009b. Hydrothermal dehydration for the "green" reduction of exfoliated graphene oxide to graphene and demonstration of tunable optical limiting properties. *Chemistry of Materials,* 21**,** 2950-2956.

Zhu, C., Guo, S., Fang, Y. & Dong, S. 2010a. Reducing sugar: New functional molecules for the green synthesis of graphene nanosheets. *ACS Nano,* 4**,** 2429-2437.

Zhu, G., Pan, L., Lu, T., Xu, T. & Sun, Z. 2011. Electrophoretic deposition of reduced graphene-carbon nanotubes composite films as counter electrodes of dye-sensitized solar cells. *Journal of Materials Chemistry,* 21**,** 14869-14875.

Zhu, M., Wang, J., Holloway, B. C., Outlaw, R. A., Zhao, X., Hou, K., Shutthanandan, V. & Manos, D. M. 2007. A mechanism for carbon nanosheet formation. *Carbon,* 45**,** 2229-2234.

Zhu, N., Huang, T.-C., Yu, Y., LaVoie, E. J., Yang, C. S. & Ho, C.-T. 2000. Identification of Oxidation Products of (−)-Epigallocatechin Gallate and (−)-Epigallocatechin with H_2O_2. *Journal of Agricultural and Food Chemistry,* 48**,** 979-981.

Zhu, X., Liu, Q., Li, C., Xu, M. & Liang, Y. 2012. Reduction of graphene oxide via ascorbic acid and its application for simultaneous detection of dopamine and ascorbic acid. *International Journal of Electrochemical Science,* 7**,** 5172-5184.

Zhu, Y., Murali, S., Stoller, M. D., Velamakanni, A., Piner, R. D. & Ruoff, R. S. 2010b. Microwave assisted exfoliation and reduction of graphite oxide for ultracapacitors. *Carbon,* 48**,** 2118-2122.

APPENDICES

Appendix A

Table A1: Zeta potential values of GO, c-GO, N_2H_4-RGO and RGO suspensions prepared at different weight ratio of GTP/GO.

Sample	Sample 1 (mV)	Sample 2 (mV)	Sample 3 (mV)	Mean (mV)	Standard deviation	Standard error
GO (25 ℃)	-57.40	-56.20	-58.70	-57.43	1.25	0.72
c-GO	-47.60	-48.00	-47.50	-47.70	0.26	0.15
RGO-1	-24.90	-30.10	-30.10	-28.37	3.00	1.73
RGO-2	-36.90	-44.00	-34.50	-38.47	4.94	2.85
RGO-3	-28.00	-26.00	-25.90	-26.63	1.18	0.68
RGO-4	-26.90	-25.40	-25.30	-25.87	0.90	0.52
RGO-5	-24.80	-28.10	-22.40	-25.10	2.86	1.65
N_2H_4-RGO	-15.20	-15.20	-16.10	-15.50	0.52	0.30

Table A2: Electrophoretic mobility values of GO, c-GO, N_2H_4-RGO and RGO suspensions prepared at different weight ratio of GTP/GO.

Sample	Sample 1 (μmcm/Vs)	Sample 2 (μmcm/Vs)	Sample 3 (μmcm/Vs)	Mean (μmcm/Vs)	Standard deviation	Standard error
GO (25 ℃)	-4.50	-4.40	-4.60	-4.50	0.10	0.06
c-GO	-3.73	-3.76	-3.72	-3.74	0.02	0.01
RGO-1	-1.95	-2.36	-2.36	-2.22	0.24	0.14
RGO-2	-2.90	-3.45	-2.71	-3.02	0.39	0.22
RGO-3	-2.19	-2.04	-2.03	-2.09	0.09	0.05
RGO-4	-2.11	-1.99	-1.99	-2.03	0.07	0.04
RGO-5	-1.95	-2.21	-1.76	-1.97	0.23	0.13
N_2H_4-RGO	-1.19	-1.19	-1.26	-1.21	0.04	0.02

Table A3: Zeta potential values of RGO suspensions prepared at different reaction temperature.

Sample	Sample 1 (mV)	Sample 2 (mV)	Sample 3 (mV)	Mean (mV)	Standard deviation	Standard error
RGO-6	-28.10	-30.90	-32.40	-30.47	2.18	1.26
RGO-7	-34.40	-30.90	-36.50	-33.93	2.83	1.63
RGO-8	-36.90	-44.00	-34.50	-38.47	4.94	2.85
RGO-9	-42.60	-40.40	-35.30	-39.43	3.74	2.16
RGO-10	-20.30	-27.70	-26.60	-24.87	3.99	2.31
RGO-11	-17.40	-16.20	-16.40	-16.67	0.64	0.37

Table A4: Electrophoretic mobility values of RGO suspensions prepared at different reaction temperature.

Sample	Sample 1 (μmcm/Vs)	Sample 2 (μmcm/Vs)	Sample 3 (μmcm/Vs)	Mean (μmcm/Vs)	Standard deviation	Standard error
RGO-6	-2.20	-2.42	-2.54	-2.39	0.17	0.10
RGO-7	-2.70	-2.42	-2.86	-2.66	0.22	0.13
RGO-8	-2.90	-3.45	-2.71	-3.02	0.39	0.22
RGO-9	-3.34	-3.17	-2.77	-3.09	0.29	0.17
RGO-10	-1.59	-2.17	-2.08	-1.95	0.31	0.18
RGO-11	-1.36	-1.27	-1.29	-1.31	0.05	0.03

Appendix B

Table B1: Percentage inhibition of CCD-18Co cell proliferation after treatment with GO, RGO-9, RGO-5 and GTP samples at different concentrations (6.25-200 µg/mL).

Sample	Concentration (µg/mL)					
	6.25	12.5	25	50	100	200
GO	47.34	58.79	51.09	59.47	69.15	64.60
	57.49	42.60	62.67	64.01	63.77	67.25
	43.23	60.18	62.47	61.52	61.01	66.03
RGO-9	26.95	36.40	49.12	55.52	60.73	54.05
	30.39	48.25	47.97	58.48	54.45	63.77
	28.73	48.21	52.91	46.23	52.24	60.69
RGO-5	27.03	48.92	49.59	51.92	42.60	51.76
	18.82	40.23	34.78	39.48	42.95	55.28
	16.41	38.65	47.42	41.85	51.25	50.30
GTP	1.01	0.49	-2.90	18.38	13.13	27.47
	-2.29	-2.53	8.51	20.91	27.11	37.66
	1.46	4.27	4.20	8.51	27.19	32.60

Table B2: Anova of Two-Factor With Replication.

SUMMARY	6.25	12.5	25	50	100	200	Total
GO							
Count	3	3	3	3	3	3	18
Sum	148.07	161.58	176.24	185.01	193.94	197.89	1062.74
Average	49.36	53.86	58.75	61.67	64.65	65.96	59.04
Variance	53.89	95.55	43.91	5.18	17.12	1.75	62.09
RGO-9							
Count	3	3	3	3	3	3	18
Sum	86.09	132.86	150.01	160.24	167.43	178.53	875.17
Average	28.70	44.29	50.00	53.41	55.81	59.51	48.62
Variance	2.95	46.66	6.68	40.82	19.41	24.66	124.42
RGO-5							
Count	3	3	3	3	3	3	18
Sum	62.27	127.81	131.80	133.26	136.82	157.36	749.31
Average	20.76	42.60	43.93	44.42	45.61	52.45	41.63

| Variance | 31.04 | 30.59 | 63.99 | 43.66 | 23.97 | 6.55 | 126.33 |

Table B2: Continued.

SUMMARY	6.25	12.5	25	50	100	200	Total
GTP							
Count	3	3	3	3	3	3	18
Sum	0.18	2.23	9.81	47.81	67.45	97.75	225.23
Average	0.06	0.74	3.27	15.94	22.48	32.58	12.51
Variance	4.23	11.66	33.24	42.97	65.56	25.97	179.16

Total						
Count	12	12	12	12	12	12
Sum	296.62	424.49	467.86	526.32	565.63	631.52
Average	24.72	35.37	38.99	43.86	47.14	52.63
Variance	356.73	489.71	521.08	348.25	293.48	181.74

ANOVA

Source of Variation	SS	df	MS	F	P-value	F crit
Sample	21496.80	3	7165.60	231.76	1.51E-28	2.7981
Concentration	5759.96	5	1151.99	37.26	2.05E-15	2.4085
Interaction	1119.92	15	74.66	2.41	0.0106	1.8802
Within	1484.06	48	30.92			
Total	29860.74	71				

Appendix C

Table C1: ΔH, ΔG and ΔS for stationary points involved in the reduction of GO by using GTP.

Species	SCF (a.u.)	H (a.u.)	G (a.u.)	S (kcal/mol·K)	$H_{correction}$ (a.u.)	$G_{correction}$ (a.u.)
GO	-305.6941	-305.5812	-305.6266	0.0784	0.1128	0.0674
GTP	-1667.3702	-1666.9506	-1667.0750	0.2150	0.4196	0.2952
reactant		-1972.5319	-1972.7017	0.2935		
= GO +						
GTP						
RGO	-230.9757	-230.8666	-230.9088	0.0728	0.1091	0.0669
Galloyl	-1666.1342	-1665.7380	-1665.8610	0.2125	0.3961	0.2731
H_2O	-75.9739	-75.9495	-75.9767	0.0468	0.0243	-0.0027
product		-1972.5542	-1972.7466	0.3323		
= RGO						
+						
Galloyl						
+ H_2O						
int	-1973.1248	-1972.5877	-1972.7285	0.2432	0.5371	0.3963
ts1	-1973.0346	-1972.5172	-1972.6442	0.2194	0.5174	0.3904
ts2	-1973.0346	-1972.5171	-1972.6442	0.2195	0.5174	0.3904

	ΔH (kcal/mol)	ΔG (kcal/mol)	ΔS (kcal/mol·K)
reactant	0.000	0.000	0.000
ts1	9.204	36.096	-0.074
int	-35.020	-16.773	-0.050
ts2	9.228	36.107	-0.074
product	-14.053	-28.132	0.039

Notes:
i) 1 a.u. = 627.51 kcal/mol
ii) H = SCF + $H_{correction}$, G = SCF + $G_{correction}$
iii) $\Delta H_{product} = H_{product} - H_{reactant}$
iv) $\Delta G_{product} = G_{product} - G_{reactant}$
v) $\Delta S_{product} = S_{product} - S_{reactant}$

Table C2: ΔH, ΔG and ΔS for stationary points involved in the reduction of GO by using N_2H_4 solution.

Species	SCF (a.u.)	H (a.u.)	G (a.u.)	S (kcal/mol·K)	$H_{correction}$ (a.u.)	$G_{correction}$ (a.u.)
GO	-305.6941	-305.5812	-305.6266	0.0784	0.1128	0.0674
N_2H_4	-111.2284	-111.1711	-111.2058	0.0599	0.0573	0.0226
reactant = GO + N_2H_4		-416.7524	-416.8325	0.1383		
RGO	-230.9757	-230.8666	-230.9088	0.0728	0.1091	0.0669
N_2H_2	-109.9922	-109.9617	-109.9929	0.0539	0.0305	-0.0006
H_2O	-75.9739	-75.9495	-75.9767	0.0468	0.0243	-0.0027
product = RGO + N_2H_2 + H_2O		-416.7779	-416.8785	0.1737		
int	-416.9750	-416.8017	-416.8583	0.0978	0.1733	0.1167
ts1	-416.8811	-416.7107	-416.7666	0.0965	0.1704	0.1145
ts2	-416.8049	-416.6438	-416.6994	0.0960	0.1611	0.1055

	ΔH (kcal/mol)	ΔG (kcal/mol)	ΔS (kcal/mol·K)
reactant	0.000	0.000	0.000
ts1	26.174	41.354	-0.042
int	-30.916	-16.193	-0.041
ts2	68.122	83.499	-0.042
product	-16.021	-28.860	0.035

Notes:
i)   1 a.u. = 627.51 kcal/mol
ii) $H = SCF + H_{correction}$, $G = SCF + G_{correction}$
iii) $\Delta H_{product} = H_{product} - H_{reactant}$
iv) $\Delta G_{product} = G_{product} - G_{reactant}$
v) $\Delta S_{product} = S_{product} - S_{reactant}$

Appendix D

Table D1: Variation of deposition weight of GFs as a function of applied voltage in EPD process.

Deposition time (s)	Applied voltage (V)	Deposition weight 1 (mg/cm^2)	Deposition weight 2 (mg/cm^2)	Deposition weight 3 (mg/cm^2)	Mean (mg/cm^2)	Standard deviation	Standard error
500	10	0.26	0.16	0.32	0.25	0.08	0.05
500	20	0.37	0.49	0.26	0.37	0.12	0.07
500	30	0.60	0.49	0.44	0.51	0.08	0.05
500	40	0.35	0.30	0.43	0.36	0.07	0.04
500	50	0.39	0.35	0.29	0.34	0.05	0.03

Table D2: Variation of deposition weight of GFs as a function of deposition time in EPD process.

Deposition time (s)	Applied voltage (V)	Deposition weight 1 (mg/cm^2)	Deposition weight 2 (mg/cm^2)	Deposition weight 3 (mg/cm^2)	Mean (mg/cm^2)	Standard deviation	Standard error
100	10	0.04	0.08	0.06	0.06	0.02	0.01
200	10	0.09	0.08	0.05	0.07	0.02	0.01
300	10	0.11	0.06	0.15	0.11	0.05	0.03
400	10	0.13	0.14	0.16	0.14	0.02	0.01
500	10	0.26	0.16	0.32	0.25	0.08	0.05